NAVAL POSTGRADUATE SCHOOL
MONTEREY, CALIFORNIA

THESIS

VIBRATION ANALYSIS OF TOPAZ II

by

Elisa Anne Raney

June, 1995

Thesis Advisor: Sandra L. Scrivener

Approved for public release; distribution is unlimited.

19960123 073

REPORT DOCUMENTATION PAGE			Form Approved OMB No. 0704-0188

1. AGENCY USE ONLY *(Leave blank)*	2. REPORT DATE June 1995	3. REPORT TYPE AND DATES COVERED Master's Thesis

4. TITLE AND SUBTITLE VIBRATION ANALYSIS OF TOPAZ II	5. FUNDING NUMBERS
6. AUTHOR(S) Raney, Elisa A.	

7. PERFORMING ORGANIZATION NAME(S) AND ADDRESS(ES) Naval Postgraduate School Monterey CA 93943-5000	8. PERFORMING ORGANIZATION REPORT NUMBER

9. SPONSORING/MONITORING AGENCY NAME(S) AND ADDRESS(ES)	10. SPONSORING/MONITORING AGENCY REPORT NUMBER

11. SUPPLEMENTARY NOTES The views expressed in this thesis are those of the author and do not reflect the official policy or position of the Department of Defense or the U.S. Government.

12a. DISTRIBUTION/AVAILABILITY STATEMENT Approved for public release; distribution is unlimited.	12b. DISTRIBUTION CODE

13. ABSTRACT *(maximum 200 words)* Topaz II is a Russian made nuclear powered satellite purchased by the United States. This thesis provides a vibration analysis of the power unit of Topaz II. Several experimental vibration tests were conducted on the actual power unit by Sandia National Laboratories, in Albuquerque, New Mexico. Utilizing Structural Dynamics Research Corporation's I-DEAS Masters Series Software, a finite element model was made of the power unit. Using the I-DEAS software, this model was tested using the same vibration test values as those performed on the actual power unit. The lateral and axial, experimental and theoretical, sine tests were then analyzed. The purpose of this analysis was to determine how accurate a representation the model was of the actual Topaz unit. This was accomplished through comparison of natural frequencies obtained experimentally with those predicted from I-DEAS testing of the finite element model. The frequency range of interest was from 0 Hz to 100 Hz. When solved for system modes, the model predicted all natural frequencies within 4.6 Hz of those found experimentally. The average variation between theoretically predicted and experimentally determined natural frequencies was 1.8 Hz.

14. SUBJECT TERMS Finite element analysis, TOPAZ, natural frequencies, system modes	15. NUMBER OF PAGES 194
	16. PRICE CODE

17. SECURITY CLASSIFICATION OF REPORT Unclassified	18. SECURITY CLASSIFICATION OF THIS PAGE Unclassified	19. SECURITY CLASSIFICATION OF ABSTRACT Unclassified	20. LIMITATION OF ABSTRACT UL

ABSTRACT

Topaz II is a Russian made nuclear powered satellite purchased by the United States. This thesis provides a vibration analysis of the power unit of Topaz II. Several experimental vibration tests were conducted on the actual power unit by Sandia National Laboratories, in Albuquerque, New Mexico. Utilizing Structural Dynamics Research Corporation's I-DEAS Masters Series Software, a finite element model was made of the power unit. Using the I-DEAS software, this model was tested using the same vibration test values as those performed on the actual power unit. The lateral and axial, experimental and theoretical, sine tests were then analyzed. The purpose of this analysis was to determine how accurate a representation the model was of the actual Topaz unit. This was accomplished through comparison of natural frequencies obtained experimentally with those predicted from I-DEAS testing of the finite element model. The frequency range of interest was from 0 Hz to 200 Hz. When solved for system modes, the model predicted all natural frequencies within 4.6 Hz of those found experimentally. The average variation between theoretically predicted and experimentally determined natural frequencies was 1.8 Hz.

TABLE OF CONTENTS

I. INTRODUCTION

A. ACQUISITION OF TOPAZ II

The United States conducts many of its military missions in space through the use of satellites. The Department of Defense has a long term requirement to develop follow-on power technologies to support these missions. Having the capability to produce a large quantity of electrical power on orbit would allow a greater spectrum of missions to be performed, such as environmental monitoring and using high power active sensors for surveillance. To determine the most effective means of supplying this power, a series of Air Force and Department of Defense mission and integration studies were begun in the late 1980's. The conclusion drawn was that compact, environmentally safe nuclear power was the best option. In the spring of 1992, a Department of Defense study considered the option of importing the Russian made TOPAZ II space nuclear reactor technology. It was decided that this technology would greatly enhance development of U.S. space nuclear reactors. [Ref. 1]

Procurement of TOPAZ II was accomplished by the Strategic Defense Initiative Organization (SDIO), now known as the Ballistic Missile Defense Organization (BMDO). They have also been responsible for the transfer of space nuclear reactor technology between the United States and Russia. This started in December of 1991, when SDIO began the investigation of the possibility of a U.S. launched Russian TOPAZ II nuclear power system. At this time, the intended destination of TOPAZ II was in the Nuclear Electric Propulsion (NEP) Space Test Mission. [Ref. 1]

The foremost consideration in launching a TOPAZ II satellite was safety. The requirement was for a safe launch, within constraints of the given budget. To find out if this were

1

possible, SDIO subpoenaed a group of twelve engineers and scientists from Sandia National Laboratories (SNL), the Air Force Phillips Laboratory (PL), Los Alamos National Laboratory (LANL), the University of New Mexico (UNM), and Advanced Sciences, Inc. (ASI). The conclusion of this comprehensive preliminary study, completed in 1992, was that the TOPAZ II could be launched safely and within budget constraints.

In the spring of 1992, two TOPAZ II reactors were delivered to the New Mexico Engineering Research Institute (NMERI). The fuel elements were not included in the package. Also obtained by NMERI was a complete satellite qualification testing facility. Under the direction of the Phillips Laboratory, non-nuclear testing of TOPAZ II was begun as part of the TOPAZ Technology Program.

The TOPAZ Technology Program, led by the BMDO, is a three phase cooperative effort with Russia. The three phases are comprised of joint evaluation, joint testing, and joint development. Each phase allows an opportunity for both the U.S. and Russia to evaluate the program and determine future direction. The United States stands to gain possession of thermionic reactor technology for use by U.S. industry. [Ref. 1]

B. MISSION DESCRIPTION

Mission goals of the NEP Space Test Program include use of the NEP Space Test Spacecraft to test an assortment of electric propulsion thrusters and conduct additional scientific experiments that would be compatible with its other mission requirements. Two specific elements of Russian space technology will also be tested and evaluated, those being the TOPAZ II nuclear reactor and the SPT-100 electric propulsion thruster. One of the programs primary goals is to

2

evaluate the NEP in orbital transfer applications and measurement of the spacecraft environment produced by NEP system operation.

The reactor system of the NEP spacecraft, shown in Figure 1, is separated from the main section of the spacecraft by an extendable boom. This arrangement is necessary to maintain the radiation dosage received by other spacecraft components to acceptable levels. [Ref. 1]

C. TOPAZ II POWER SYSTEM DESCRIPTION

The power system of TOPAZ II consists of a reactor power system, which generates electricity from nuclear heat through the use of in-core thermionic conversion units. This system was designed by Russian engineers to meet the following specifications: [Ref. 1]

1. Under no circumstances should the reactor system operate before reaching orbit altitude.

2. The system shelf life must be 10 or more years

3. The coolant shall not freeze before operation

4. The system must be capable of providing 6 kWe at 27 volts for a lifetime of 3 years with a reliability of 0.95.

5. The mass of the power system must not exceed 1061 kilograms, excluding the controller and supply system masses.

The main subsystem of the TOPAZ II power system are the reactor subsystem, the radiation shield, the primary coolant loop, the cesium supply system, the instrumentation and control system, gas systems, thermal cover, and the primary power system structure. (see Figure 2)
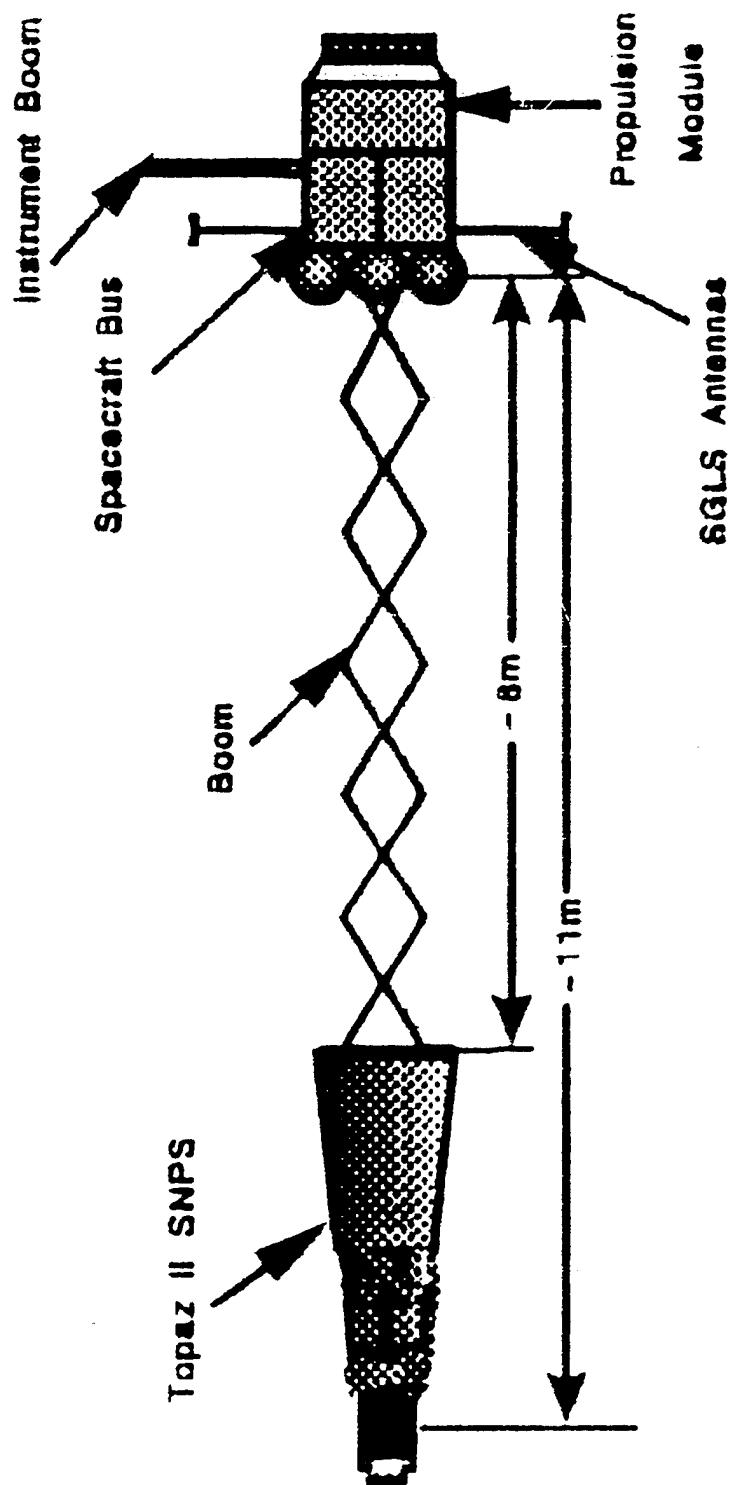
Figure 1. TOPAZ [Ref. 1].

4

The nuclear reactor is a small zirconium hydride-moderated, epi-thermal reactor with in-core thermionic converters. The reactor incorporates 37 in-core single cell thermionic fuel elements (TFEs). Prior to fuel being loaded into the TFEs, electric heaters can be loaded into the TFE cavity to simulate heat generated from the reactor. The advantage of using heaters is the capability to perform non-nuclear testing of the thermionic converters and the complete power system. With heaters, this can be accomplished at conditions near what the nominal operating conditions would be.

The purpose of the radiation shield is to attenuate neutron and gamma radiation. Located behind the reactor, it is a truncated cone composed of a stainless steel shell containing lithium hydride (LiH) which is the neutron shield. The radiation shield is attached by support legs to the lower end of the reactor.

The reactor coolant loop is comprised of a single EM pump, stainless steel piping, sodium-potassium (NaK) coolant, and a heat rejection radiator. From a lower plenum, the NaK passes through the reactor core where it is heated, to an upper plenum to two stainless steel pipes to the radiator, the NaK flows through two coolant pipes dividing into three pipes each, prior to reaching the EM pump. The pump then sends the NaK back to the reactor lower plenum.

Cesium is supplied to the TFE interelectrode gap via the cesium supply system. This is necessary to increase the efficiency of the thermionic converters through suppression of the space charge that occurs near its emitters.

The Instrumentation and Control system is required for the monitoring, controlling, and telemetering of the power system status. Its primary duties are the following: 1) to start the power system, 2) maintenance of the system operation under nominal operating conditions, 3)

5
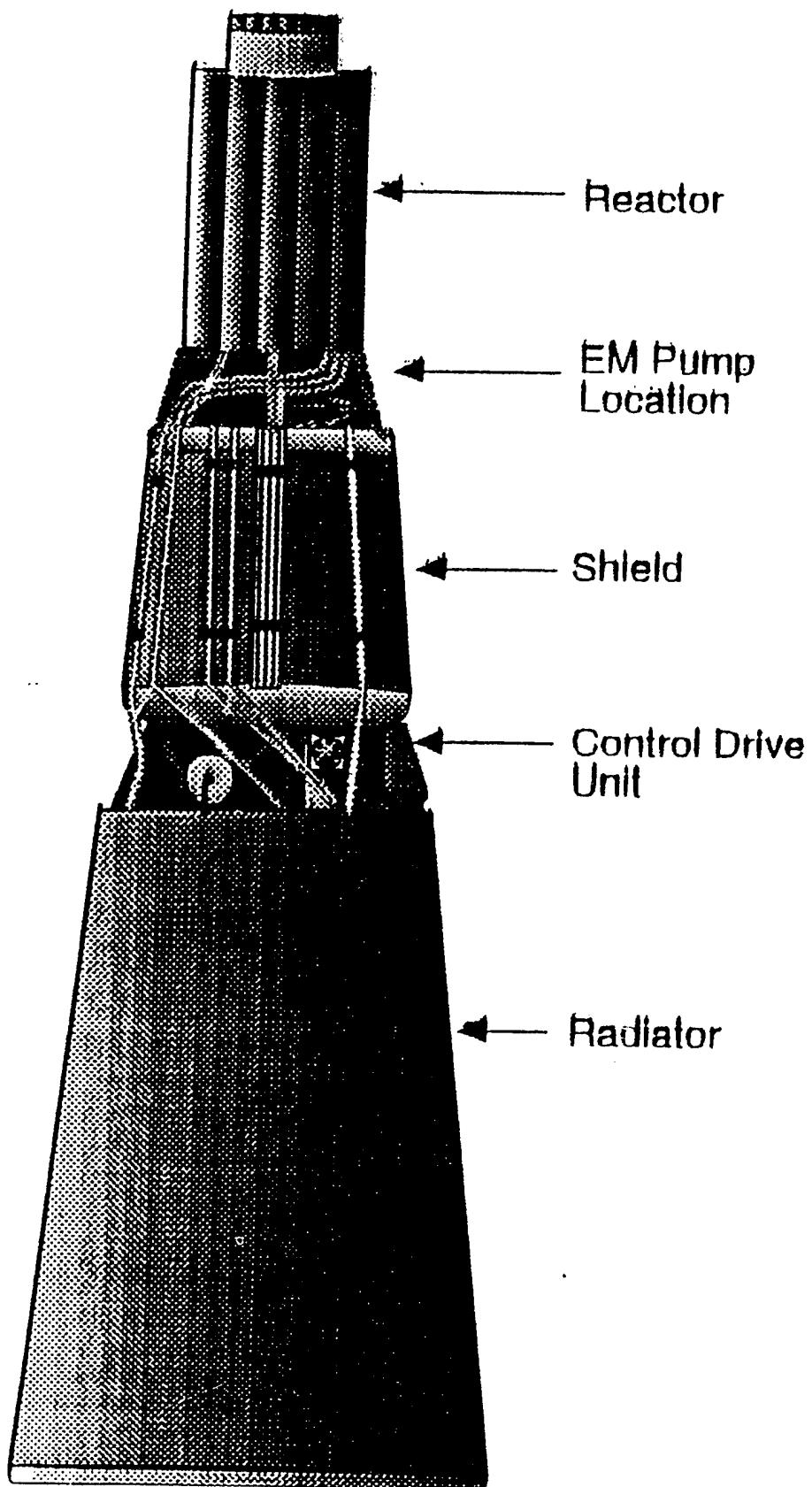
Figure 2. Primary Power System [Ref. 1].

stabilization of the voltage received by the payload 4) performance of the commands from the ground control station, 5) shutdown of the power system, 6) maintain safety control during land-based operations, 7) telemetering performance data to the ground, 8) shunting of excess electrical power to ballast resistors, and 9) to keep the storage battery charged. [Ref. 1]

There are four gas systems on board TOPAZ II. These are the CO_2/He moderator cover gas, the He TFE-gap gas, the Ar/He gas in the volume accumulator and the helium gas in the radiation shield. The gas pressure is monitored during filling, electric ground testing, and throughout the first few thousand hours of space operation by pressure gauges connected to each of these gas systems.

The purpose of the thermal cover is to reduce the heat loss from the power system on the launch pad and during the flight to orbit. If the TOPAZ II coolant were allowed to freeze, coolant circulation would cease, and the system would no longer operate properly.

The primary power system structure consists of the reactor, the shield, and the frame. These are the three main structural members of the power system. The frame supports the radiator, the gas bottles, coolant piping, and the volume accumulator. It is attached to the shield, and is also used to attach the spacecraft boom. [Ref. 1]

A more indepth analysis of the nuclear power system was done by LT Steve Benke and LT Rich Venable. Their theses may be obtained through the Naval Postgraduate School, Monterey, CA. [Ref. 2].

II. TOPAZ II - THE MODEL

A. DEVELOPMENT / PURPOSE OF TOPAZ II FINITE ELEMENT MODEL

The Finte Element Model of TOPAZ II was developed by J.M. Lacy, of Idaho National Laboratories [Ref. 3]. One of the first problems encountered was that of which system of units to use. American engineers tend to favor the SAE system whereas the Russians use their version of the SI system. Mr. Lacy elected to use the Russian modified metric system. The following units conversion table may prove useful. [Ref. 3]

Unit	Dimension	Equivalencies	
length	1 mm	0.03937 in	0.00329 ft
mass	1 kg	2.2 lbm	0.00571 lb-s^2/in
force	1 N	0.2248 lb	0.1019 kgf
stress	1 MPa	1 N/mm^2	145.04 psi

The finite element model was made for the reactor unit and its support frame. The frame has three legs whose feet, when connected by an imaginary circle, form a circle of 2440 mm in diameter. The upper end of the frame, to which the reactor unit is attached, has a diameter of 680 mm. This platform is 2116 mm above the feet. (see Figure 3) On the launch pad, the power system and frame will weigh approximately 1043 kg. The center of gravity will be 2304 mm above the feet.

Some of the TOPAZ frames are constructed of 12X18H10T stainless steel while others are reported as 08X18H10T material. These designations are interpreted below and their properties are listed in Table 1. [Ref. 3]

8

2903 mm
r = 223.5 mm

2116 mm
r = 340 mm

1822 mm
r = 362 mm

0 mm
r = 610 mm
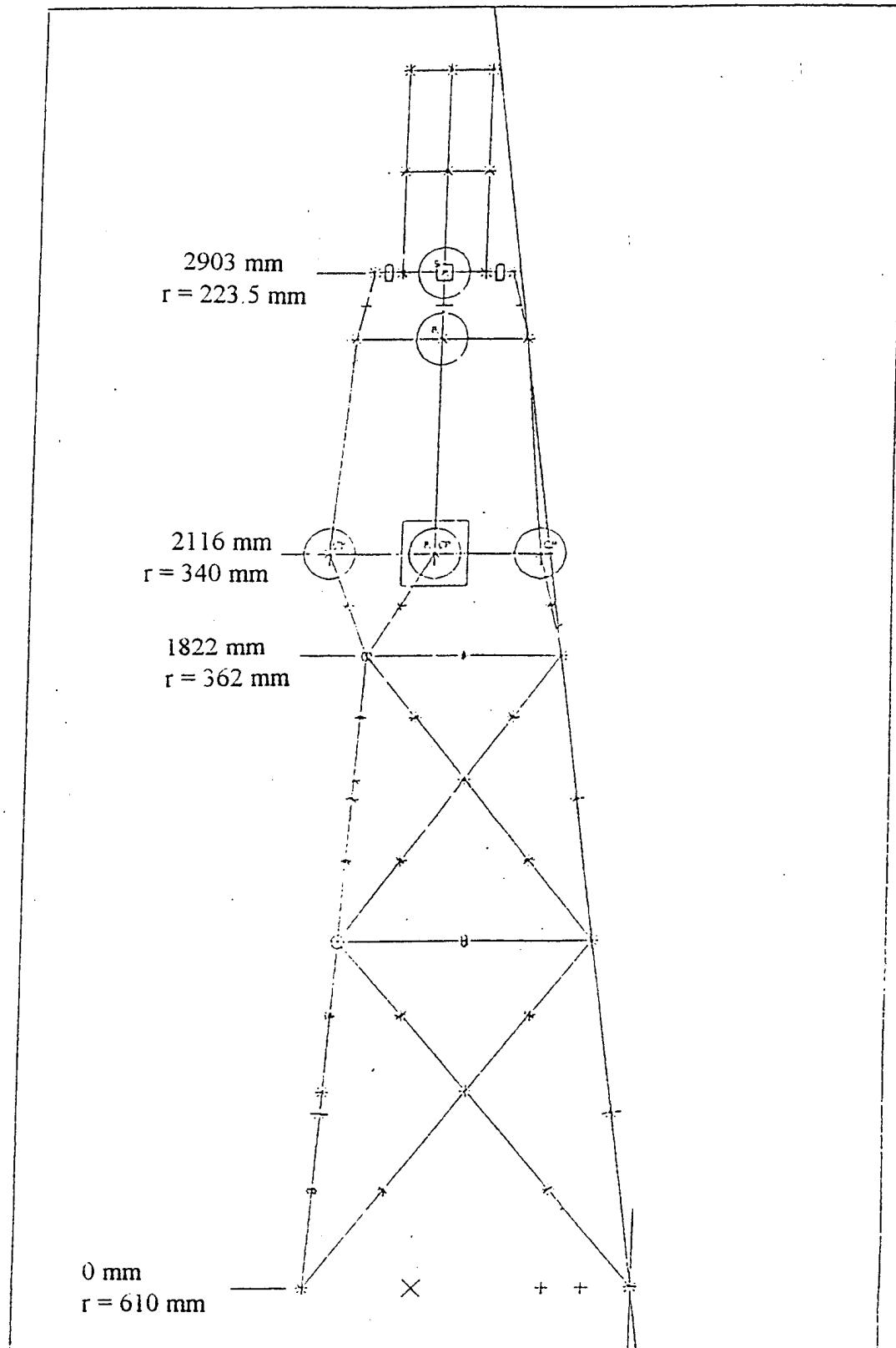
Figure 3. TOPAZ Finite Element Model [Ref. 3].

12		less than 0.12% Carbon
X18		18% Chromium
H10		10% Nickel
T		Titanium is 5 times the Carbon content, but less than 0.8%
density, p		7.95 g/cm^3
modulus of elasticity, E		195.12 GPa (28.3×10^6 psi)*
		* an assumption, to correspond with ASME stainless steel properties

Designation	Temperature (^{0}C)	Ultimate Strength (MPa)	Yield Strength (MPa)	Elongation (%)	Reduction in Area (%)
08X18H10T	unknown	490	196	40	55
12X18H10T	350	549	216	35	NA
	600	510	196	40	55

Table 1. TOPAZ II Frame Properties [Ref. 3].

One purpose of creating the FEM, and the one addressed by this thesis, is the determination of the natural frequency of the reactor system. This is a major concern during the launch phase, due to the vibration forces that will be imparted to TOPAZ. The natural frequency determines how the system is going to respond to these inputs and whether or not it will withstand the launch loads. If the natural frequencies are accurately calculated, then the stiffness, mass, and mass distribution of the system are known to have been modeled correctly. Having accomplished this, the model can then be used reliably to predict what stresses and displacements will occur under actual loading conditions.

Through testing of an actual TOPAZ unit in 1992, the Russian scientists found the first natural frequency of the reactor unit to be 4.5 - 5.0 Hz. This presented a problem because the

natural frequency of the entire system would be far lower than that of the rector unit alone. Due to interference from launch loads, a payload whose natural frequency is less than 4 Hz cannot be launched in the United States.

When E.D. Schaefer of APL [Ref. 8] created a FEM to confirm the frequency range of 4.5 to 5 Hz, he instead found the first natural frequency of the system to be closer to 10.5 Hz. Early in 1993, Lacy [Ref. 3] was tasked to study this problem independently. His results were the same as Schaefer's. At this point, the discrepancy explanation was thought to lie in differences between the reactor system and its documentation. Through hands-on measurements, this was disproved. Properties that could not be directly measured were confirmed with the Russian scientists.

During the summer of 1993, Sandia National Laboratories performed a modal survey of an actual reactor unit. This system massed 899 kg (as opposed to 1043 kg used the previous FEM) and the first natural frequency was found to be 20.3 Hz. In their testing, Sandia used both the reactor unit and the seismic mass. When this mass was included in Lacys' FEM and the reactor mass reduced to 899 kg, he predicted the first natural frequency to be 21.6 Hz. Therefore, Sandia's modal survey supported both Lacys' and Schaefer's theoretical results of 10 Hz.

Lacy produced another FEM of TOPAZ in the fall of 1993 [Ref. 3]. This model weighed 899 kg and had small refinements made to the mass distribution of the system, and to the frame geometry. His results continued to agree with Schaefer's results and those of Sandia National Laboratories. The first natural frequency of the seismic mass was only 2% below that reported by the modal survey, and the first lateral fixed base frequency of the system was found to be 10.8 Hz. [Ref. 3].

The results presented in this work were derived through vibrational analysis of this updated FEM model.

III. EXPERIMENTAL SHOCK AND VIBRATION TESTING OF TOPAZ II

A. SETUP

Early in September, 1994, shock and vibration testing was performed on TOPAZ II at Sandia National Laboratories in Albuquerque, N. M. Specifically, the vibration tests performed were lateral and longitudinal sine vibration tests, random vibration tests, and shock tests. The sine tests are examined in this thesis. Analysis of the random vibration tests has been performed by LT Sheryl Campbell from the Naval Postgraduate School, in a companion thesis completed in June 1995.

There were twelve accelerometers mounted on the power system. The accelerometers were placed where the anticipated responses were deemed most critical. Their locations are given in Tables 2 and 3 for the lateral and longitudinal tests respectively. Also shown in this table are the instrument axes from which responses were read by the testing equipment. Data were not taken from all axes from each accelerometer during each test because the testing equipment could only read a maximum of 24 channels concurrently.

There were three different coordinate systems used between the experimental set-up and theoretical analysis. The actual TOPAZ unit, the FEM, and the accelerometers each had their own coordinate directions. The relationship between the instrument and accelerometer axes is given in Table 4. Figure 4 shows the relationship between the FEM and TOPAZ coordinate axes. Table 4 does not include accelerometer numbers 11 and 12. These accelerometers were mounted on the cesium unit and the start-up unit of TOPAZ. In the FEM, these units were not individually modeled so that there was no theoretical result obtained from these locations. In future research,

Accel. No.	Instrument Location	Axis Used X	Axis Used Y	Axis Used Z
1	Mount on -Z leg of frame at base	x	x	x
2	Mount on leg between +Y and +Z of frame at base		x	x
3	Mount on bottom collector of radiator on -Z axis	x		
4	Mount on bottom collector of radiator on +Y axis		x	
5	Mount on -Z leg of frame at top of radiator	x		x
6	Mount on leg between +Y and +Z of frame at top of radiator	x	x	
7	Mount on reactor leg bracket most closely aligned with -Z axis			x
8	Mount on reactor leg bracket most closely aligned with +Y axis		x	
9	Mount on reactor top plenum on -Z axis	x	x	x
10	Mount on reactor top plenum on +Y axis			
11	Mount to "hard point" on cesium unit	x	x	x
12	Mount to "start-up unit" frame	x	x	x

Table 2. Lateral Sine Sweep Accelerometers [Ref. 6].

these units should be modeled and their responses evaluated.

In this thesis, the terms lateral and longitudinal refer to the lateral (Z) and axial (X) directions of the actual TOPAZ unit. The position of the accelerometers on TOPAZ are depicted in Figures 4 and 5. Also shown are the coordinate systems of both the actual TOPAZ unit and the FEM, for future reference in later chapters.

The values of the sine vibration applied to TOPAZ were chosen as common launch frequencies that might be imparted to the satellite. The specific values and test parameters are listed below. (A graphical repesentation of the sine input is given in Figure 6) [Ref. 6]

Accel. No.	Instrument Location	Axis Used X	Axis Used Y	Axis Used Z
1	Mount on -Z leg of frame at base	x	x	x
2	Mount on leg between +Y and +Z of frame at base	x	x	
3	Mount on bottom collector of radiator on -Z axis			x
4	Mount on bottom collector of radiator on +Y axis			x
5	Mount on -Z leg of frame at top of radiator	x		
6	Mount on leg between +Y and +Z of frame at top of radiator	x	x	
7	Mount on reactor leg bracket most closely aligned with -Z axis	x		
8	Mount on reactor leg bracket most closely aligned with +Y axis	x		
9	Mount on reactor top plenum on -Z axis	x		x
10	Mount on reactor top plenum on +Y axis	x	x	
11	Mount to "hard point" on cesium unit	x	x	x
12	Mount to "start-up unit" frame	x	x	x

Table 3. Longitudinal Sine Sweep Accelerometer Locations [Ref. 6].

SINE-VIBRATION INPUT

Frequency(Hz)	Level: g (1 min. @ axis)
5	.25
5 - 8	linear increase
8 - 40	1.0
40 - 100	.9
100 - 200	.8

1. The input was ramped

2. The test duration (sweep rate) was 0.25 octaves/minute which corresponds to a test duration of about 7 minutes.

3. A standard test tolerances of +/-10% was placed on the test parameters.

4. Three additional control accelerometers were used. Their purpose was to limit the response of the TOPAZ system to prevent overstressing it. These were accelerometers number 2, 5, and 9. See Figures 4 and 5 for their locations. [Ref. 7]. These controls were limited to responses of 6, 9, and 12 dB respectively. [Ref. 9].

The sine vibration was applied to the TOPAZ unit twice, once in the longitudinal X direction and once in the lateral Z direction. Due to the geometry of TOPAZ, the Z direction was determined by the Russians to be the most critical of the two lateral axes directions for testing purposes.

Accel #	On Node #	Instrument Axis	Topaz Axis	Accelerometer ID
1	5	X	-X	I01/C13:-Z LEG@BASE Axis: -X
1	5	Y	-Z	I01/C14:-Z LEG@BASE Axis: -Z
1	5	Z	-Y	I01/C15:-Z LEG@BASE Axis: -Y
2	12	X	-X	I02/C16:LEG/+Y AND +Z/BASE Axis: -X
2	12	Y	+Y(30 degree offset)	I02/C17:LEG/+Y AND +Z/BASE Axis: +Y
2	12	Z	-Z	I02/C18:LEG/+Y AND +Z/BASE Axis: -Z
5	29	X	-X	I05/C31:JOINT ON LEG Axis: -X
5	29	Y	Y	
5	29	Z	-Z	I05/C33:JOINT ON LEG Axis: -Z
6	55	X	-X	I06/C19:LEG +Y AND +Z/RAD.TOP Axis: -X
6	55	Y	+Z(30 degree offset)	I06/C20:LEG/+Y AND +Z/RAD.TOP Axis: +Z(30)
6	55	Z	+Y(30 degree offset)	
7	79	X	-X(20 degree slant)	I07/C05:REAC.LEG BRACKET/-Z Axis: -X(20)
7	79	Y	+Y	
7	79	Z	-Z(20 degree slant & 15 degree offset)	I07/C08:REAC.LEG BRAK./-Z Axis: -Z(15)
8	75	X	-X(20 degree slant)	I08/C01:REAC.LEG BRACKET/+Y Axis: -X(20)
8	75	Y	+Z	I08/C04:REACT.LEG BRAKET/+Y Axis: +Z

Accel #	On Node #	Instrument Axis	Topaz Axis	Accelerometer ID
8	75	Z	+Y (15 degree offset & 20 degree slant)	
9	97	X	-X	I09/C09:REACT.TOP PLENUM/-Z Axis: -X
9	97	Y	+Y	I09/C11:REACT.TOP PLENUM/-Z Axis: +Y
9	97	Z	-Z	I09/C12:REAC.TOP PLENUM/-Z Axis: -Z
10	92	X	-X	I10/C03.REAC.TOP PLENUM/+Y Axis: -X
10	92	Y	+Z	
10	92	Z	+Y	I10/C02:REAC.TOP PLENUM/+Y Axis: +Y

Table 4. Correlation of Coordinate Systems.
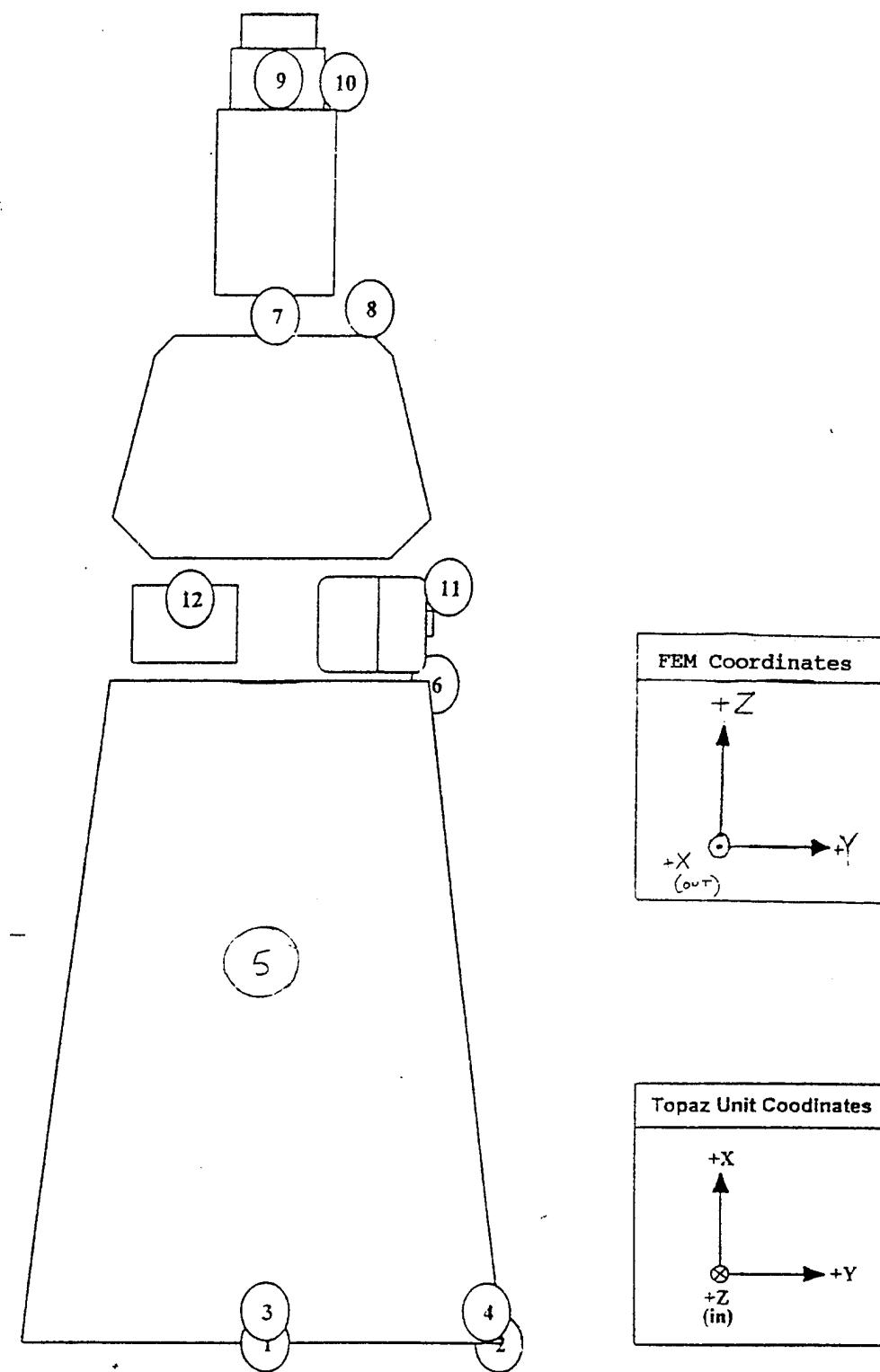
Figure 4. Location of Accelerometers, +XY Topaz Plane [Ref. 7].
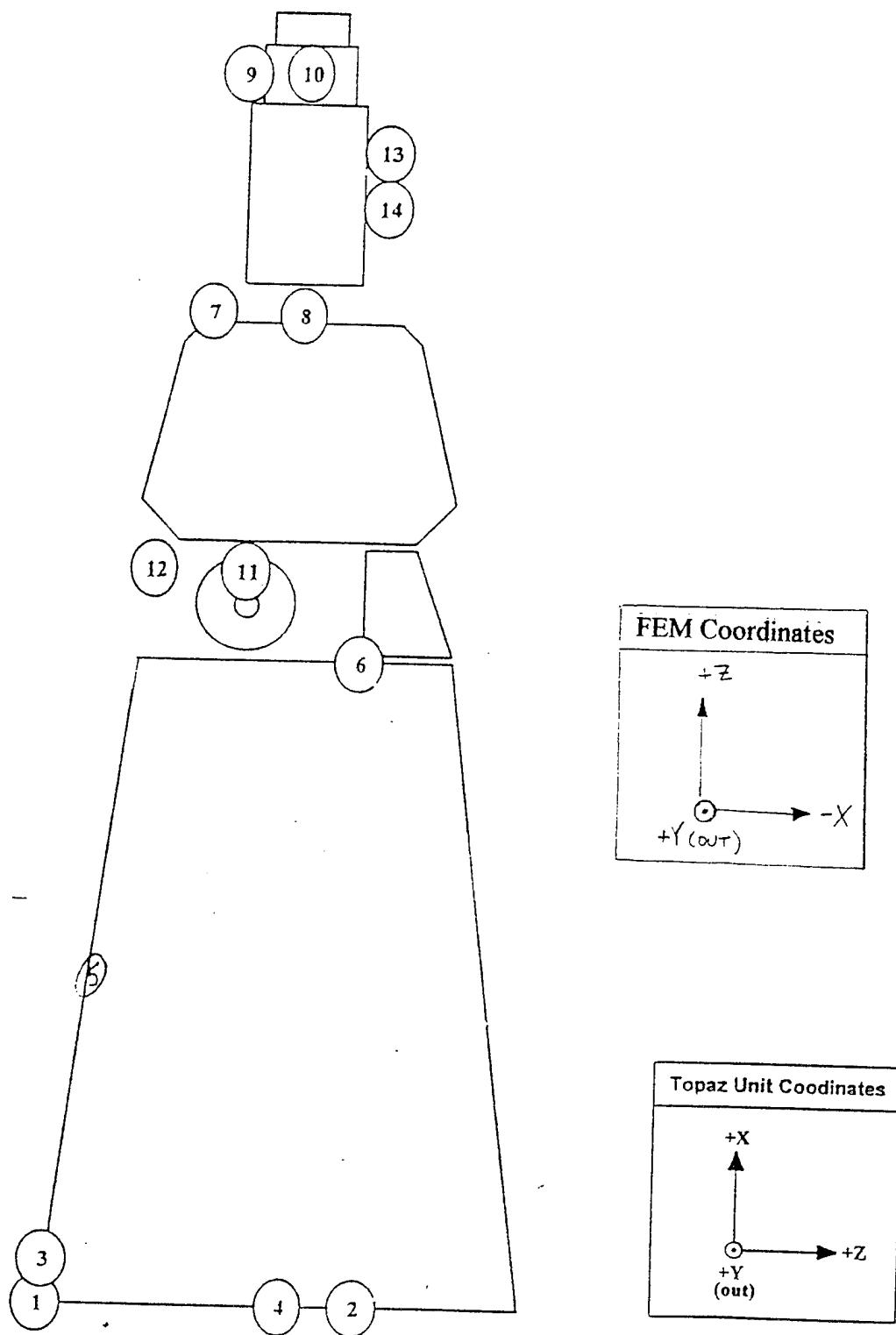
**Figure 5. Location of Accelerometers, +XZ Topaz Plane [Ref. 7].**
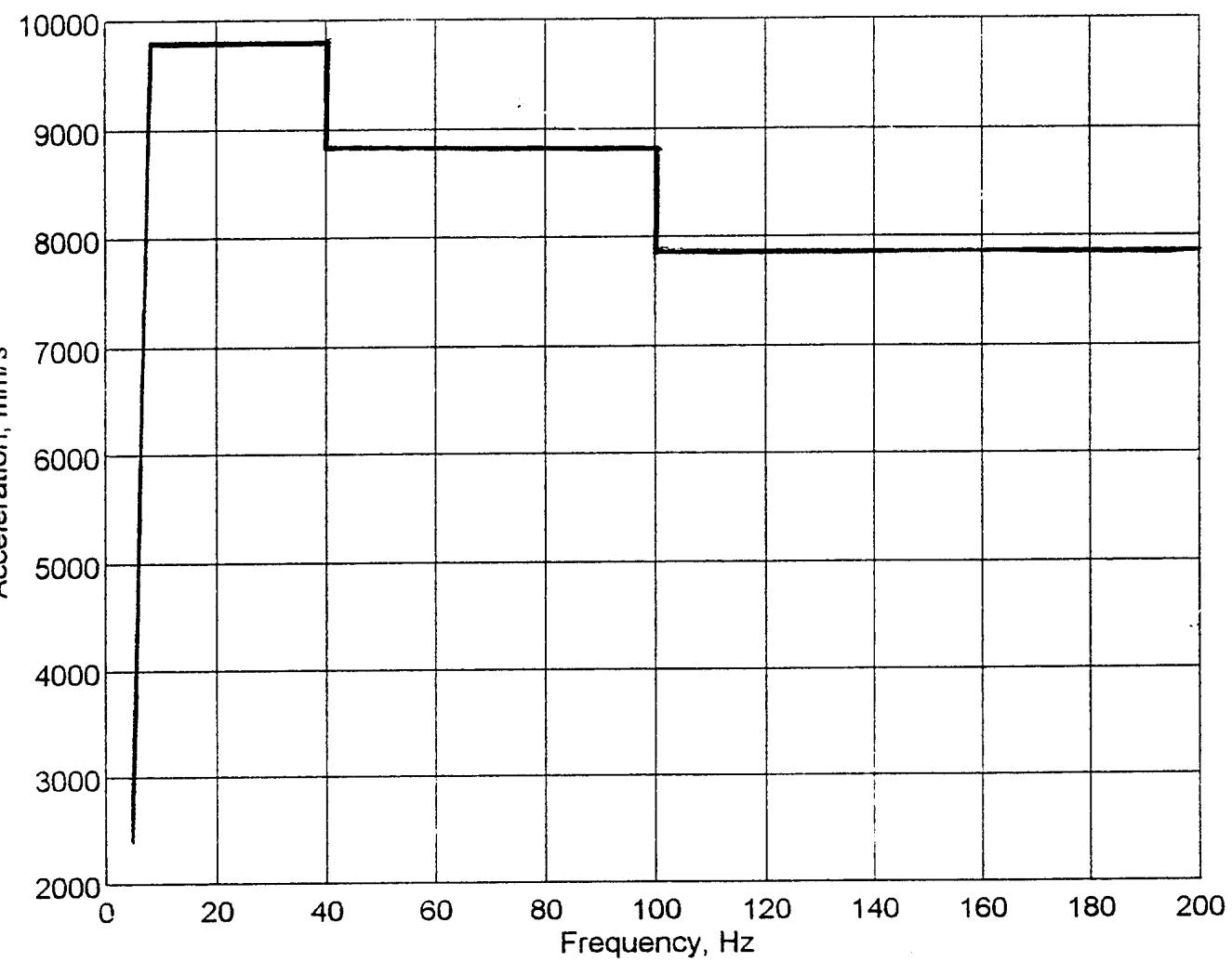
Figure 6. Sine-Vibration Input.

B. DATA MANAGEMENT

The data received from these tests were converted over to DOS readable ASCII format. Results were then manipulated by a simple MATLAB program and plotted as acceleration versus frequency. One such plot was obtained for each accelerometer axis from which data were taken, for both the lateral and longitudinal sine tests. These graphs are contained in Appendix D.

Each of these graphs has been analyzed to determine at which frequencies peaks occurred. These peaks represent natural frequencies of the TOPAZ system which were excited by the vibration input. Below 100 Hz, most peaks are easily distinguishable. Above 100 Hz, there are many smaller peaks appearing in the data. This was due to a combination of noise in the equipment and interference from excitation of lower system modes. Only prominent peaks are tabulated.

One example of these graphs is given in Figure 7. Peaks are indicated by 'x' marks. The corresponding data are given in Table 5. The values were obtained by first analyzing the plot and then going into the converted data files to locate the actual frequency and amplitude values. One such plot and table were made for each accelerometer axis from which data was taken, for each test. The remaining graphs and tables may be found in Appendices D and E, respectively.

The system was tested up to 200 Hz. Frequencies above this value are insignificant during a launch scenario and are typically determined during acoustic testing. They are also more difficult to accurately distinguish.
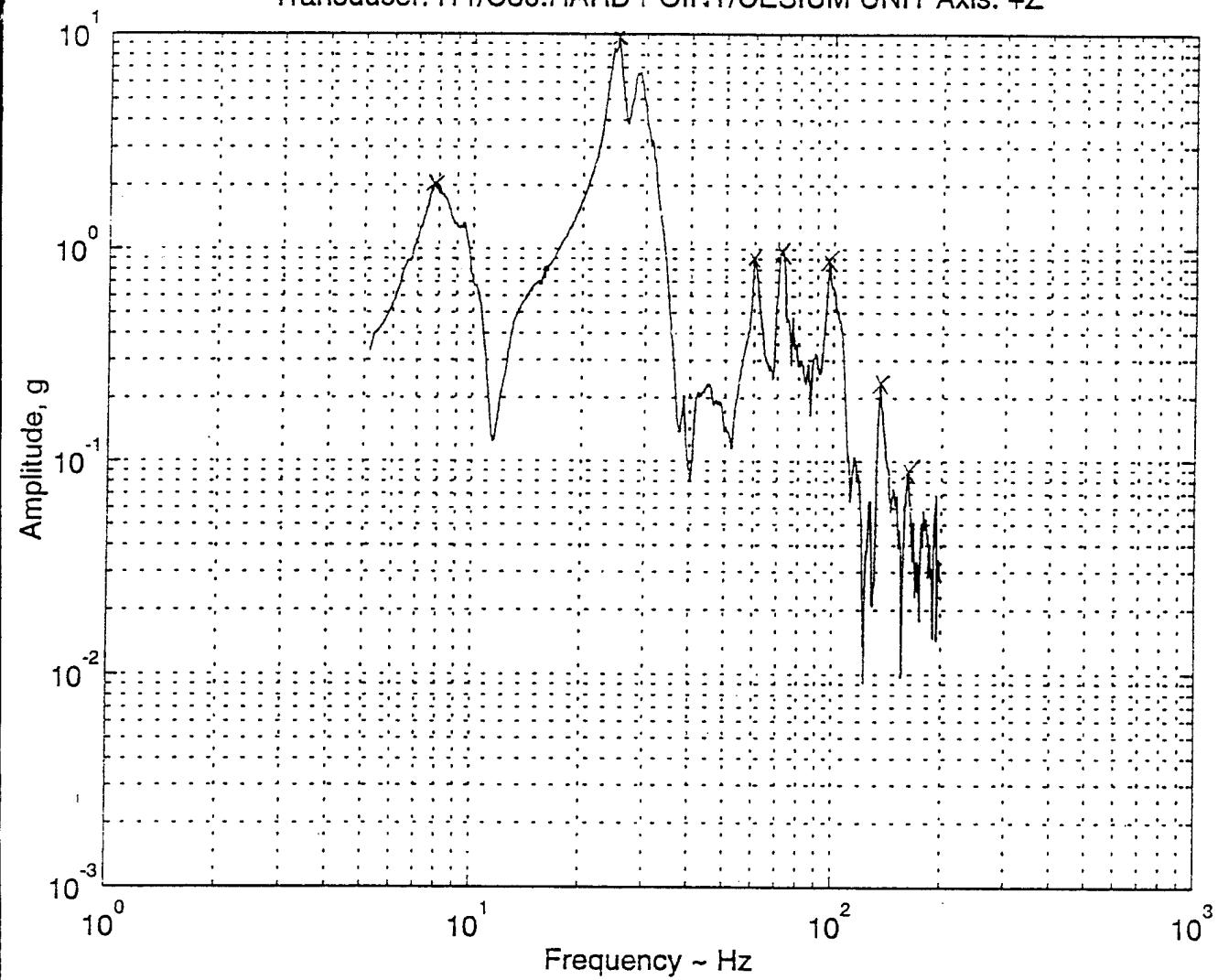
Figure 7. Example Experimental Data Plot.

TRANSDUCER:	I11/C30:HARD POINT/CESIUM UNIT Axis: +Z	
PEAK	FREQUENCY (Hz)	AMPLITUDE (g)
1	7.81651	2.05755
2	.24.9373	9.57841
3	60.0392	0.904517
4	71.8386	0.974768
5	97.2413	0.865449
6	135.027	0.232790
7	161.199	8.948593E-02

Table 5. Data Derived From Figure 7.

IV. DESIGN TOOLS

A. I-DEAS SOFTWARE

I-DEAS [Ref. 4] is a product of the Structural Dynamics Research Corporation (SDRC). I-DEAS is an integrated package of mechanical engineering software tools. Among the applications available with the software are solid modeling design, drafting, finite element simulation, dynamics, post-processing and testing.

In the vibrational analysis of the TOPAZ II power system, the finite element model solution, post-processing, and dynamics applications are the most useful. The model solution application has the capability of creating a "solution set" which describes the type of solution (statics, dynamics, etc), the type of output to store, and other options. Using this application, the TOPAZ II finite element model was analyzed under both linear statics and dynamics. The restraints used were a clamp located on each of the three feet, restraining the model against all six possible rigid body motions. The model was solved in order to obtain the natural frequencies of the structure. This solution also gave the displacements and stresses for each mode. These results were listed, and displayed two-dimensionally and color-coded, using the post-processing application. The modes were animated to determine each mode shape. Figure 8 is a snapshot of mode one.

After the model was solved, the dynamics application was used to apply the vibration sine values of acceleration vs. frequency to the model. These loads were applied through the clamped feet. A viscous damping ratio of 0.02, determined from the previous modal test, was applied and the model response obtained and graphed. From these graphs the theoretical natural frequencies were obtained. [Ref. 4]

VALUE OPTION: ACTUAL

1. 00E+03

9. 01E+02

8. 01E+02

7. 01E+02

6. 01E+02

5. 01E+02

4. 00E+02

3. 00E+02

2. 00E+02

1. 00E+02

0. 00E+00
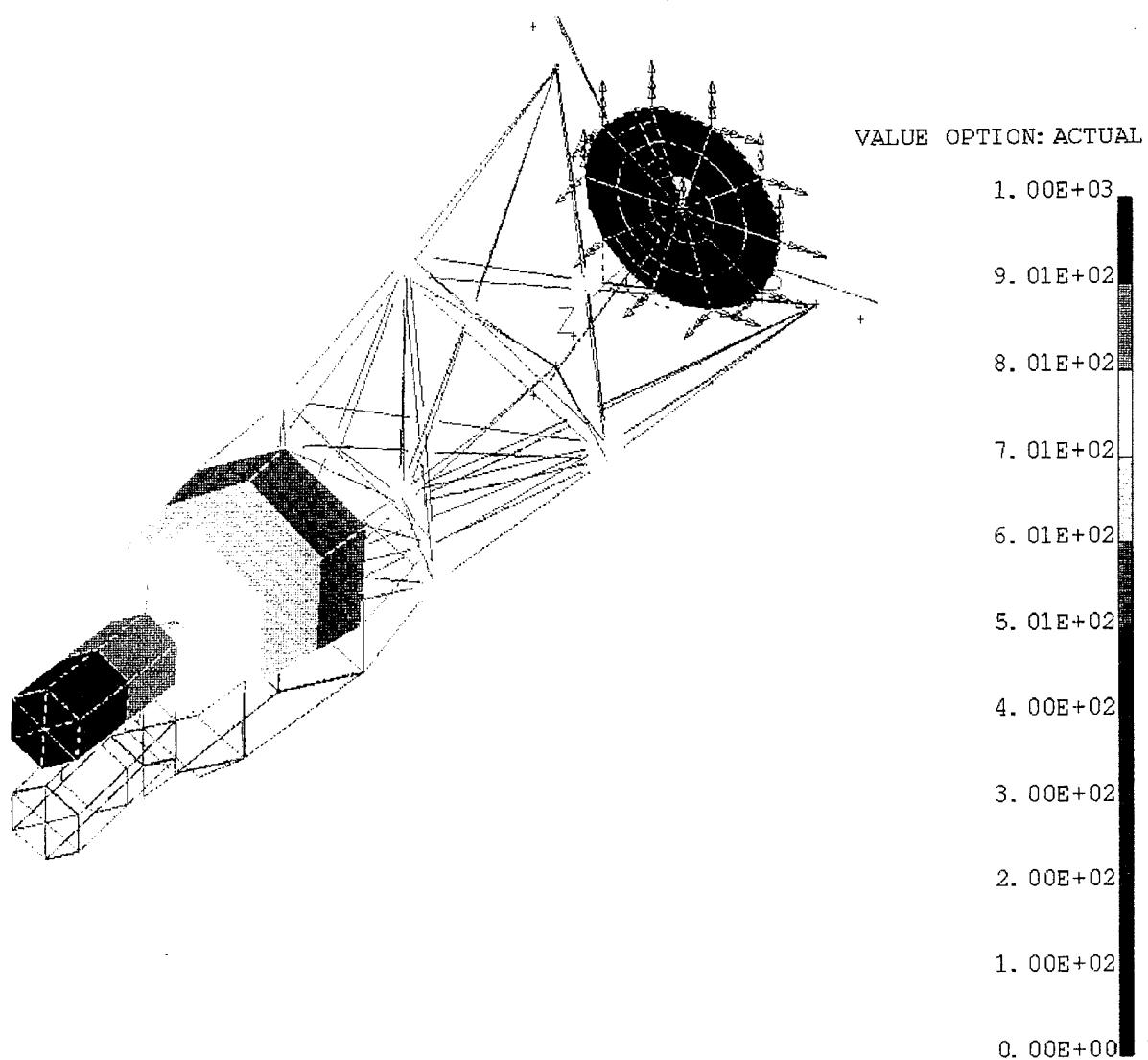
Figure 8. Mode 1, Displacement

V. FINITE ELEMENT MODELING AND ANALYSIS

A. FINITE ELEMENT ANALYSIS - THEORY

The finite element method provides a formulation which can use digital computer automation for the analysis of irregular systems. To accomplish this, the method sees a complex structure as an assembly of finite elements, where each element is part of a continuous structural member. By requiring that the displacements be computed and the internal forces in balance at points shared by several elements, called nodes, the entire structure reacts as a single entity. The finite element method expresses the displacement at any point of the continuous element in terms of a finite number of displacements at the nodal points multiplied by given interpolation functions. [Ref. 5]

The advantage of the finite element method over other methods is that the equations of motion for the system can be derived by first deriving the equations of motion for a typical finite element and then assembling the individual elements' equations of motion. The motion at any point inside the element is obtained by means of interpolation, where the interpolation functions are the same for every element. Complicated structures can be modeled by simpler one or two dimensional elements, resulting in less computation time. [Ref. 6]

The I-DEAS software utilizes the displacement based finite element method to solve finite element models. To derive the equilibrium equations, the principal of virtual work is used. The principle of virtual work is basically a statement of the static equilibrium of a mechanical system and is defined as follows: *the work performed by the applied forces through infinitesimal virtual displacements compatible with the system constraints is zero.* [Ref. 5]

27

The principle can be used to calculate the portion of static equilibrium of a system. For a conservative system, the equation is

$$\overline{\delta W} = \sum_{i=1}^{N} \vec{F}_i \cdot \delta \vec{r}_i = -\sum_{i=1}^{N} \left(\frac{\partial V}{\partial x_i} \delta x_i + \frac{\partial V}{\partial y_i} \delta y_i + \frac{\partial V}{\partial z_i} \delta z_i \right) = 0 \qquad (1)$$

where

$$\overline{\delta W} = \text{virtual work}$$

$$F_i = \text{the applied force}$$

$$\delta r_i = \text{virtual displacement vector of the}$$

$$\delta V = \text{virtual potential}$$

$$\delta x_i = \text{virtual displacement in the X direction}$$

$$\delta y_i = \text{virtual displacement in the Y direction}$$

$$\delta zi = \text{virtual; displacement in the Z direction}$$

As utilized by I-DEAS, the equation is as follows

$$\int_V (\hat{\epsilon})^T (\sigma) \, dV = (\hat{U}_i)^T (F_i) + \int_s (\hat{U})^T (f_s) \, dS + \int_V (\hat{U})^T (f_B) \, dV \qquad (2)$$

where

$$(\hat{U}) = \text{virtual displacement}$$

$$(\sigma) = \text{strain due to the virtual displacement}$$

28

$(\hat{\varepsilon})$ = actual stress at current time t due to applied loads

(F_i) = nodal forces

(f_s) = surface forces

(f_B) = body forces

This equation states that the work done by point loads, surface loads, and body forces are equal to the internal strain energy due to the virtual displacement when integrated over the volume. Given a set of nodal values, the forces and displacements can be evaluated anywhere on the body. This is accomplished through the introduction of (N), continuous element interpolation functions, and (B), the derivatives of (N). Cancelling the virtual displacement vector from above, leaves

$$\sum_{elem\ V_e} \int [B]^T(\sigma) dV_e = (F_i) + \sum_{elem\ S_e} \int [N]^T(f_s) dS_e + \sum_{elem\ V_e} \int [N]^T(f_B) dV_e \qquad (3)$$

A global set of equations are formed from the integrations over each element. When considering the linear case, this equation is reduced to

$$[K](u) = (F_i) + (F_s) + (F_b) \qquad (4)$$

where

(u) = displacement

$[K]$ = linear stiffness matrix

The linear stiffness matrix is equal to

$$[K] = \sum_{elem \ V_e} [B]^T[D][B]dV_e \qquad (5)$$

where

$$[D] = \text{matrix of elastic constants}$$

To determine strain and stress, the following equations are used

$$(\epsilon) = [B](u) \qquad (6)$$

$$(\sigma) = [D](\epsilon) \qquad (7)$$

A finite element model can be made of more than one type of element. The idea is to model the deflection of the structure, not its appearance. The FEM is the idealization of the entire structural problem. This includes the elements node locations, both the physical and material properties, boundary conditions and loads. [Ref. 4]

1. Modal Analysis

The FEM was tested using I-DEAS software. The restraints used were clamps on each of the three feet. The model was solved, using the parameters from Appendix A, to determine its natural frequencies. Because the model used ideal clamps, these natural frequencies were expected to be higher than those found experimentally. No losses were modeled, also contributing to higher theoretical natural frequencies. These frequencies are listed in Table 6.

When the FEM was solved, post processing revealed the results shown in Table 6. Using I-DEAS, modes up through 200 Hz were animated to determine each mode shape present. The upper bound of 200 Hz was chosen because that was as far as the experimental testing went. The mode shapes demonstrate how the structure moves when a particular natural frequency is excited. Figures 8 - 12 are snapshots of five of these mode shapes. Each snapshot gives the mode number, corresponding frequency, and color-coded scale relating to either stress or displacement. Displacement values are displayed in Figures 8, 9, 10, and 11, and stress values in Figure 12. Either parameter may be selected.

The numerical stress and displacement values on these pictures are significant as relative quantities only. Using Figure 9 as an example, it is known that any "red" section will deflect ten times as far as any "royal blue" section of TOPAZ. If the figure were displaying relative stress, the same would hold true for values of stress.

When solving for natural frequencies, the I-DEAS software is solving an eigenvalue problem. The shapes of the functions are known as the eigenfunctions. Because the equations being solved are homogeneous, the shape of the function can be determined uniquely but the amplitude of the functions are arbitrary. Each natural frequency has a corresponding

31

THEORETICAL DATA				
MODE	FREQ (Hz)	DISPLACED AMPLITUDE	RELATIVE AMPLITUDE	ANIMATED MODE SHAPE
1	9.2949	1.00E+03	35-36-37	beam, structure, +/- Y
2	9.4301	1.00E+03	35-36-37	beam, structure, +/- X
3	27.6152	3.37E+02	11	torsion, about Z
4	40.5769	8.58E+02	3	mode 2 beam, +/- Y
5	40.9074	8.46E+02	4	mode 2 beam, +/- X
6	56.7768	1.00E+03	35-36-37	axial +/- Z
7	59.0425	5.33E+02	6	bottom +/- Y, top +/- Y
8	59.05082	5.36E+02	5	bottom +/- X
9	63.30842	4.69E+02	7	bottom only, radial +/- Z
10	81.85867	4.29E+02	9	structure mode 3, XZ plane
11	81.94865	4.3E+02	8	YZ deflection of reactor support
12	99.2141	3.55E+02	10	torsion, frame
13	115.4492	2.04E+02	16	XY plane, deflection 2 lower bays, opposite
14	115.6353	1.71E+02	21	mode 3, ZX plane
15	120.2439	2.03E+02	17	torsion in lower 2 bays
16	125.5667	2.99E+02	13	axial, structure
17	126.487	2.44E+02	15	mode 3 beam, XY plane
18	127.1178	2.69E+02	14	mode 3 XZ
19	129.8433	2.02E+02	18	torsion about Z, top opposite bottom half
20	130.4791	1.47E+02	25	mode 3 ZY
21	130.483	1.57E+02	22-23	mode 3 ZX
22	150.6242	2.00E+02	19	mode 3 ZY
23	150.7446	1.90E+02	20	mode 3 ZX
24	170.473	3.30E+02	12	mode 3 ZX

THEORETICAL DATA, CONT.				
MODE	FREQ (Hz)	DISPLACED AMPLITUDE	RELATIVE AMPLITUDE	ANIMATED MODE SHAPE
25	174.9176	1.32E+02	26	torsion of bottom bay
26	177.8734	1.28E+02	27	mode 3 ZY
27	178.1774	1.48E+02	24	mode 4 ZX
28	181.3174	1.24E+02	29	mode 4 ZY
29	182.0637	1.15E+02	31-32	torsion, structure
30	183.776	1.57E+02	22-23	mode 3 ZX
31	185.9247	8.96E+01	1	torsion, lower 2 bays
32	189.7822	1.01E+02	34	torsion, structure
33	190.003	8.80E+01	2	torsion, structure
34	193.3796	1.15E+02	31-32	axial, torsion, structure
35	193.6082	1.26E+02	28	mode 3 ZY, torsion lower half
36	199.7701	1.18E+02	30	axial, torsion
37	212.4125	1.10E+02	33	---

Table 6. Theoretical Results.

VALUE OPTION: ACTUAL

3.38E+02

3.04E+02

2.70E+02

2.36E+02

2.03E+02

1.69E+02

1.35E+02

1.01E+02

6.75E+01

3.38E+01

0.00E+00
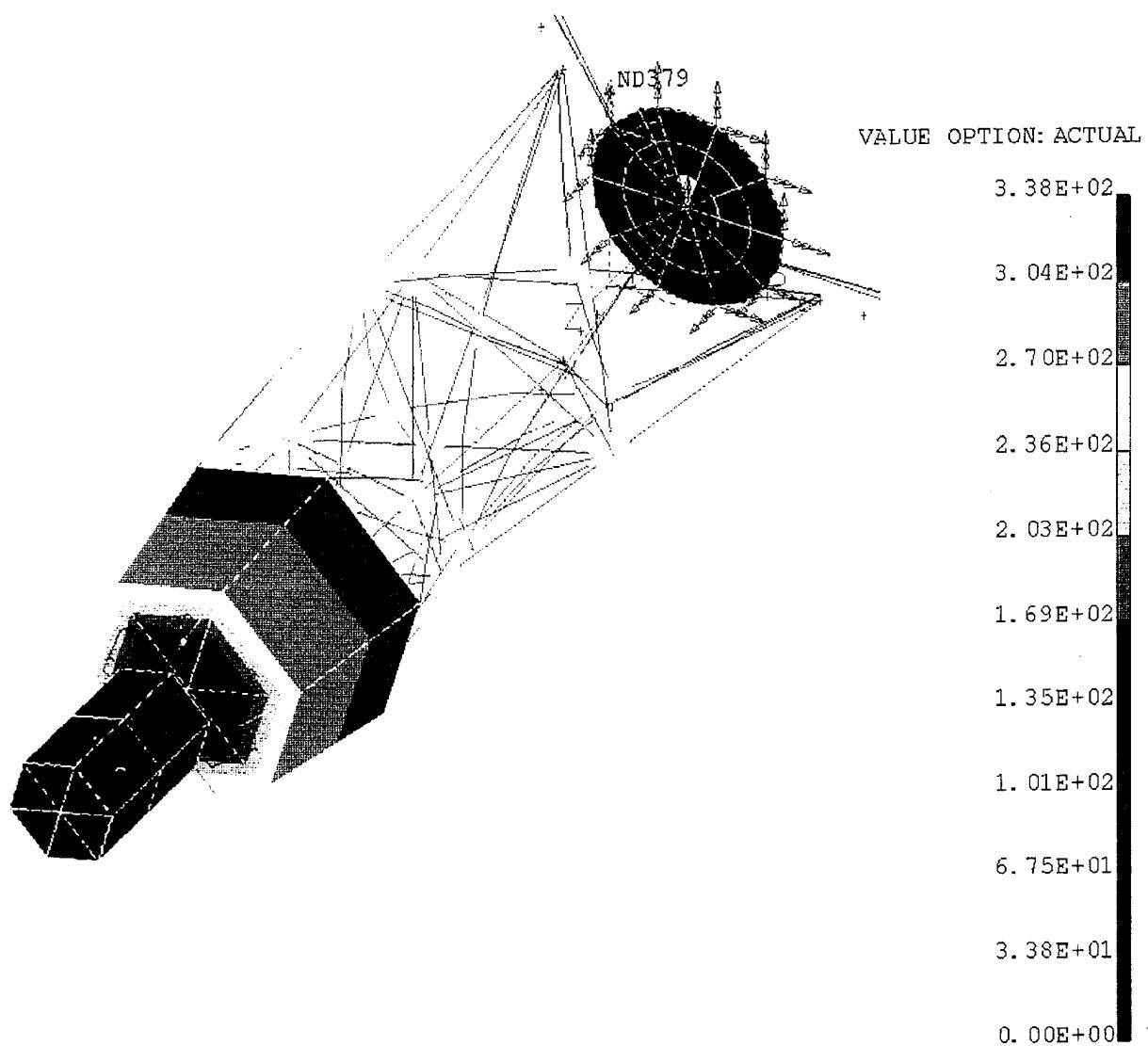
Figure 9. Mode 3, Displacement

34

VALUE OPTION: ACTUAL

1.00E+03

9.00E+02

8.00E+02

7.00E+02

6.00E+02

5.00E+02

4.00E+02

3.00E+02

2.00E+02

1.00E+02

0.00E+00
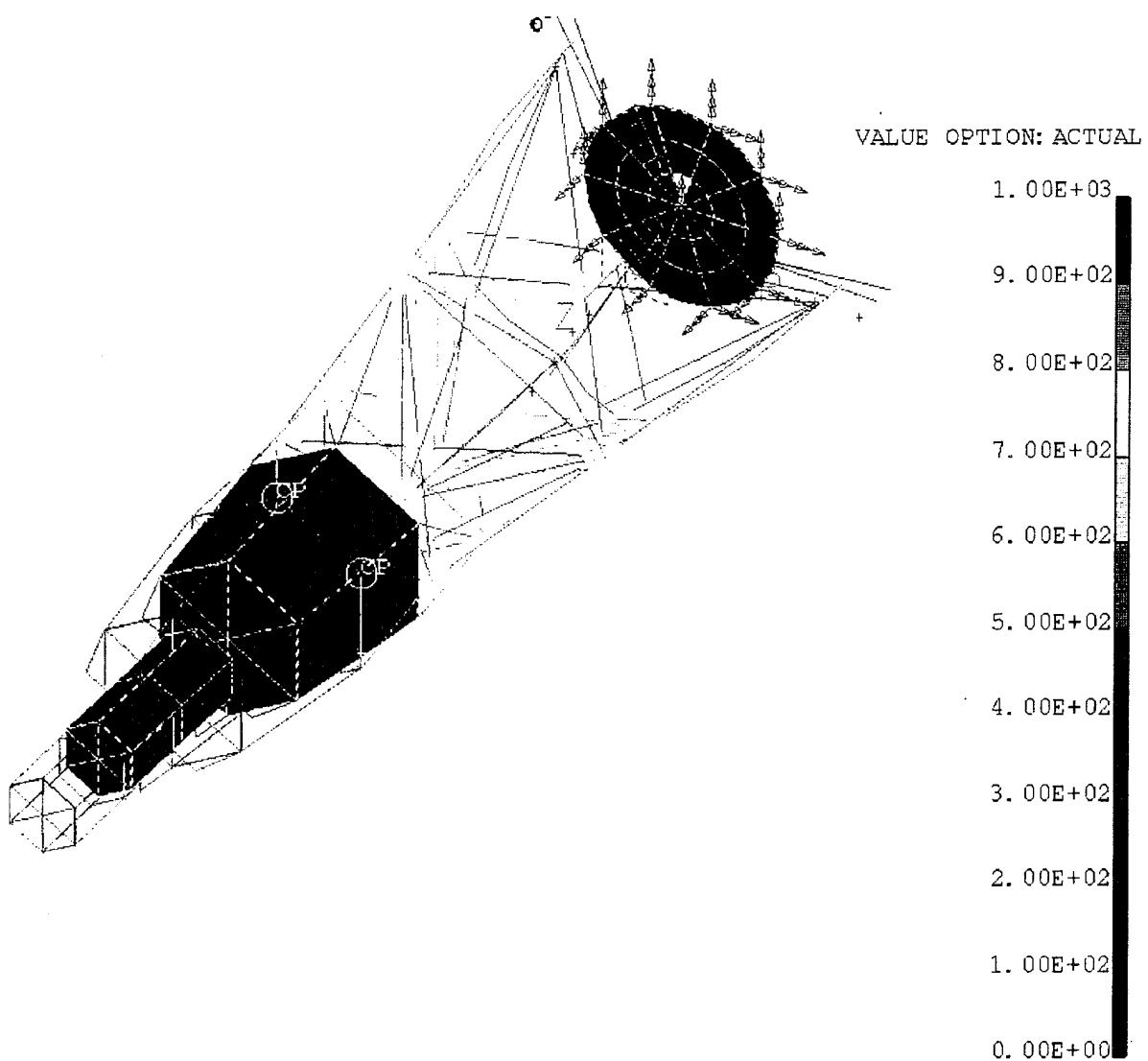
Figure 10. Mode 6, Displacement

VALUE OPTION: ACTUAL

1. 03E+02

9. 29E+01

8. 26E+01

7. 22E+01

6. 19E+01

5. 16E+01

4. 13E+01

3. 10E+01

2. 06E+01

1. 03E+01

0. 00E+00
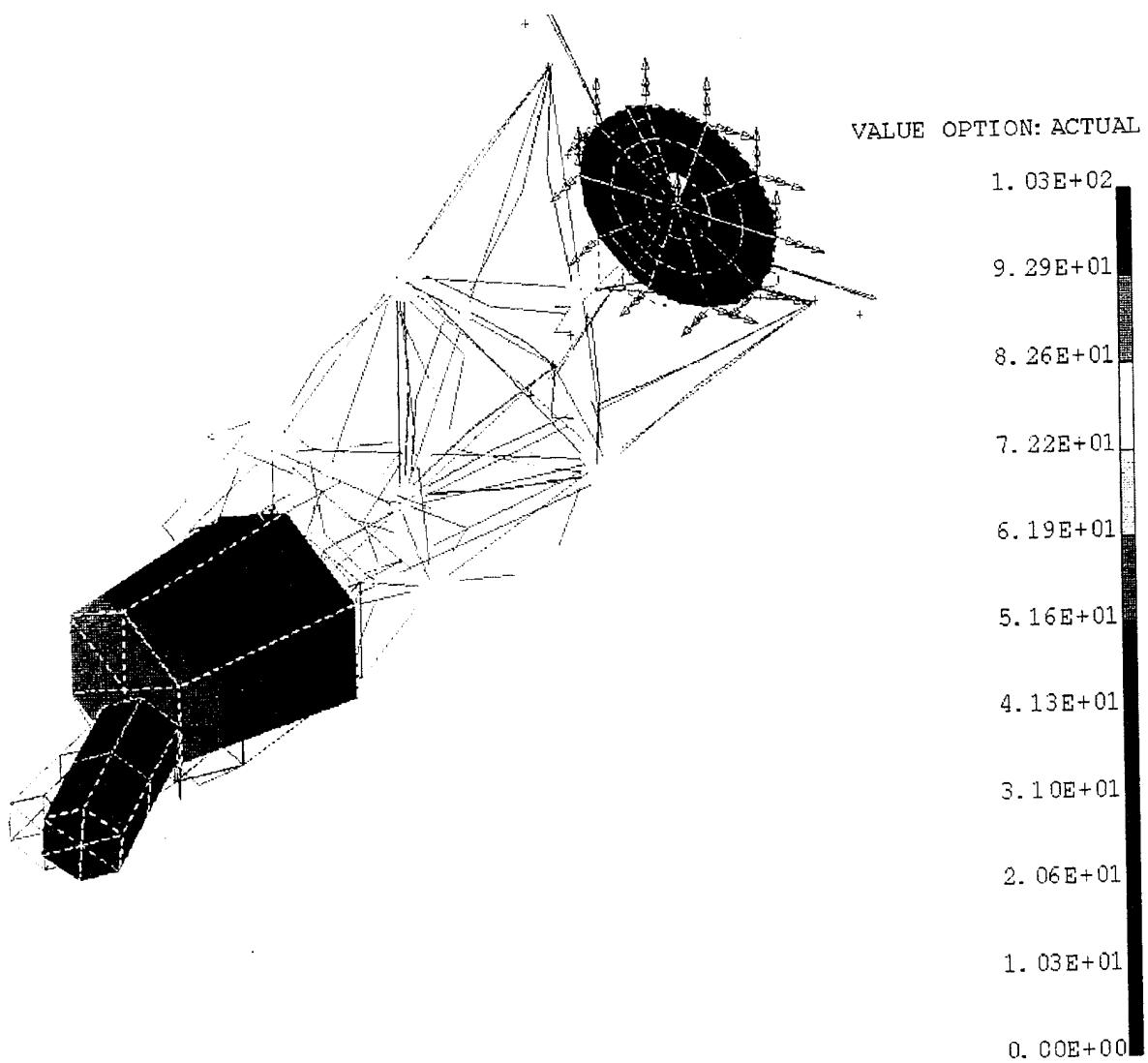
Figure 11. Mode 38, Displacement

VALUE OPTION: ACTUAL
SHELL SURFACE: TOP

2.48E+06

2.23E+06

1.98E+06

1.73E+06

1.49E+06

1.24E+06

9.91E+05

7.44E+05

4.96E+05

2.49E+05

1.41E+03
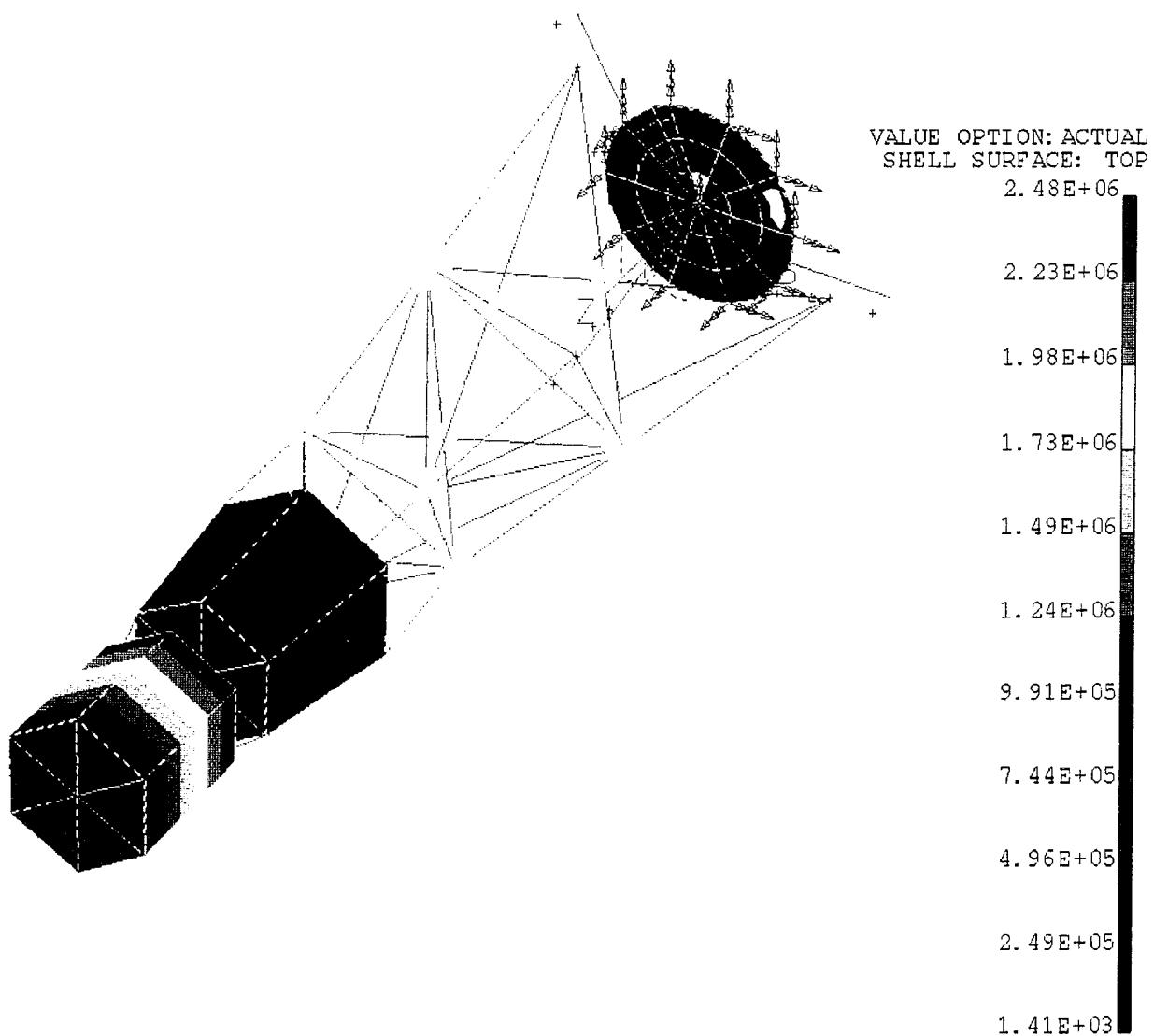
Figure 12. Mode 39, Stress

eigenfunction, or natural mode. Because the problem is homogeneous, any constant multiplier of a natural mode represents the same natural mode. Therefore, amplitudes are relative values only. [Ref. 6]

Table 6 also lists the relative amplitudes of the displaced mode shapes. This is important to determine, when excited, which mode shapes will deflect the structure the greatest amount. This information also gives a feeling of where the maximum areas of stress will occur. A description of the animated mode shapes are listed in the last column of the Table. All axis references in this table are to the FEM coordinate system. Again, these may be used to predict the structural deflection when the corresponding frequencies are excited.

2. Forced Response

In order to determine the accuracy of the FEM, it had to be tested in the same manner as was the actual structure. Table 7 gives the sine-vibration input that was applied to the actual TOPAZ unit. This same input was applied to the FEM. The sine vibration is shown graphically in Figure 6. This function was applied to the FEM through each of the clamped feet. A damping ratio of 0.02 was applied to all elements of the FEM, corresponding to the damping ratio of the actual structure.

SINE VIBRATION	
Frequency (Hz)	Acceleration (mm/s^2)
5	2452.5
5 - 8	linear increase
8 - 40	9810
40 - 100	8829
100 - 200	7848

Table 7. Applied Sine Vibration [Ref. 6].

The sine-vibration test was applied twice, once in the lateral direction and once in longitudinally, as was done in the experimental testing. The same lateral direction (Z of the actual unit) was used for testing of the FEM.

When post processing the theoretical results, data was taken from locations on the FEM

which corresponded to accelerometer locations on the actual structure. As with the experimental data, the theoretical results were graphed. Each of these graphs were then compared to each of the experimental graphs obtained from the same location on TOPAZ. An example of one of the theoretical graphs may be seen in Figure 13. This graph came from node 92 of the FEM, which corresponds to accelerometer number 10 of the actual TOPAZ structure. This accelerometer was mounted on the reactor top plenum. (See Table 3) As explained in Chapter II, this comparison is necessary to determine the accuracy of the FEM. The results of this analysis are explained in Chapter V.

In Figure 13, under the graph, the ID number of 3021 represents this particular function in I-DEAS. Each function was assigned a different number automatically. The functions were then plotted. The data from this figure were obtained from the X direction of the FEM. The Y axis labeled 'modulus' represents a non-dimensional number. The theoretical amplitude values were not necessary in determining which natural frequencies were excited. As with the experimental data, prominent peaks were tabulated from the graphs (See Figure 13 and the corresponding data listed in Table 8). The phase plots, such as the one in Figure 13, were useful in identifying which peaks were significant. When the phase changes 180 degrees, a natural frequency of the system has been crossed. As the frequency values increase, the phase plot becomes less angular and phase changes less distinct. This is because lower natural frequencies are also contributing to phase changes. 'X' marks are indicated on Figure 13 to show which peaks were tabulated.

The remainder of the theoretical graphs and tabulated data may be found in Appendices B and C, respectively.
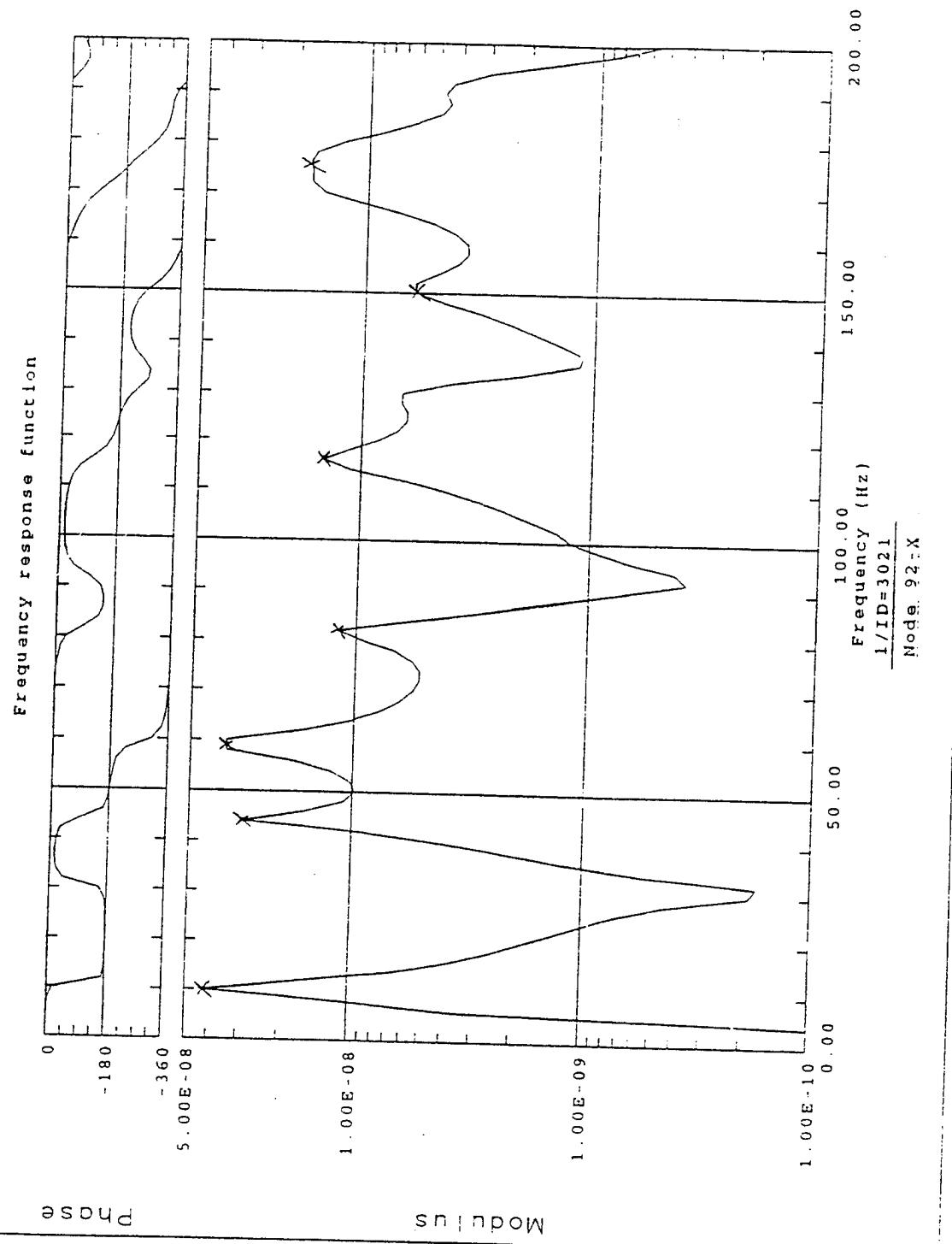
Figure 13. Sample Theoretical Plot.

41

NODE 92 - X	
PEAK	FREQUENCY (Hz)
1	10.0
2	44.0
3	58.0
4	82.0
5	116.0
6	150.0
7	176.0

Table 8. Data Derived From Figure 13.

VI. ANALYSIS AND CONCLUSIONS

A. ANALYSIS OF EXPERIMENTAL AND THEORETICAL RESULTS

The theoretical and experimental graphs of Appendices B and D, respectively, were analyzed the same way. Prominent peaks, indicating natural frequencies of the system, were marked on the graphs. The raw data were then examined so that the frequencies at which these peaks occurred could be exactly identified. This procedure was followed for both the lateral and longitudinal tests of both the theoretical and experimental data. The lateral and longitudinal test results were analyzed separately. This was done because different natural frequencies would be excited during the two tests.

At this point, there were four sets of tabulated results. These were the lateral and longitudinal results from the theoretical and experimental tests. Each of these sets were individually studied to determine which frequencies had peaks commonly occurring. The experimental lateral and longitudinal frequencies are listed in Table 9. The theoretical lateral and longitudinal results were combined and listed as the theoretically predicted natural frequencies of the system. (See Table 9)

As expected, the experimentally determined natural frequencies were lower than those theoretically predicted. As mentioned earlier, this is in part due to the ideal restraints used by the computer model. Also, no losses were simulated on the FEM, but losses would occur in an actual system. Some of the theoretically predicted frequencies were not found in the experimental data. This was due, in part, to the accelerometer placements on TOPAZ. They may not have been located properly to register each natural frequency. Some frequencies may have been damped out by losses in the system. This accounts for the "missing" experimental frequencies in Table 9.

43

THEORETICAL DATA				
MODE	THEORETICAL NATURAL FREQ (Hz)	SINE-X ACTUAL (Hz)	SINE-Z ACTUAL (Hz)	ANIMATED MODE SHAPE
1	9.2949	7.26	7.6	beam, structure, +/- Y
2	9.4301		8.8	beam, structure, +/- X
3	27.6152	28	28	torsion, about Z
4	40.57694	40	44	mode 2 beam, +/- Y
5	44.111	44	46	mode 2 beam, +/- X
6	56.7768	53	55	axial +/- Z
7	59.0425	58	56	bottom +/- Y, top +/- Y
8	59.05082		59	bottom +/- X
9	63.30842	64	60	bottom only, radial +/- Z
10	81.85867	75	81	structure mode 3, XZ plane
11	81.94865	83	81	YZ deflection of reactor support
12	99.2141	101	97	torsion, frame
13	115.4492	112		XY plane, deflection 2 lower bays, opposite
14	115.6353	113	111	mode 3, ZX plane
15	120.2439	119	119	torsion in lower 2 bays
16	125.5667		121	axial, structure
17	126.487	124		mode 3 beam, XY plane
18	127.1178			mode 3 XZ
19	129.8433			torsion about Z, top opposite bottom half
20	130.4791		131	mode 3 ZY
21	130.483		133	mode 3 ZX
22	150.6242	148	144	mode 3 ZY
23	150.7446	150	154	mode 3 ZX
24	170.473	169	170	mode 3 ZX

	THEORETICAL DATA, CONT.			
MODE	THEORETICAL NATURAL FREQ (Hz)	SINE-X ACTUAL (Hz)	SINE-Z ACTUAL (Hz)	ANIMATED MODE SHAPES
25	174.9176	172	171	torsion of bottom bay
26	177.8734		175	mode 3 ZY
27	178.1774		177	mode 4 ZX
28	181.3174	181		mode 4 ZY
29	182.0637			torsion, structure
30	183.776			mode 3 ZX
31	185.9247			torsion, lower 2 bays
32	189.7822			torsion, structure
33	190.003		190	torsion, structure
34	193.3796		191	axial, torsion, structure
35	193.6082		193	mode 3 ZY, torsion lower half
36	199.7701			axial, torsion
37	212.4125			---

Table 9. Theoretical and Experimental Result Tabulation .
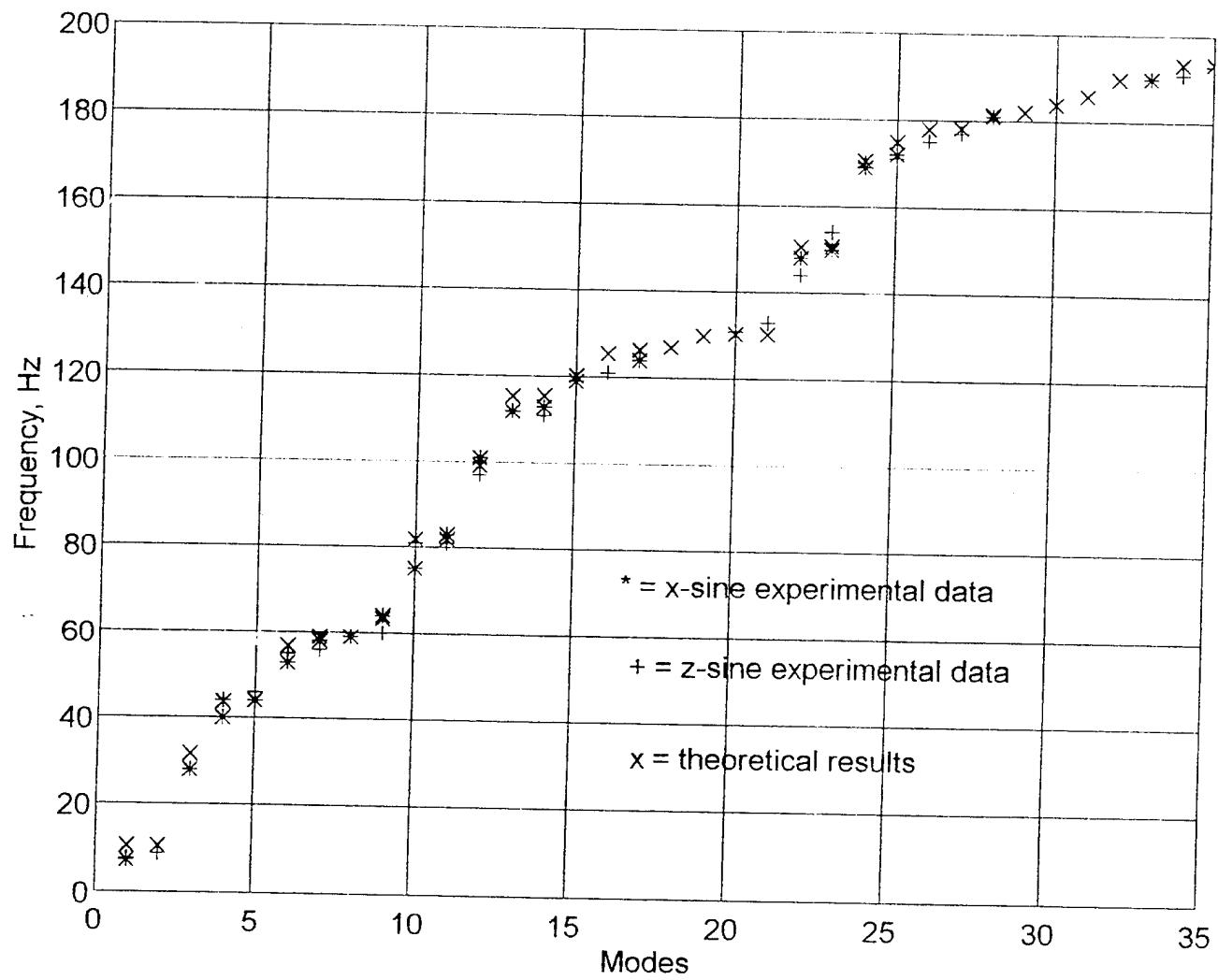
Figure 14. Theoretical and Experimental Result Comparison.

46

The theoretically predicted natural frequencies were then plotted against the experimentally found frequencies. This graph is shown in Figure 14. For 70% of the predicted modes, there exists a corresponding experimentally determined natural frequency. Modes where experimental frequencies were not found were most likely a result of inadequate accelerometer placement. In a one to one comparison, theoretically predicted and experimentally found natural frequencies were within 4.6 Hz of each other, with an average difference of 1.8 Hz.

B. CONCLUSIONS

The finite element method is a very useful tool for structural analysis. Complex structures can be modeled, have forces applied, and be tested for failure in a number of ways, using only computer software. This provides a substantial cost savings when used to complement prototype or actual unit testing. The I-DEAS software proved invaluable for the analysis work presented in this thesis.

In order to obtain reliable useful data from finite element modeling, the model must accurately represent how the actual structure will deflect under loading. One method of checking the accuracy of the model is to solve it for its natural frequencies. If the system modes predicted by the model resemble the actual system modes, the model is considered reliable. Through the testing completed for this thesis, the results show the two sets of natural frequencies, theoretical and experimental, to be very close, and therefore the model is an accurate representation of the TOPAZ structure.

C. RECOMMENDATIONS FOR FUTURE STUDY

Further study of the finite element model test data should be done to locate the highest amplitude response, thereby identifying the frequencies which correspond to the worst case loading. As mentioned previously, individual components such as the cesium block or starter unit should be analyzed to see if they exceeded the limits of the test. If the power system must be launched in an upright position to conform to the shape of U.S. launch vehicles, structural analysis of the frame must be done to see if it will withstand launch loads. From previous testing in Russia, the interface between the shield and reactor can be a problem source. Further research needs to be completed in this area.

When data were analyzed in this thesis, only relative values of stress and displacement were obtained. Further analysis needs to be done to predict the actual stress and displacement that will occur during a typical launch sequence.

LIST OF REFERENCES

1. U. S. Topaz II Flight Safety Team, *NEP Space Test Program Preliminary Nuclear Safety Assessment*, November 1992.

2. Benke, S.M. and Venable, J.R., "Operational Testing and Thermal Modelling of a TOPAZ-II Single-Cell Thermionic Fuel Element Stand", AIP Conference Proceedings 324, XIIth Symposium on Space Nuclear Power and Propulsion, Albuquerque, NM, (8-12 January, 1995).

3. Lacy, J.M., *TOPAZ II Structural Analysis FY 1993 Activity Report*, Idaho National Laboratories, September 30, 1993.

4. I-DEAS Software On-Line Help Database, *Understanding the Linear Statics Formulation*, Structural Dynamics Research Corporation, 1993.

5. Donaldson, B.K., *Analysis of Aircraft Structures*, McGraw-Hill Inc., New York, NY, 1993.

6. Meirovitch, L., *Elements of Vibration Analysis*, Second Edition, McGraw-Hill Inc., New York, NY, 1986.

7. Wyant, F.J., and Schmidt, G., *Shock and Vibration Testing of Ya-21U, TSET Experiment #93-16*, TOPAZ International Program, August 1994.

8. Schaefer, E.D., *Preliminary Test Report Ya-21U*, Johns Hopkins University / Applied Physics Laboratory, September, 1994.

9. Mayes, R.L., *TOPAZ Ya-21 Modal Test Series Results*, Sandia National Laboratories, Albuquerque, NM, May 1993.

APPENDIX A.

This Appendix contains the parameters used in the I-DEAS [Ref. 4] software to solve the finite element model.

SOLUTION SET

Type of solution: Normal Mode Dynamics

BOUNDARY CONDITION SET

Normal Mode Dynamics - SVI   Selected
Restraint Set (Pinned Feet)   Selected
Constraint Set (Base Constraints)   Selected
Temperature Set   Room Temperature

OUTPUT SELECTION

Mode Shapes   Store/List
Stress   Store/List

OPTIONS

Method   Solution No Restart
Mass Lumping   Selected
Enforced Motion   Selected
Number of Rigid Body Modes   0

SOLUTION CONTROL

Number of Flexible Modes   43
Number of Iteration Vectors   58
Maximum Iterations   10
Frequency Accuracy (digits)   3
Start Vector Creation   Automatic
Frequency Shift Method   Shift and Number of Modes
Frequency Shift in Hertz   0

A minimum of 10 iterations were required to converge on a solution.

APPENDIX B.

This Appendix contains 54 theoretical graphs obtained using the I-DEAS [Ref. 4] software. The FEM was solved after applying a sine vibration input. Results were taken from nodes of interest, corresponding to accelerometer locations on the actual unit. These results were then plotted and the graphs are contained herein.

Pages 54-80 contain graphs from the longitudinal-sine input. Pages 81-107 contain graphs from the lateral-sine input.

Frequency response function

Phase

Modulus

Frequency (Hz)
1/ID=3000
Node 5-X
Force

5.000

1.000

0.1000

0.0500

0.00

50.00

100.00

150.00

200.00

0

-180

-360

Frequency response function

Phase

Modulus

Frequency (Hz)
1/ID=3001
Node 5-y
Force

Frequency response function

Phase

Modulus

0

-180

-360

2.000

1.000

0.1000

0.0100

0.00

50.00

100.00

150.00

200.00

Frequency (Hz)

1/ID=3002

Node 5-Z

Force

0.00

0.1000

1.000

56

Phase

Modulus

0

-180

-360

2.000

1.000

0.2000

0.00

50.00

100.00

150.00

200.00

Frequency (Hz)

1/ID=3003

Node 12-X

Force

Frequency response function

Phase

Modulus

0
-180
-360

1.0E+00

1.0E-01

1.0E-02

2.0E-03
0.00

50.00

100.00
Frequency (Hz)
1/ID=3004
Node 12-Y
Force

150.00

200.00

58

Phase

Modulus

Frequency (Hz)
1/ID=3005
Node 12-Z
Force

0
-180
-360
1.0E+00
1.0E-01
1.0E-02
2.0E-03

0.00
50.00
100.00
150.00
200.00

Frequency response function

Phase

Modulus

0
-180
-360
2.000

1.000

0.2000
0.00

50.00

100.00
Frequency (Hz)
1/ID=3006
Node 24-X
Force

150.00

200.00

Phase

Modulus

Phase

Modulus

0

-180

-360

1.0E+00

1.0E-01

1.0E-02

1.0E-03

0.00

50.00

100.00

150.00

200.00

Frequency (Hz)

1/ID=3007

Node 24-Y

Force

Frequency response function

Phase

Modulus

Frequency (Hz)
1/ID=3008
Node 24-Z,
Force

62

Phase

Modulus

Frequency (Hz)

1/ID=3009

Node 29-X

Displacement

63

Frequency response function

Phase

Modulus

0
-180
-360
5.00E-11

1.00E-11

1.00E-12
5.00E-13

0.00   50.00   100.00   150.00   200.00

Frequency (Hz)
1/ID=3010
Node 29-Y
Displacement

64

Phase

Modulus

Frequency (Hz)
1/ID=3011
Node 29-Z
Displacement

65

Frequency response function

Phase

0
-180
-360

Modulus

5.00E-08
1.00E-08
1.00E-0.9
1.00E-10

0.00
50.00
100.00
150.00
200.00

Frequency (Hz)

1/ID=3012

Node 55-X
Displacement

Phase

Modulus

0
-180
-360

5.00E-08
1.00E-08
1.00E-09
1.00E-10
5.00E-11

0.00   50.00   100.00   150.00   200.00

Frequency (Hz)

1/ID=3013

Node 55-Y

Displacement

Frequency response function

Phase
Modulus

Frequency (Hz)
1/ID=3014
Node 55-Z
Displacement

Node 75-X
Displacement

Frequency (Hz)

1/ID=3015

Frequency response function

Phase

Modulus

Phase

0
-180
-360

5.00E-10

1.00E-10

1.00E-11

5.00E-12

0.00   50.00   100.00   150.00   200.00

Frequency (Hz)

1/ID=3016

Node 75-y

Displacement

70

Phase

Modulus

0
-180
-360

2.00E-10
1.00E-10
1.00E-11
2.00E-12

0.00
50.00
100.00
150.00
200.00

Frequency (Hz)
1/ID=3017
Node 75-z
Displacement

71

Frequency response function

Phase

Modulus

-180   -360
0

5.00E-08   1.00E-08   1.00E-09   1.00E-10   5.00E-11

0.00   50.00   100.00   150.00   200.00

Frequency (Hz)

1/ID=3018

Node 79-X
Displacement

72

Phase

Modulus

Frequency (Hz)
1/ID=3019
Node 79-Y
Displacement

73

Frequency response function

Phase

Modulus

Frequency (Hz)
1/ID=3020
Node 79-Z
Displacement

Frequency (Hz)
1/ID=3021
Node 92-X
Displacement

Phase

Modulus

Frequency response function

Phase

Modulus

Frequency (Hz)
1/ID=3022
Node 92-Y
Displacement

Phase

Modulus

0

-180

-360

1.00E-08

1.00E-09

1.00E-10

1.00E-11

0.00

50.00

100.00

150.00

200.00

Frequency (Hz)

1/ID=3026

Node 97-Z

Displacement

Frequency response function

Phase

Modulus

Frequency (Hz)
1/ID=3023
Node 92-Z
Displacement

Phase

Modulus

0
-180
-360

5.00E-08
1.00E-08
1.00E-09
1.00E-10

0.00
50.00
100.00
150.00
200.00

Frequency (Hz)
1/ID=3024
Node 97-X
Displacement

79

Frequency response function

Phase

Modulus

Frequency (Hz)

1/ID=3025

Node 97-Y

Displacement

Node 5-X
Force

1/ID=2000

Frequency response function

Phase

0
-180
-360

Modulus

1.00E-02

1.00E-03

5.00E-04

0.00   50.00   100.00   150.00   200.00

Frequency (Hz)
1/ID=2001

Node 5-Y
Force

82

Phase

Modulus

Frequency (Hz)

1/ID=2002

Node 5-Z
Force

200.00

150.00

100.00

50.00

0

-180

-360

1.000

0.1000

0.00

Frequency response function

Phase

Modulus

0
-180
-360
5.00E-02
1.00E-02
1.00E-03
1.00E-04

0.00
50.00
100.00
150.00
200.00

Frequency (Hz)
1/ID=2003
Node 12-X
Force

84

Phase

Modulus

Frequency (Hz)

1/ID=2004

Node 12-Y
Force .

85

Frequency response function

Phase

Modulus

0 -180 -360 1.000

Phase

Modulus

0.00   50.00   100.00   150.00   200.00

Frequency (Hz)
1/ID=2005
Node 12-Z
Force

0.1000

86

Phase

Modulus

Frequency (Hz)

1/ID=2006

Node 24-X

Force

200.00   150.00   100.00   50.00   0.00

0   -180   -360

5.00E-02   1.00E-02   1.00E-03   1.00E-04

87

Frequency response function

Phase

Modulus

Phase

0
-180
-360

5.00E-02

1.00E-02

1.00E-03

1.00E-04
5.00E-05

0.00

50.00

100.00
Frequency (Hz)
1/ID=2007
Node 24-Y
Force

150.00

200.00

88

Phase

Modulus

Frequency (Hz)

1/ID=2008

Node 24-Z

Force

0.00   50.00   100.00   150.00   200.00

0   -180   -360   1.000   0.1000

89

Frequency response function

Phase

Modulus

Frequency (Hz)
1/ID=2009
Node 29-X
Displacement

Phase

Modulus

Phase

0
-180
-360
1.00E-10
1.00E-11
1.00E-12

200.00
150.00
100.00
50.00
0.00

Frequency (Hz)
1/ID=2010
Node 29-y
Displacement

Frequency response function

Phase

Modulus

0

-180

-360

5.00E-09

1.00E-09

1.00E-10

1.00E-11

5.00E-12

0.00

50.00

100.00

Frequency (Hz)

1/ID=2011

Node 29-Z,
Displacement

150.00

200.00

Phase

0
−180
−360

Modulus

2.00E-09
1.00E-09
1.00E-10
5.00E-11

0.00   50.00   100.00   150.00   200.00

Frequency (Hz)
1/ID=2012
Node 55-X
Displacement

Frequency response function

Phase

Modulus

0
-180
-360

2.00E-09
1.00E-09

1.00E-10

1.00E-11
5.00E-12

0.00   50.00   100.00   150.00   200.00
Frequency (Hz)
1/ID=2013
Node 55-Y
Displacement

Node 55-Z
Displacement

1/ID=2014

Frequency (Hz)

Phase

Modulus

Frequency response function

Phase

Modulus

Frequency (Hz)

1/ID=2015

Node 75-X
Displacement

96

Frequency (Hz)
1/ID=2016
Node 75-Y
Displacement

Frequency response function

Frequency (Hz)
1/ID=2017
Node 75-Z
Displacement

Phase

Modulus

Frequency (Hz)
1/ID=2018
Node 79-X
Displacement

Frequency response function

Phase

Modulus

Frequency (Hz)
1/ID=2019
Node 79-Y
Displacement

Frequency response function

Phase

Modulus

0

-180

-360 1.00E-09

1.00E-10

2.00E-11 0.00

50.00

100.00
Frequency (Hz)
1/ID=2019
Node 79-Y
Displacement

150.00

200.00

Phase

Modulus

Frequency response function

Phase

Modulus

0
-180
-360
1.00E-11

1.00E-12

5.00E-13

0.00
50.00
100.00
150.00
200.00

Frequency (Hz)
1/ID=2021
Node 92-X
Displacement

102

Phase

Modulus

Frequency (Hz)

1/ID=2022

Node 92-Y

Displacement

103

Frequency response function

Phase

Modulus

0

-180

-360

1.00E-08

1.00E-09

1.00E-10

0.00

50.00

100.00

150.00

200.00

Frequency (Hz)
1/ID=2023
Node 92-Z
Displacement

104

Phase

Modulus

Phase

Modulus

0

−180

−360

1.00E−11

1.00E−12

5.00E−13

0.00

50.00

100.00

Frequency (Hz)

1/ID=2024

Node 97-X

Displacement

150.00

200.00

Frequency response function

Phase

Modulus

Frequency (Hz)
1/ID=2025
Node 97-Y
Displacement

Phase

Modulus

Frequency (Hz)

1/ID=2026

Node 97-Z

Displacement

APPENDIX C.

This Appendix contains the theoretical results obtained from analysis of 25 of the graphs from Appendix B. Only the graphs corresponding to experimental testing accelerometer locations were analyzed. Prominent peaks were located and the corresponding frequencies tabulated. A table was made corresponding to each of the 25 graphs.

Pages 110-113 contain results from the longitudinal-sine input. Pages 114-117 contain results from the lateral-sine input.

X-AXIS SINE (LONGITUDINAL)		THEORETICAL RESULTS

NODE 92 - Y		
PEAK	FREQUENCY (Hz)	AMPLITUDE
1	178.0	-

NODE 92 - X		
PEAK	FREQUENCY (Hz)	AMPLITUDE
1	10.0	-
2	44.0	-
3	58.0	-
4	82.0	-
5	116.0	-
6	150.0	-
7	176.0	-

NODE 97 - X		
PEAK	FREQUENCY (Hz)	AMPLITUDE
1	10.0	-
2	44.0	-
3	58.0	-
4	82.0	-
5	116.0	-
6	150.0	-
7	176.0	-

NODE 97 - Z		
PEAK	FREQUENCY (Hz)	AMPLITUDE
1	10.0	-
2	44.0	-
3	60.0	-
4	82.0	-
5	116.0	-
6	172.0	-

NODE 5 - X		
PEAK	FREQUENCY (Hz)	AMPLITUDE
1	8.0	-
2	58.0	-
3	84.0	-
4	118.0	-
5	132.0	-
6	178.0	-

NODE 5 - Z		
PEAK	FREQUENCY (Hz)	AMPLITUDE
1	8.0	-
2	60.0	-
3	116.0	-
4	130.0	-
5	178.0	-

111

NODE 5 - Y		
PEAK	FREQUENCY (Hz)	AMPLITUDE
1	10.0	-
2	44.0	-
3	60.0	-
4	80.0	-
5	116.0	-
6	130.0	-
7	178.0	-

NODE 12 - X		
PEAK	FREQUENCY (Hz)	AMPLITUDE
1	58.0	-
2	118.0	-
3	176.0	-
4	188.0	-

NODE 12 - Y		
PEAK	FREQUENCY (Hz)	AMPLITUDE
1	10.0	-
2	44.0	-
3	58.0	-
4	82.0	-
5	116.0	-
6	132.0	-
7	182.0	-

NODE 55 - X		
PEAK	FREQUENCY (Hz)	AMPLITUDE
1	10.0	-
2	44.0	-
3	58.0	-
4	82.0	-
5	116.0	-
6	130.0	-
7	150.0	-
8	180.0	-

NODE 29 - X		
PEAK	FREQUENCY (Hz)	AMPLITUDE
1	10.0	-
2	44.0	-
3	60.0	-
4	80.0	-
5	116.0	-
6	132.0	-
7	182.0	-

113

Z-AXIS SINE (LATERAL)		THEORETICAL RESULTS
NODE 75 - Z		
PEAK	FREQUENCY (Hz)	AMPLITUDE
1	8.0	-
2	44.0	-
3	58.0	-
4	176.0	-

NODE 79 - Z		
PEAK	FREQUENCY (Hz)	AMPLITUDE
1	8.0	-
2	56.0	-
3	176.0	-

NODE 97 - X		
PEAK	FREQUENCY (Hz)	AMPLITUDE
1	10.0	-
2	168.0	-

NODE 97 - Y		
PEAK	FREQUENCY (Hz)	AMPLITUDE
1	8.0	-
2	42.0	-
3	50.0	-
4	58.0	-
5	176.0	-

NODE 97 - Z		
PEAK	FREQUENCY (Hz)	AMPLITUDE
1	8.0	-
2	56.0	-

NODE 5 - X		
PEAK	FREQUENCY (Hz)	AMPLITUDE
1	8.0	-
2	58.0	-
3	62.0	-
4	100.0	-

NODE 5 - Z		
PEAK	FREQUENCY (Hz)	AMPLITUDE.
1	56.0	-

NODE 5 - Y		
PEAK	FREQUENCY (Hz)	AMPLITUDE
1	56.0	-

NODE 12 - Y		
PEAK	FREQUENCY (Hz)	AMPLITUDE
1	8.0	-
2	44.0	-
3	58.0	-
4	62.0	-
5	100.0	-

NODE 12 - Z		
PEAK	FREQUENCY (Hz)	AMPLITUDE
1	56.0	-

NODE 55 - X		
PEAK	FREQUENCY (Hz)	AMPLITUDE
1	8.0	-
2	56.0	-
3	62.0	-
4	100.0	-

116

NODE 55 - Z		
PEAK	FREQUENCY (Hz)	AMPLITUDE
1	8.0	-
2	42.0	-
3	56.0	-
4	64.0	-
5	100.0	-

NODE 29 - X		
PEAK	FREQUENCY (Hz)	AMPLITUDE
1	8.0	-
2	56.0	-
3	100.0	-
4	124.0	-

NODE 29 - Z		
PEAK	FREQUENCY (Hz)	AMPLITUDE
1	8.0	-
2	56.0	-
3	100.0	-
4	126.0	-

APPENDIX D.

This Appendix contains experimental graphs obtained from testing of the actual TOPAZ unit. Data were taken from accelerometers placed at various locations on the unit, manipualted by a MATLAB routine, and then plotted.

Pages 120-143 contain graphs from the longitudinal-sine input. Pages 144-167 contain graphs from the lateral-sine input.

Transducer: A1:RESP.;INBD.SPIDER FX.LEG Axis: +X
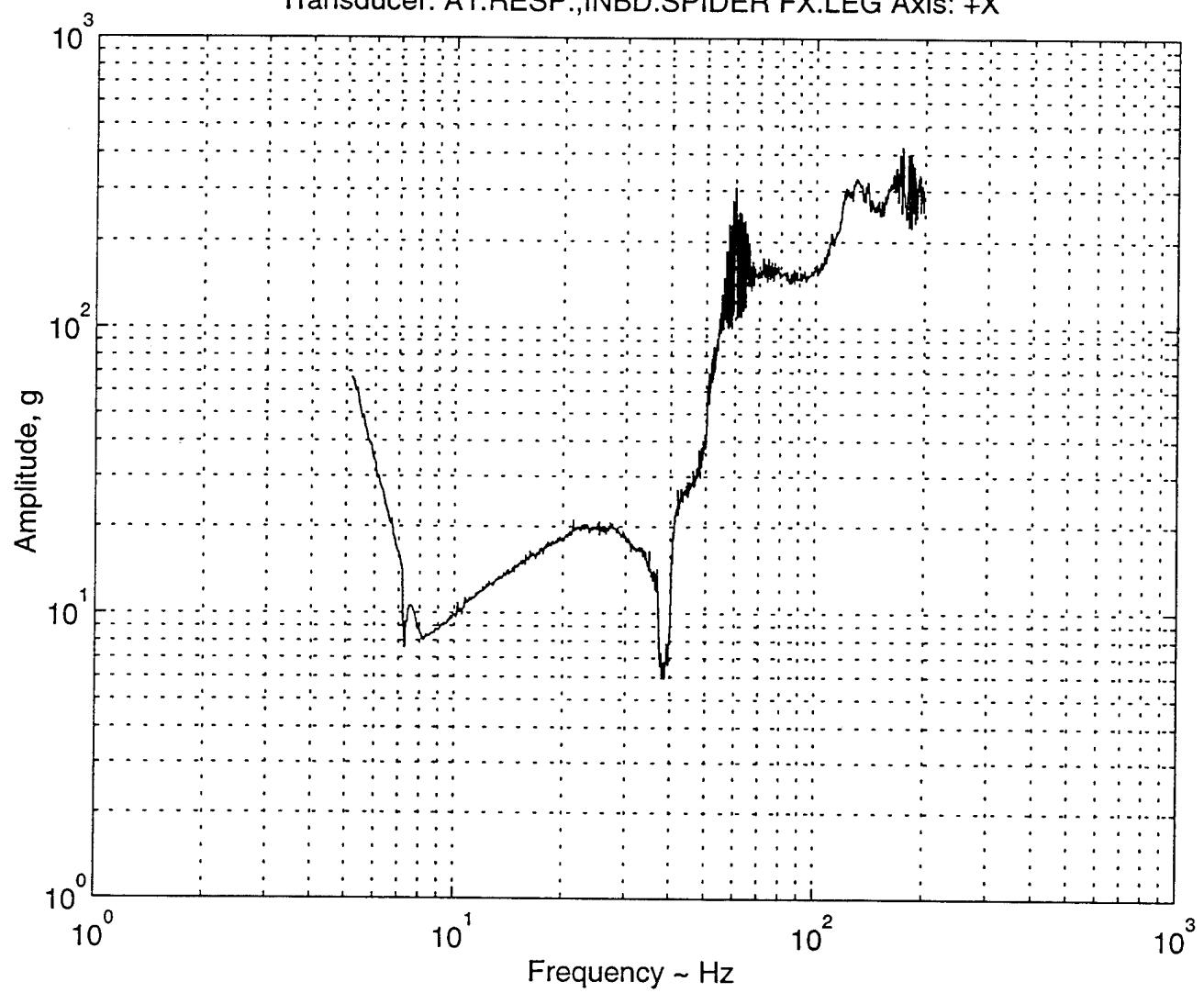
Transducer: A2:CTL.;TBL.FX.NEAR INB.SPDR. Axis: +X

Transducer: I08/C01:REAC. LEG BRACKET/+Y Axis: -X(20)

122
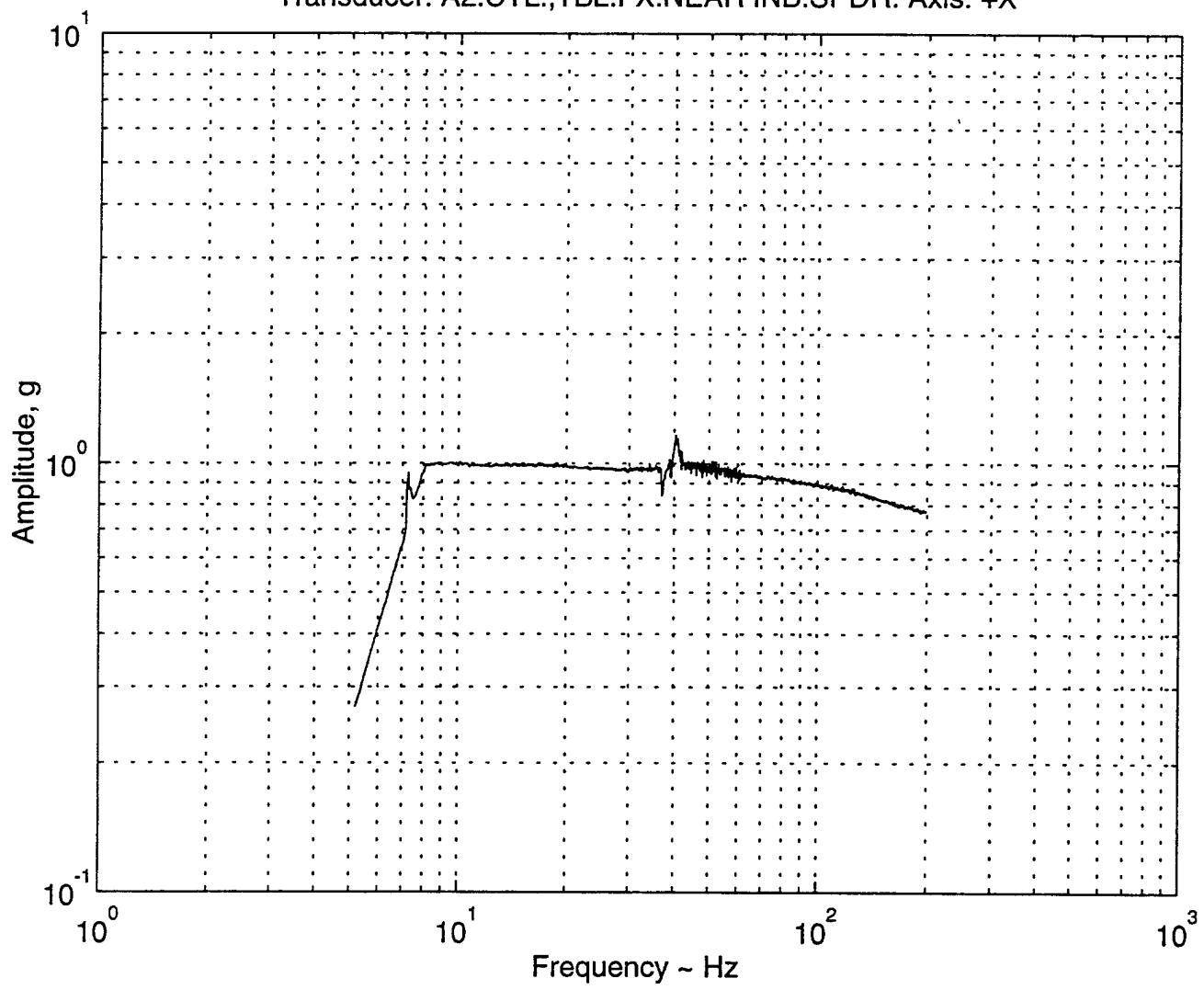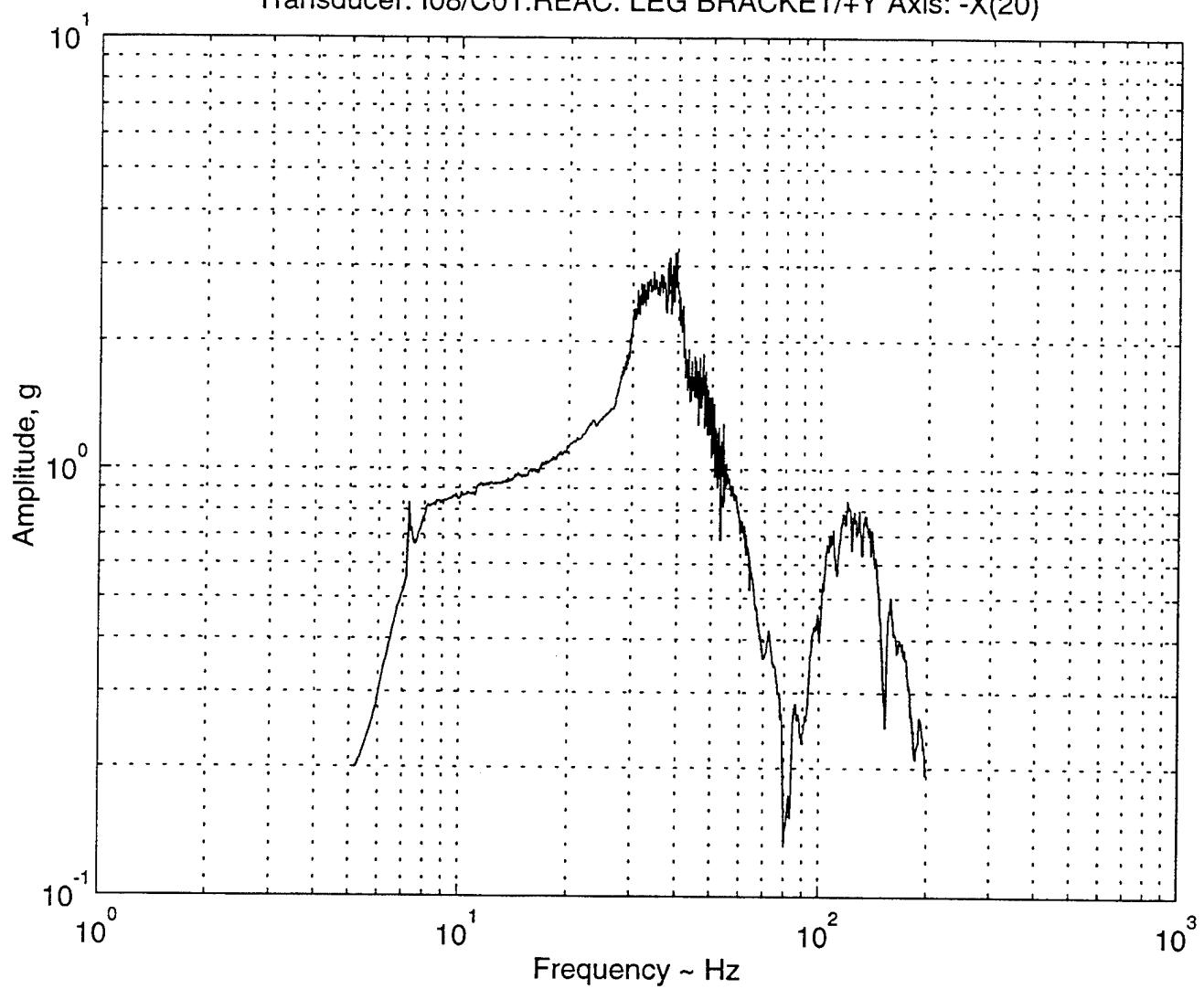
Transducer: I10/C02:REAC.TOP PLENUM/+Y Axis: +Y

Transducer: I10/C03:REAC.TOP PLENUM/+Y Axis: -X

124

Transducer: I07/C05:REAC. LEG BRACKET/-Z Axis: -X(20)

125

Transducer: I09/C09:REACT. TOP PLENUM/-Z Axis: -X

126

Transducer: I09/C12:REAC.TOP PLENUM/-Z Axis: -Z

127

Transducer: I01/C13:-Z LEG @ BASE Axis: -X

Transducer: I01/C14:-Z LEG @ BASE Axis: -Z

129

Transducer: I01/C15:-Z LEG @ BASE Axis: -Y

130

Transducer: I02/C16:LEG/+Y AND +Z/BASE Axis: -X

131

Transducer: I02/C17:LEG/+Y AND +Z/BASE Axis: +Y

132

Transducer: I06/C19:LEG/+Y AND +Z/RAD. TOP Axis: -X

133

Transducer: I06/C20:LEG/+Y AND +Z/RAD. TOP Axis: +Y(30)

134

Transducer: I04/C24:BOTTOM COLL.RAD./+Y Axis: +X

Transducer: I03/C27:BOTTOM COLL.RAD./-Z Axis: +X

136

Transducer: I11/C28:HARD POINT/CESIUM UNIT Axis: -X

137

Transducer: I11/C29:HARD POINT/CESIUM UNIT Axis: -Y

138

Transducer: I11/C30:HARD POINT/CESIUM UNIT Axis: -Z

139
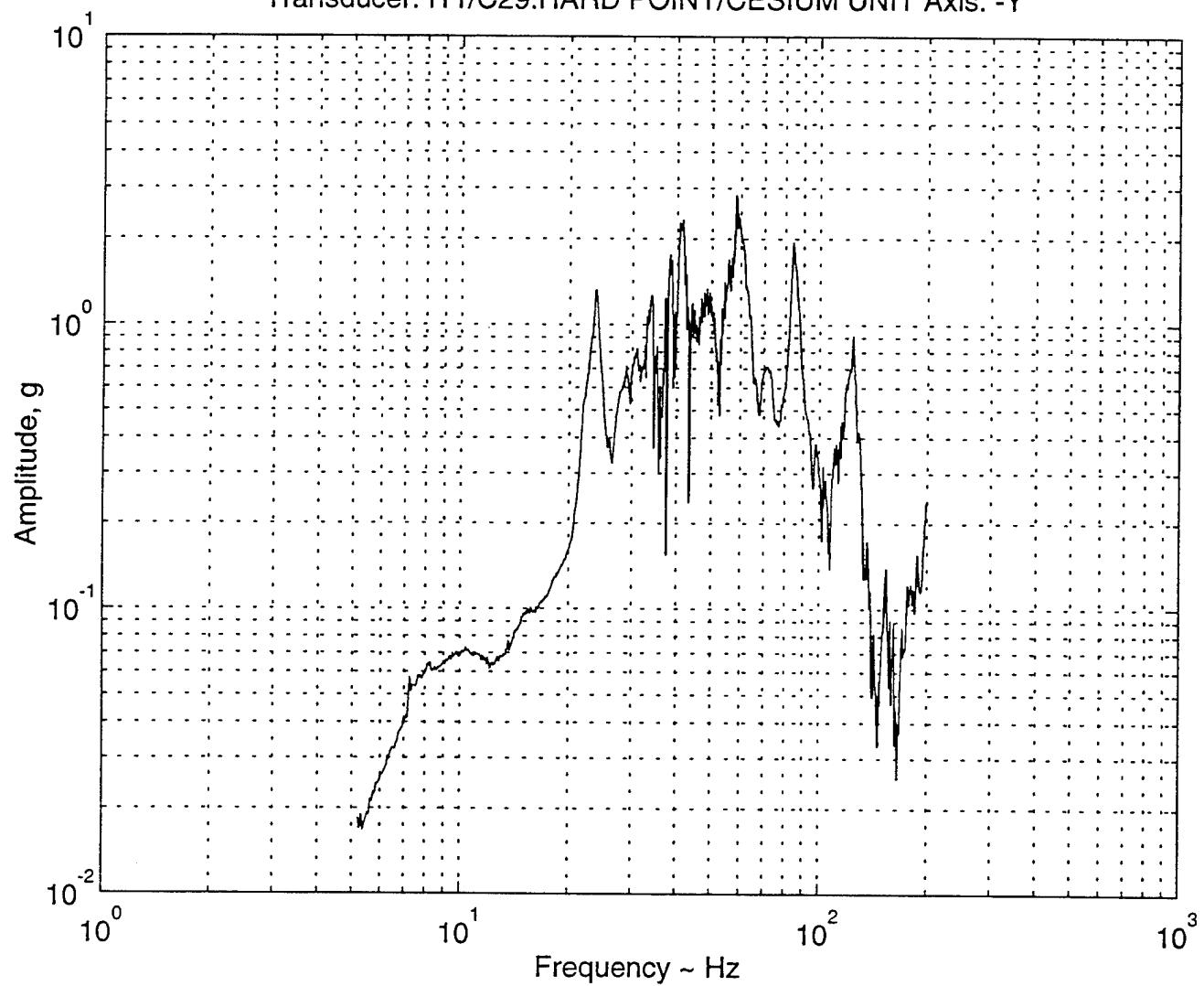
Transducer: I05/C31:JOINT ON LEG Axis: -X

Transducer: I12/C34:STARTUP UNIT FRAME Axis: -X
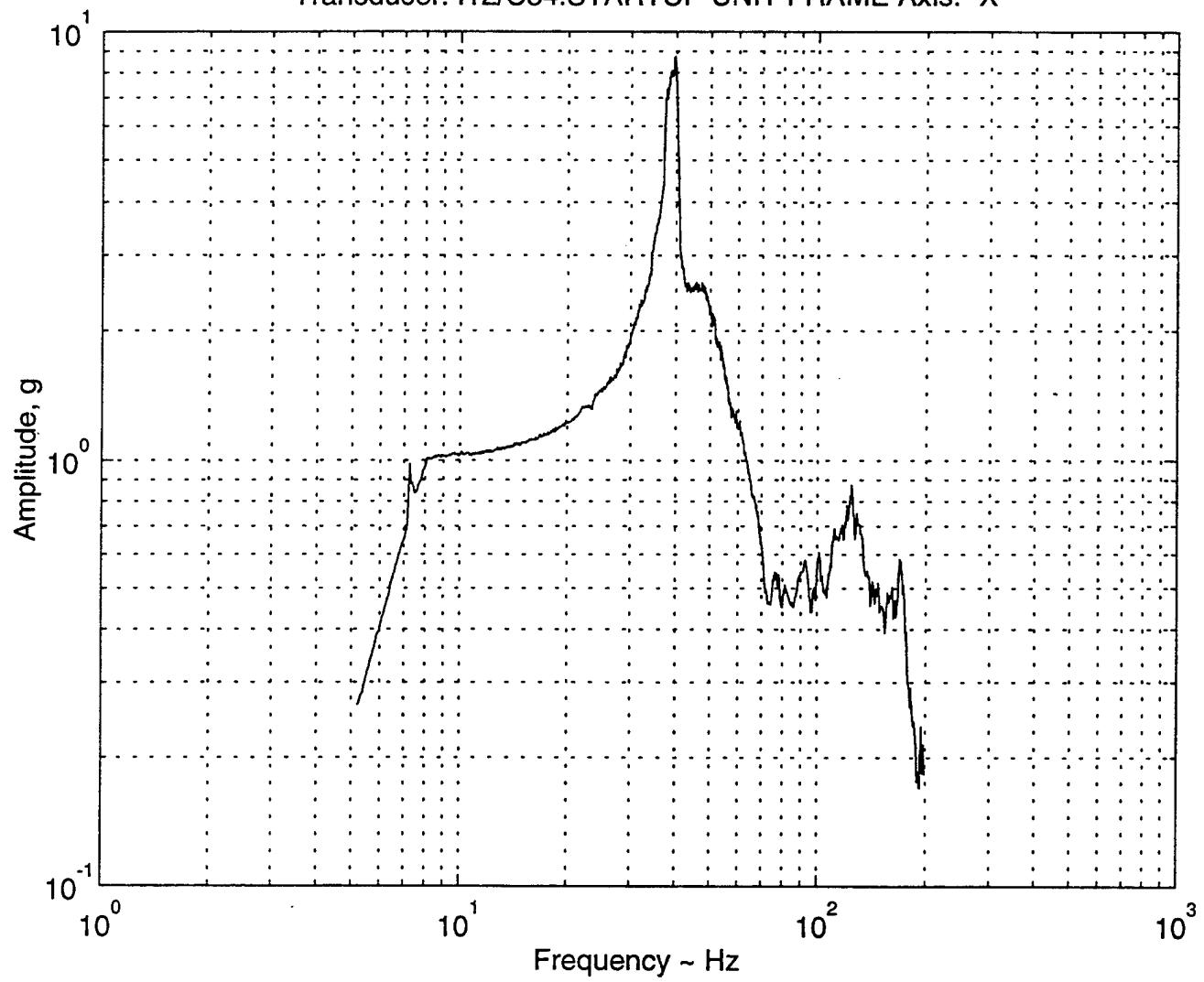
141

Transducer: I12/C35:STARTUP UNIT FRAME Axis: -Z(60)

Transducer: I12/C36:STARTUP UNIT FRAME Axis: -Y(60)

Transducer: A1:SINE CTL.1;INBOARD LEG(N.) Axis: +Z
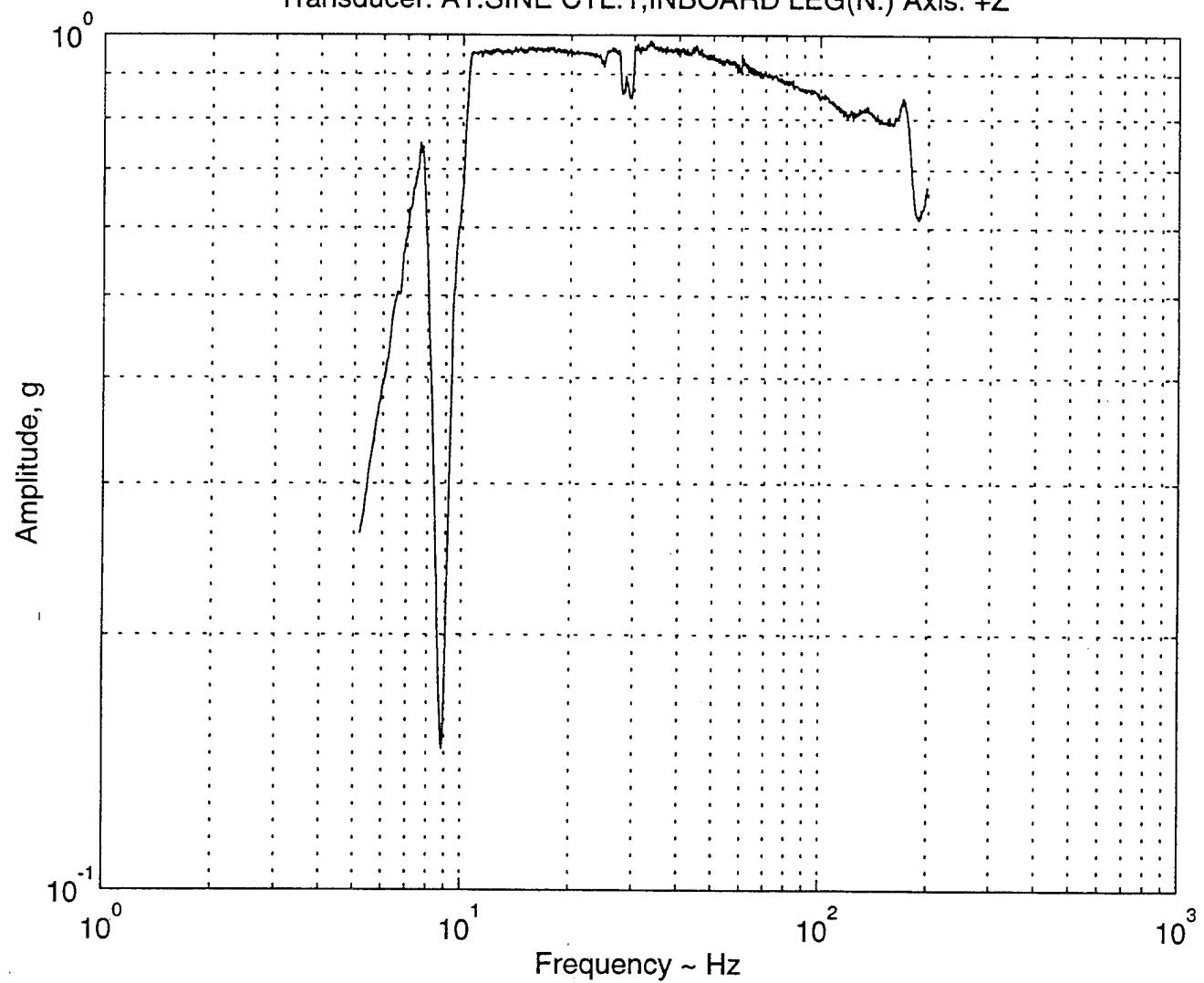
Transducer: A2:SINE CTL.2;OUTBOARD LEG(E.) Axis: +Z

145

Transducer: I08/C04:REACT. LEG BRAKET/+Y Axis: +Z

146
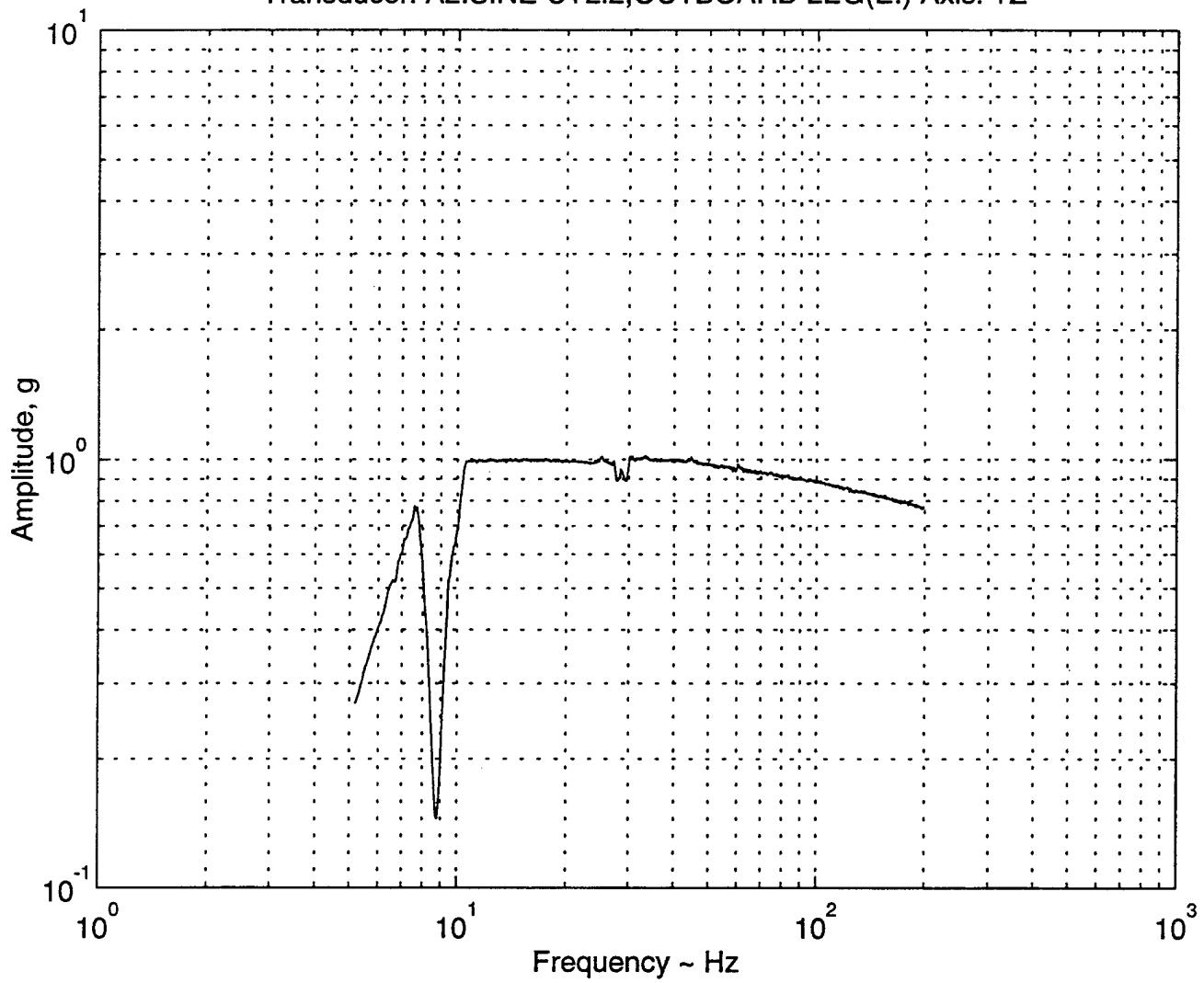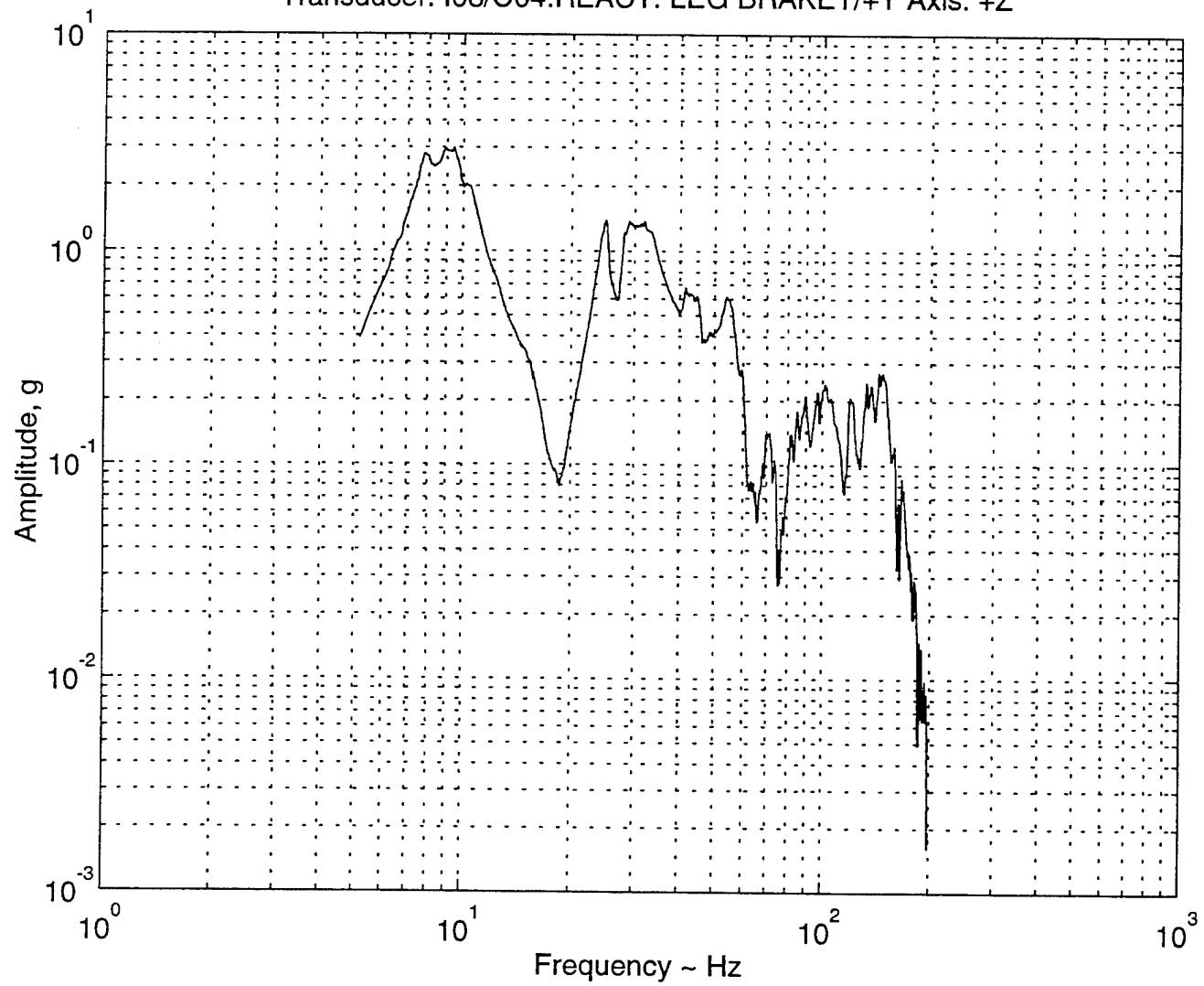
Transducer: I07/C08:REACT. LEG BRAK./-Z Axis: -Z(15)

Transducer: I09/C09:REACT. TOP PLENUM/-Z Axis: -X
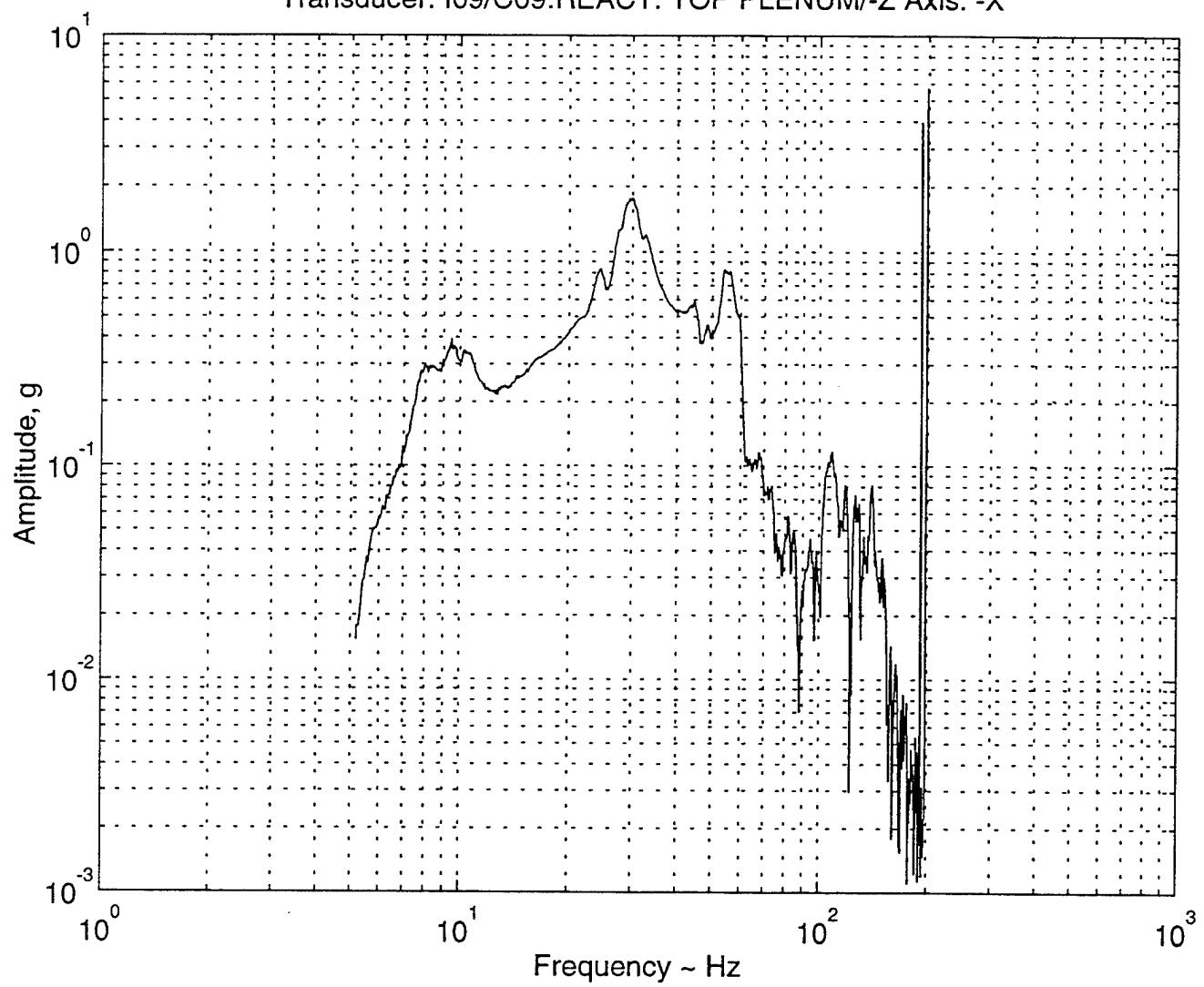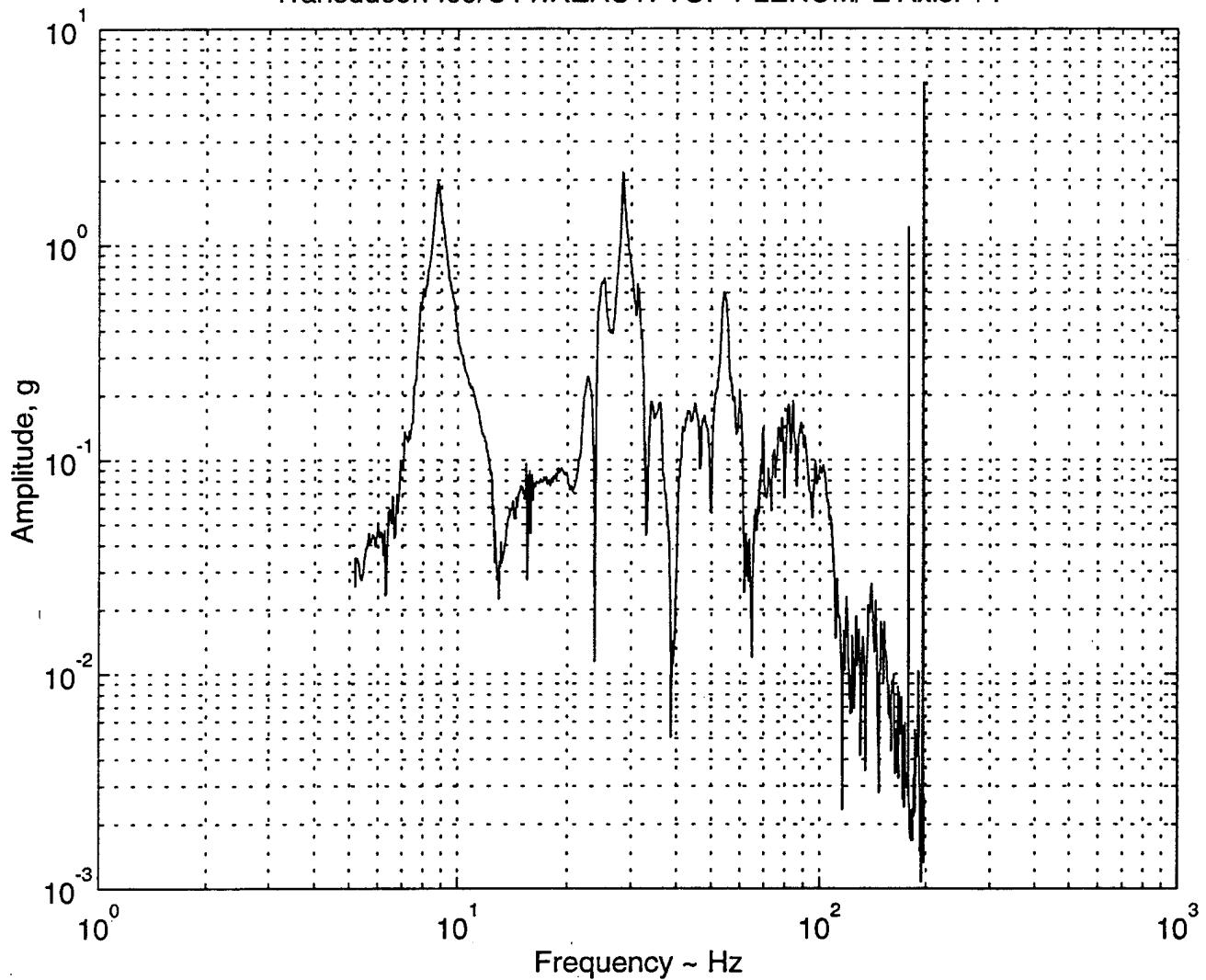
148

Transducer: I09/C11:REACT. TOP PLENUM/-Z Axis: +Y

149

Transducer: I09/C12:REACT. TOP PLENUM/-Z Axis: -Z

150
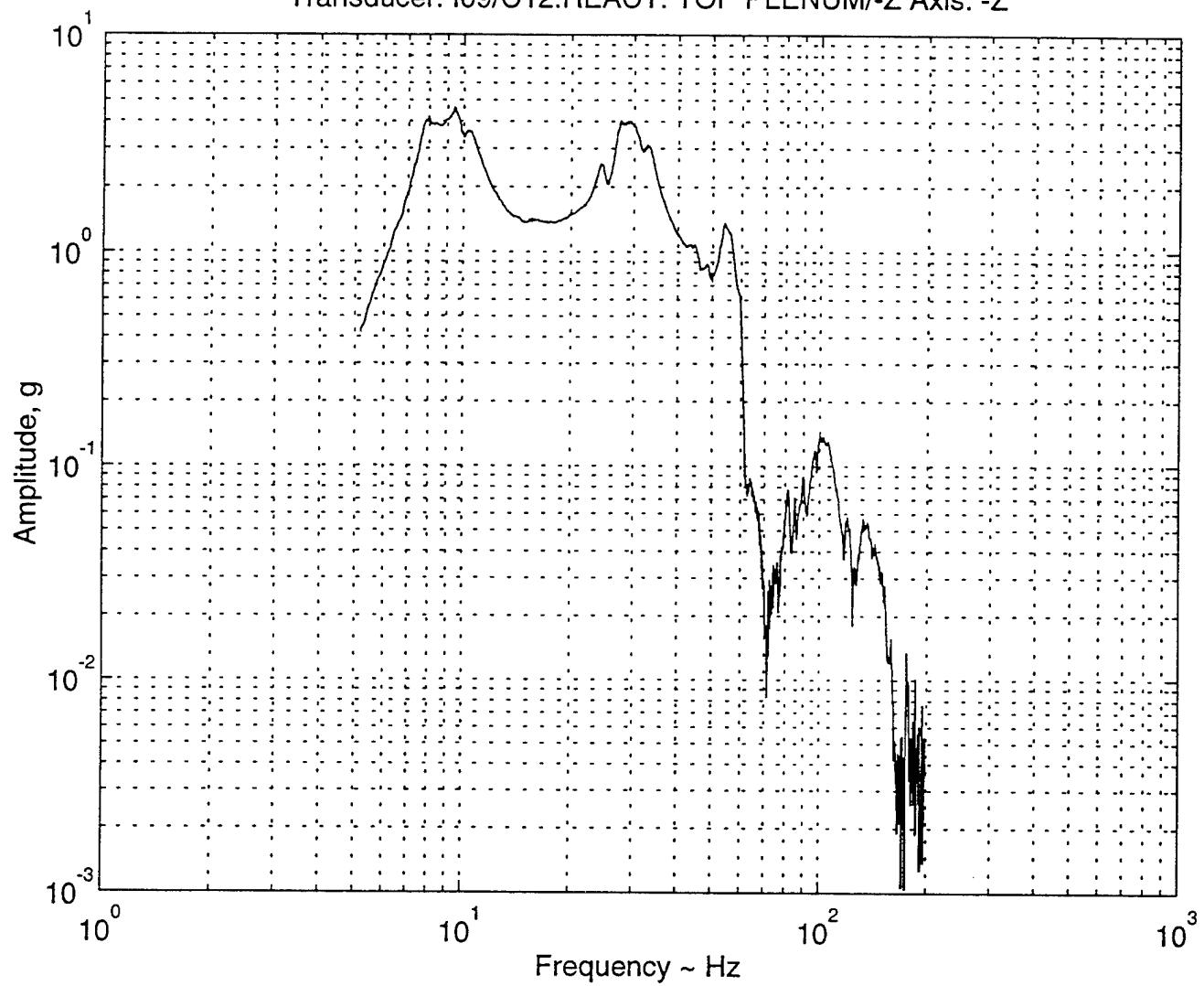
Transducer: I01/C13:-Z LEG @ BASE Axis: -X
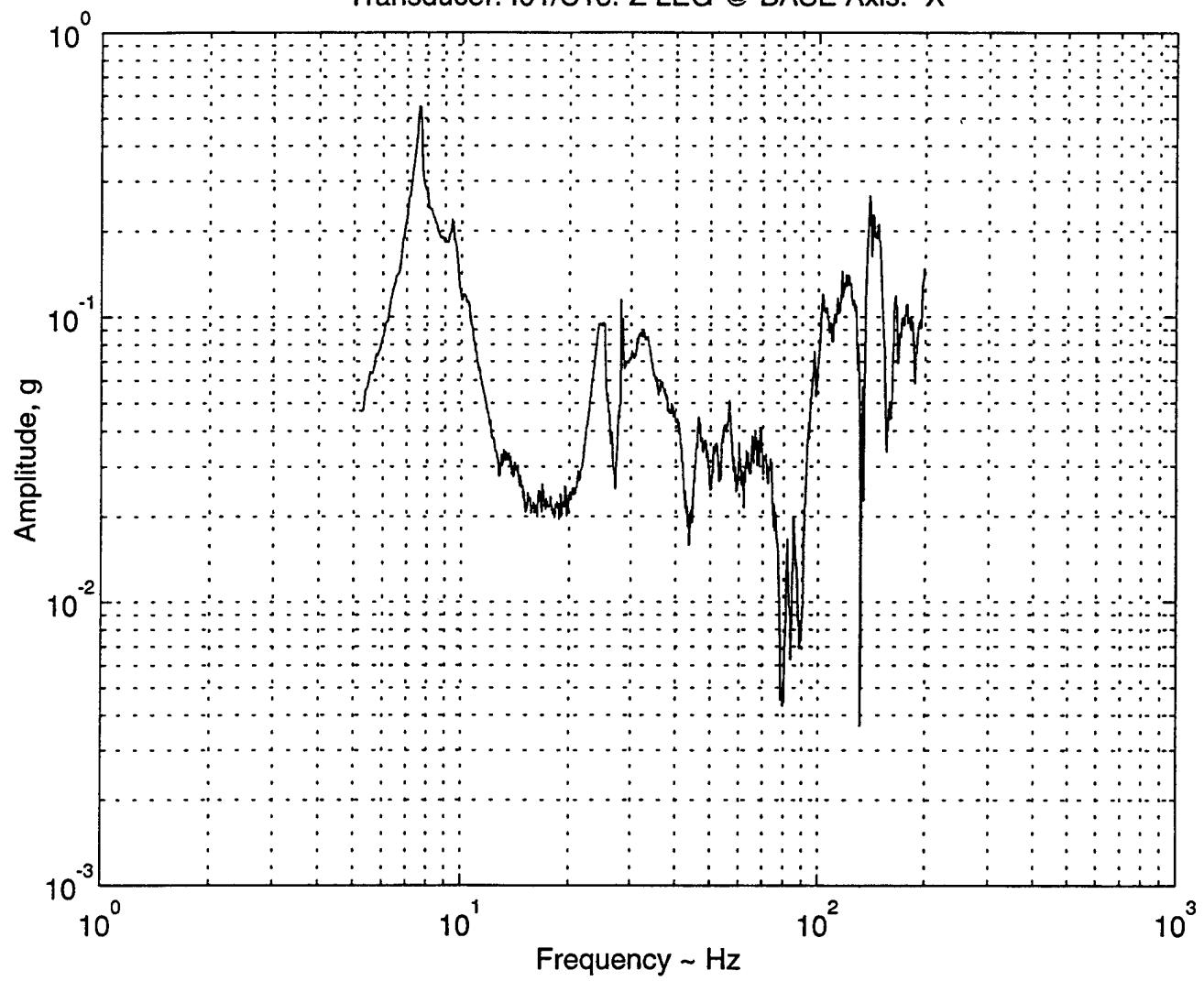
Transducer: I01/C14:-Z LEG @ BASE Axis: -Z
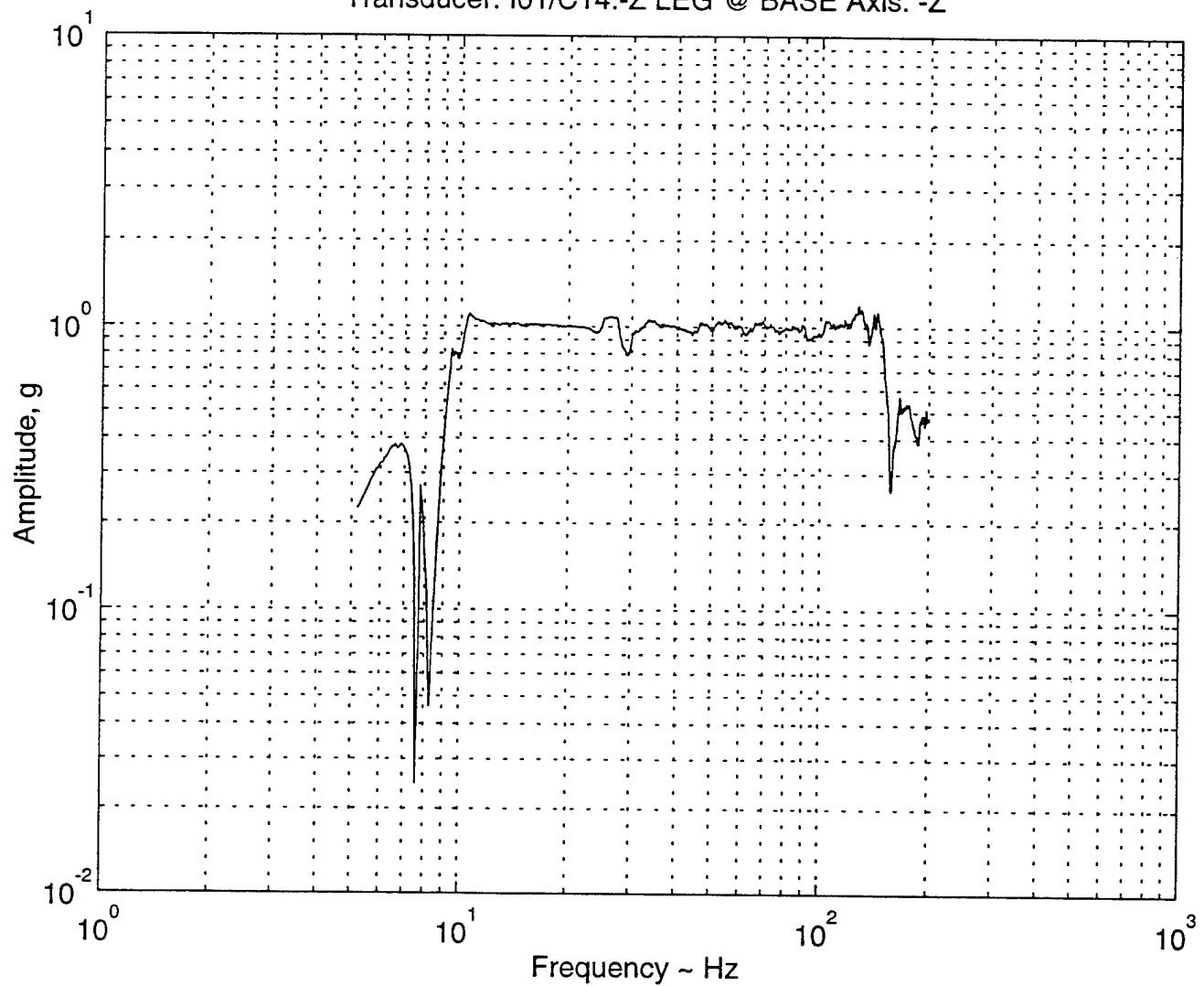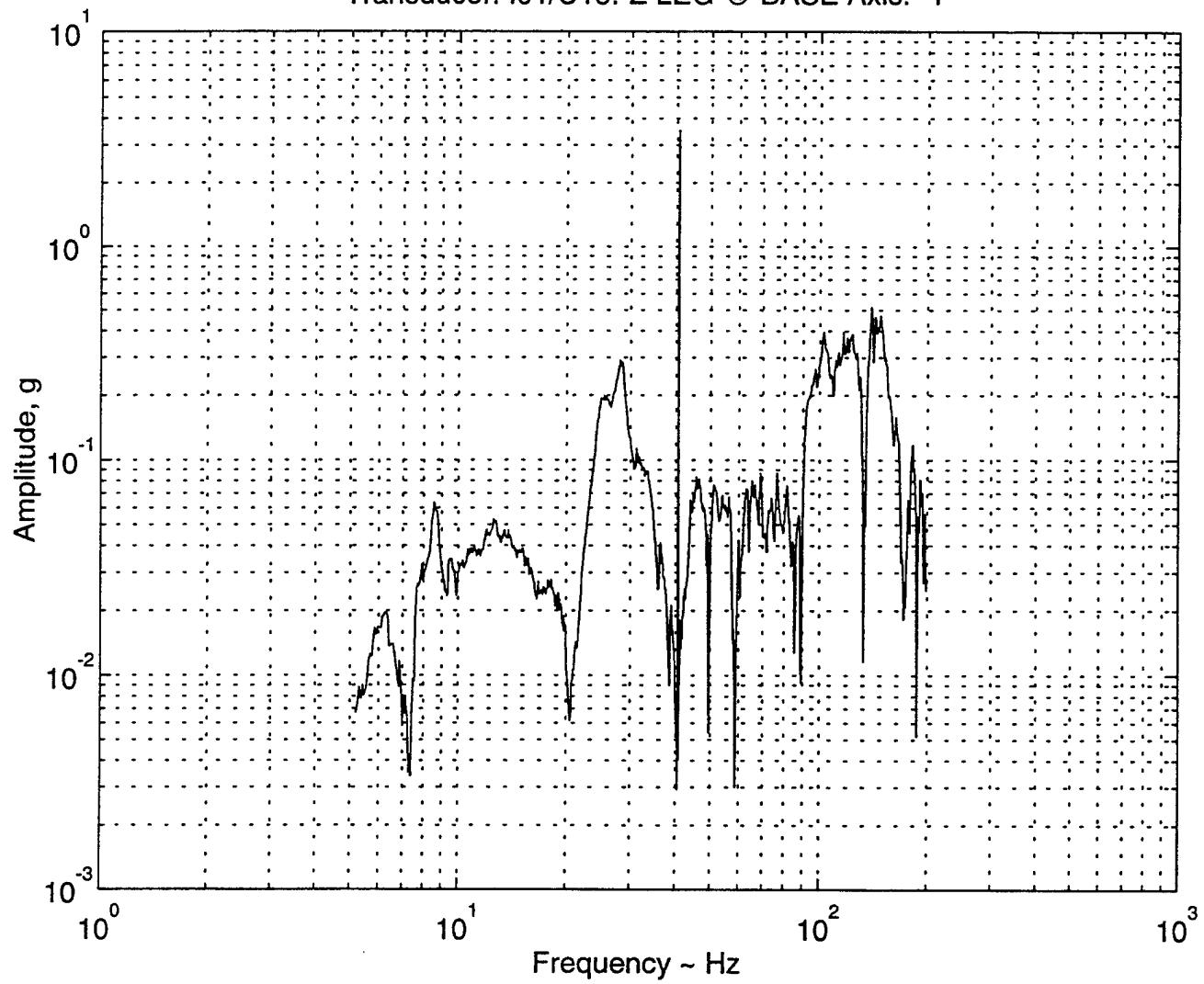
Transducer: I01/C15:-Z LEG @ BASE Axis: -Y

Transducer: I02/C17:LEG/+Y AND +Z/BASE Axis: +Y

154
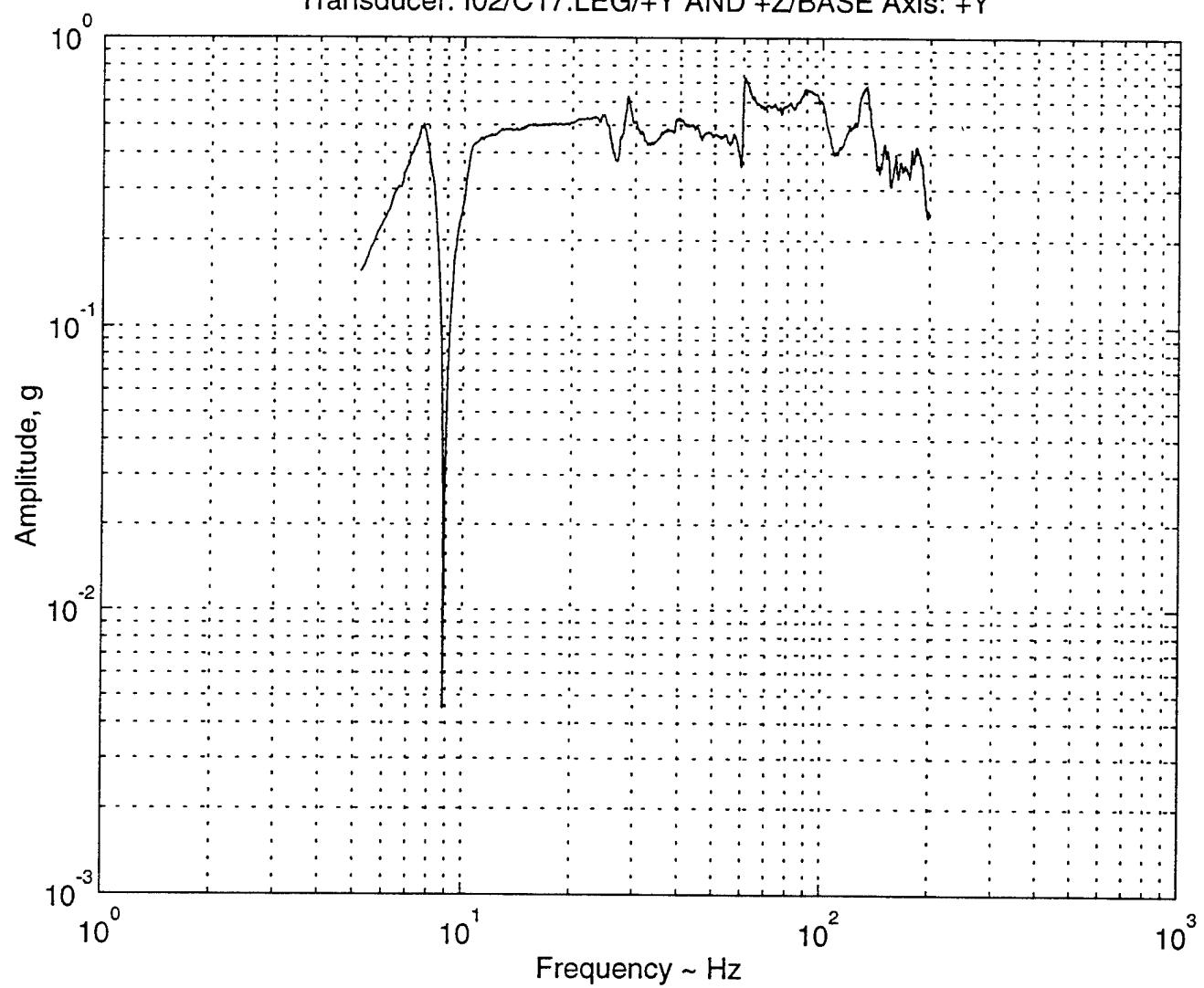
Transducer: I02/C18:LEG/+Y AND +Z/BASE Axis: -Z
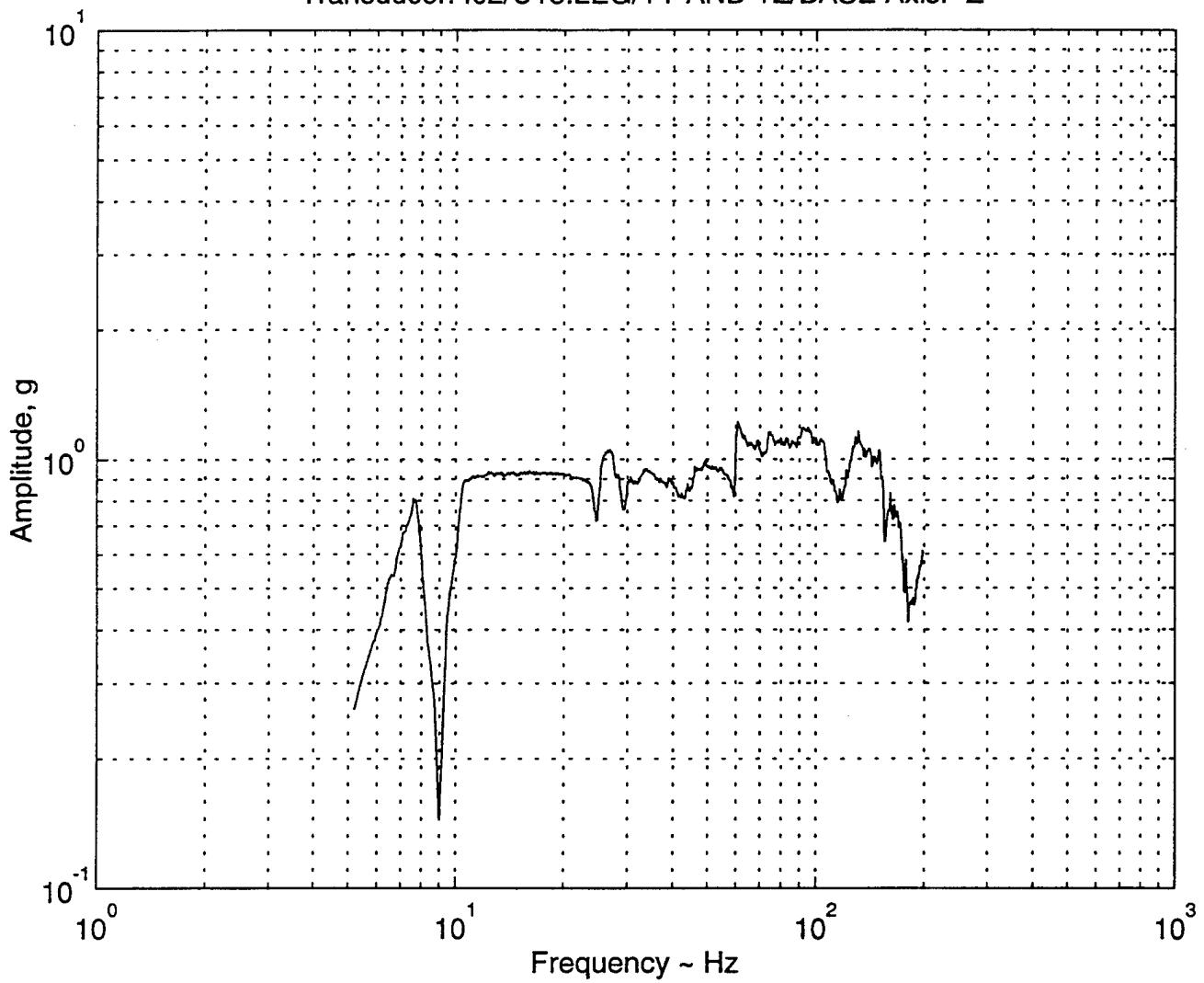
Transducer: I06/C19:LEG/+Y AND +Z/RAD. TOP Axis: -X
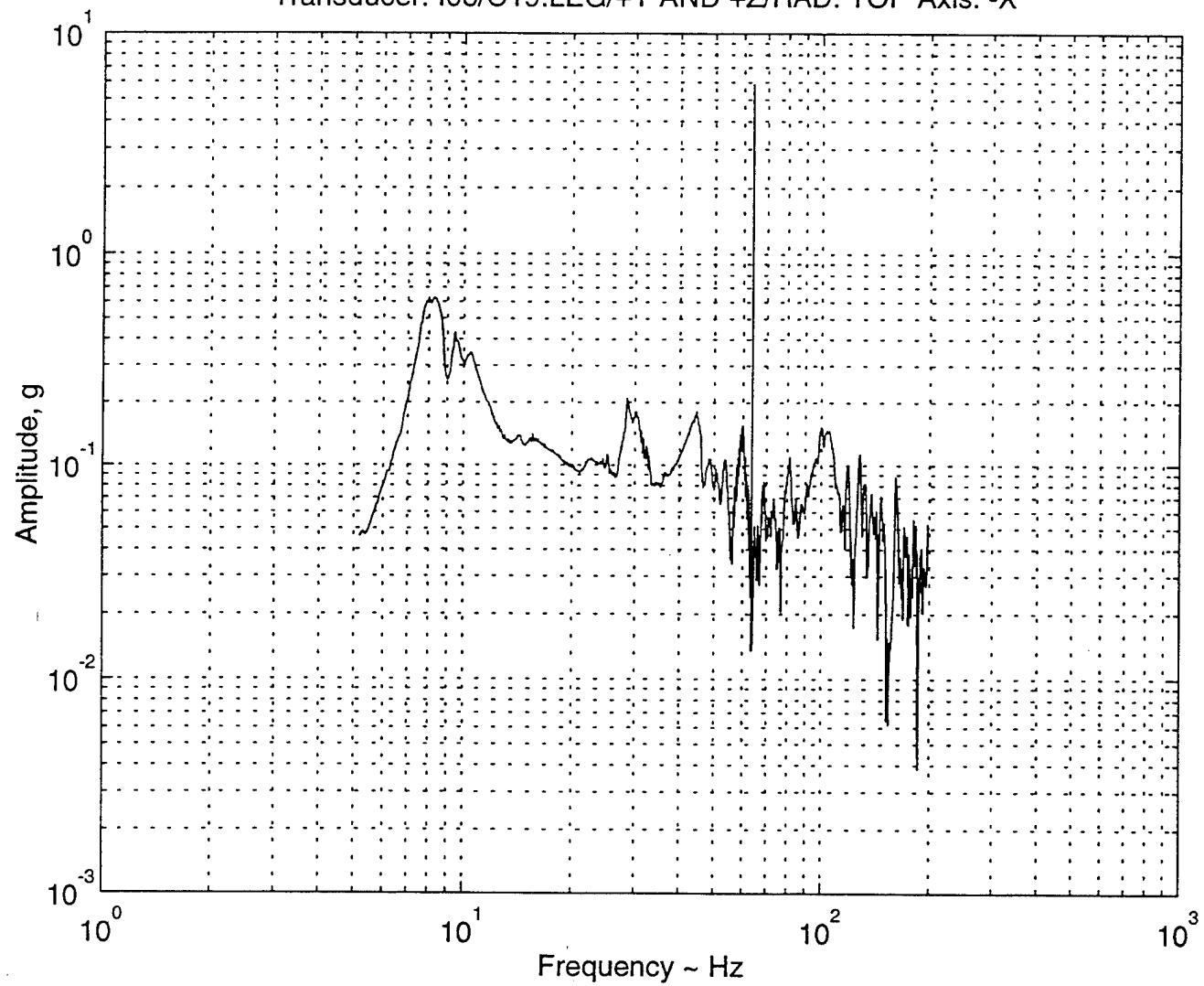
Transducer: I06/C20:LEG/+Y AND +Z/RAD. TOP Axis: +Z(30)

157

Transducer: I04/C23:BOTT. COLL. RAD./+Y Axis: +Y

158
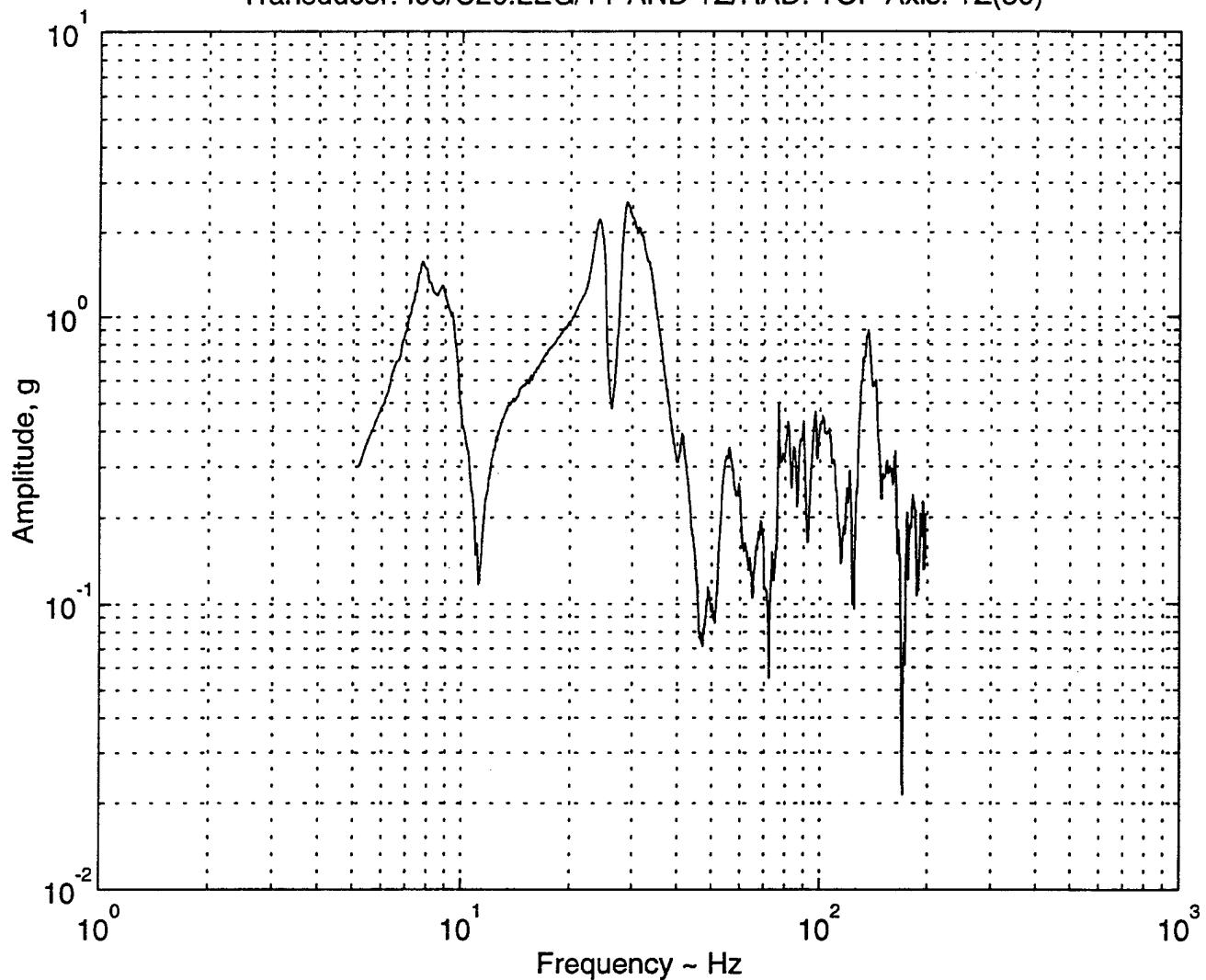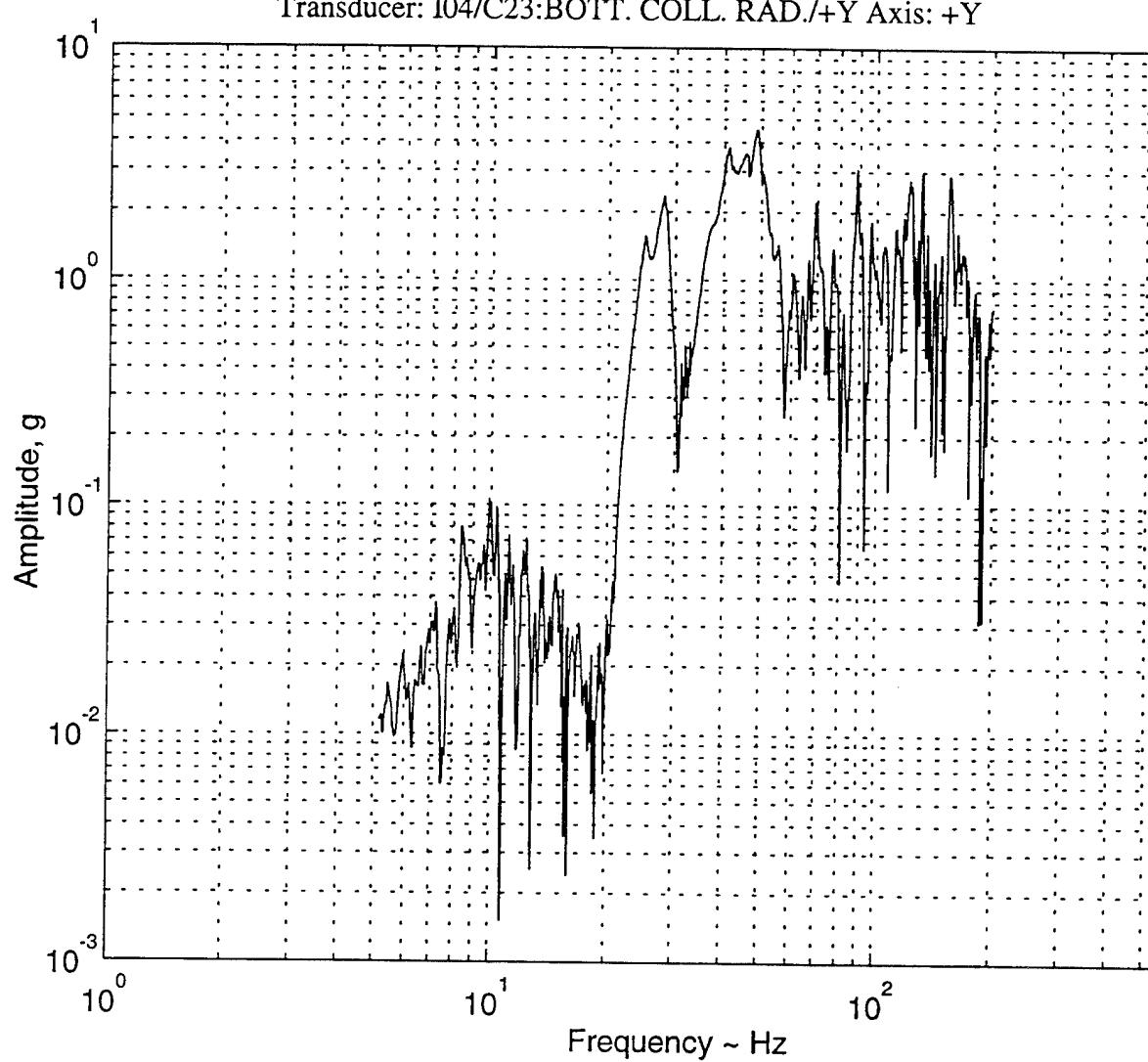
Transducer: I03/C25:BOTT. COLL. RAD./-Z Axis: -Z

Transducer: I11/C28:HARD POINT/CESIUM UNIT Axis: -X

160
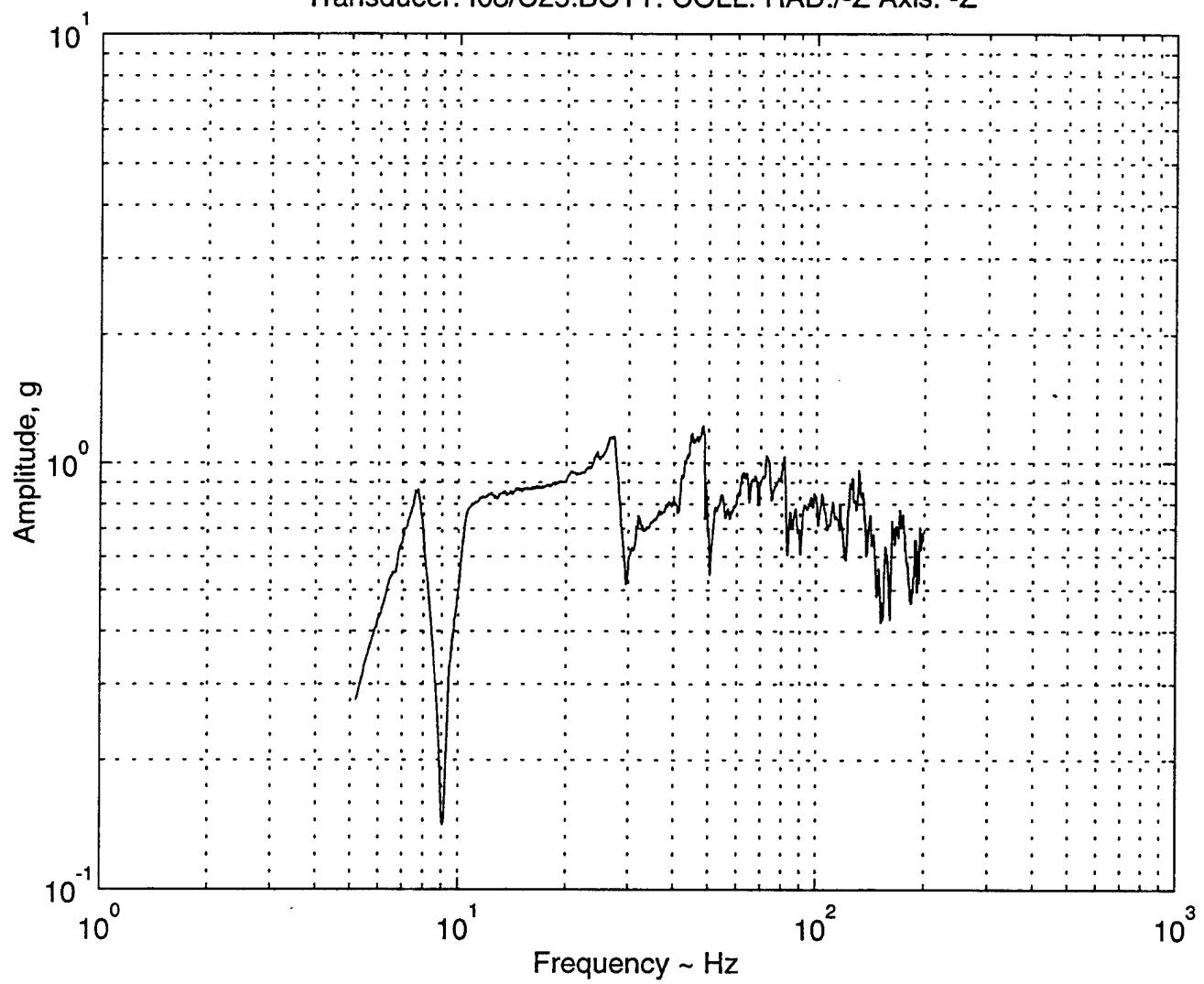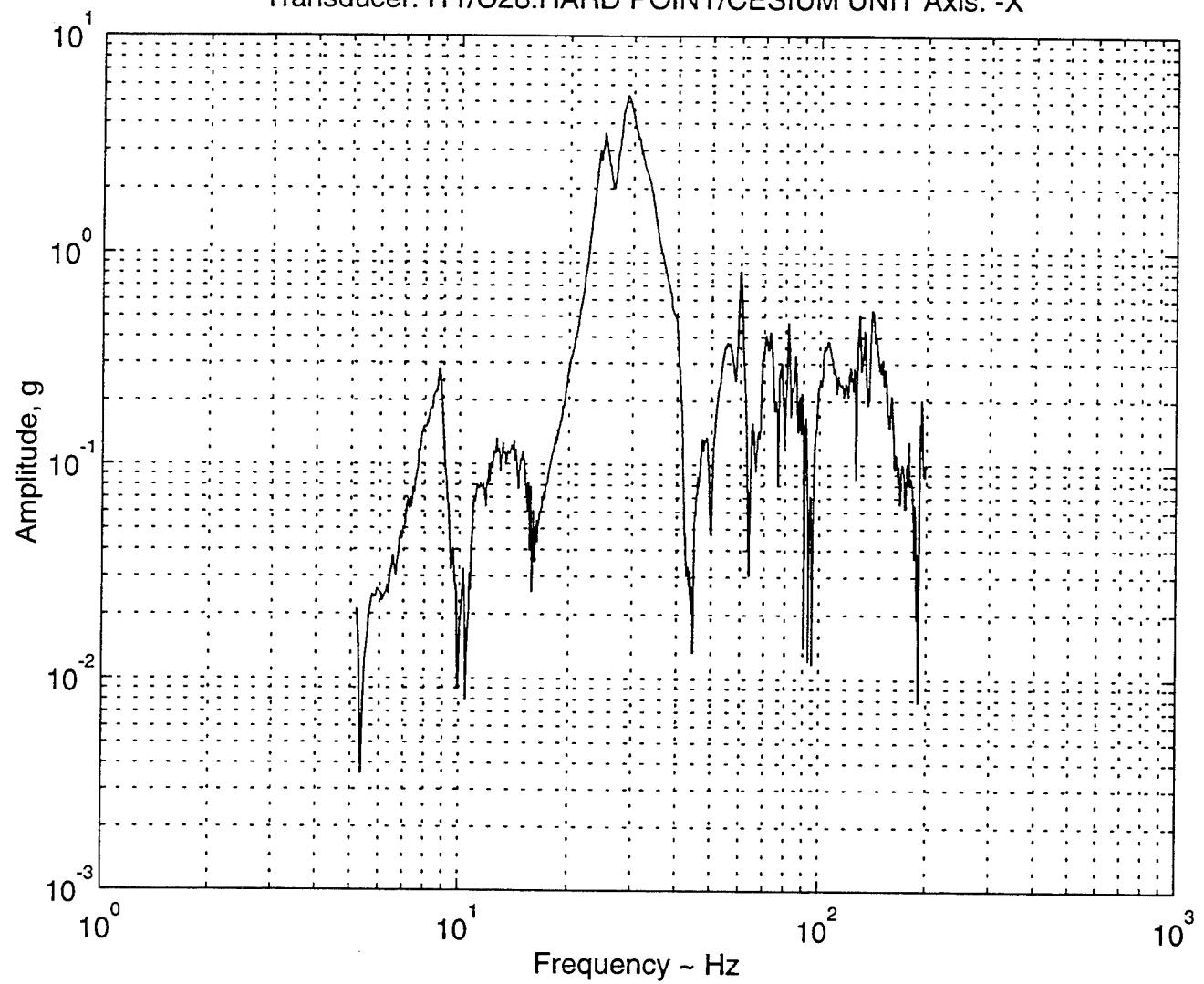
Transducer: I11/C29:HARD POINT/CESIUM UNIT Axis: -Y

Transducer: I11/C30:HARD POINT/CESIUM UNIT Axis: +Z

162

Transducer: I05/C31:JOINT ON LEG Axis: -X

163

Transducer: I05/C33:JOINT ON LEG Axis: -Z

164
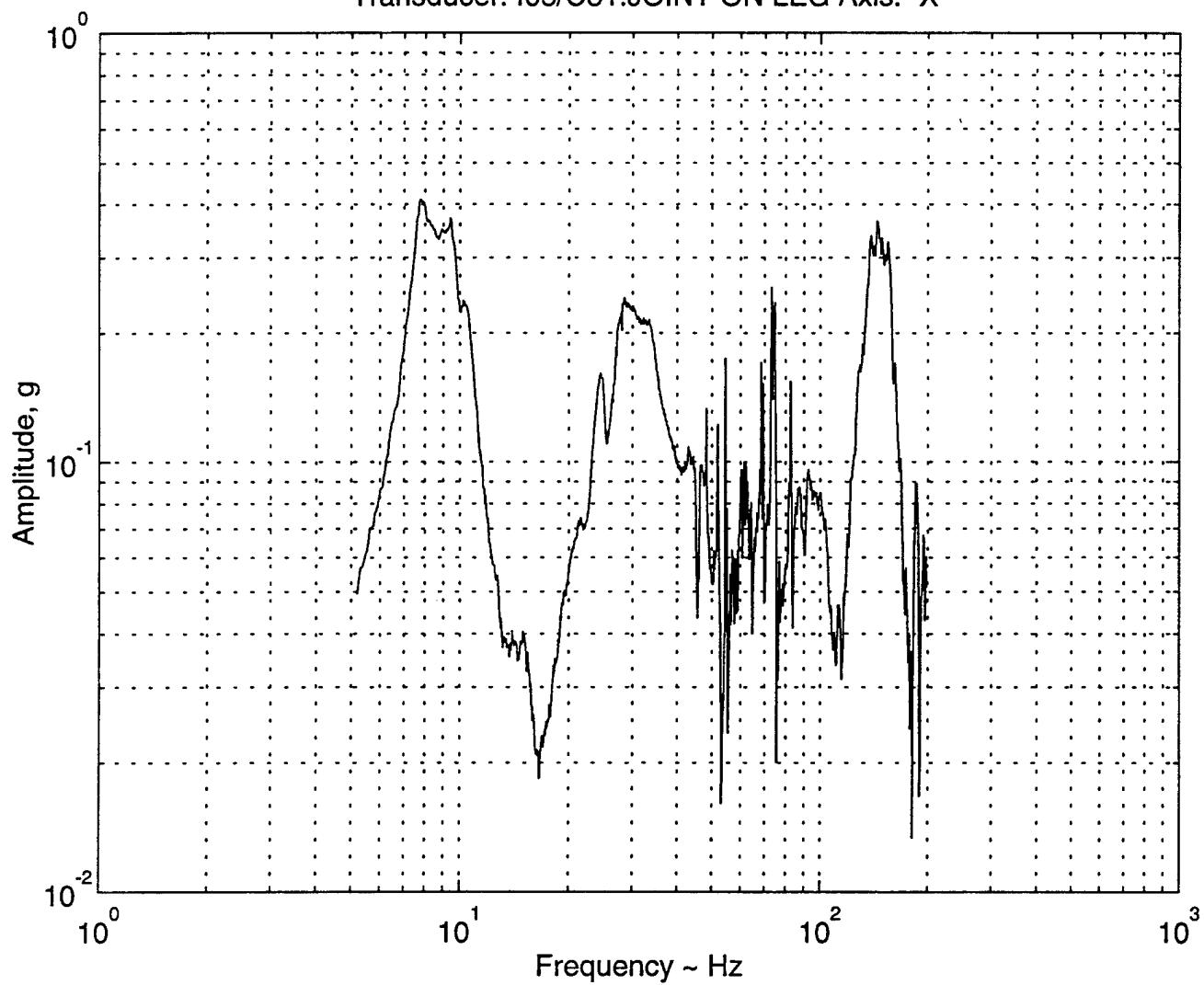
Transducer: I12/C34:STARTUP UNIT FRAME Axis: -X

Transducer: I12/C35:STARTUP UNIT FRAME Axis: -Z(60)

Transducer: I12/C36:STARTUP UNIT FRAME Axis: -Y(60)

167
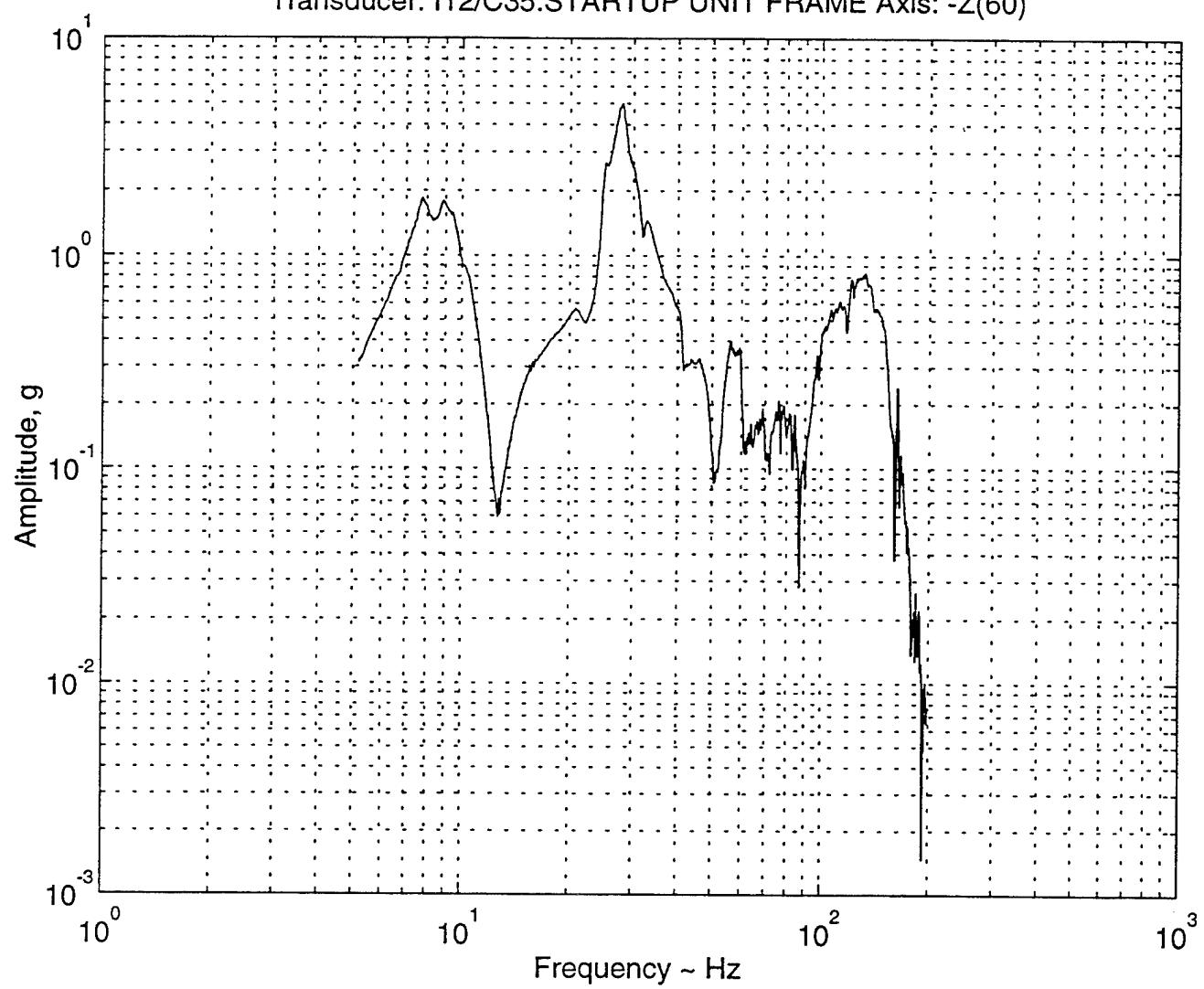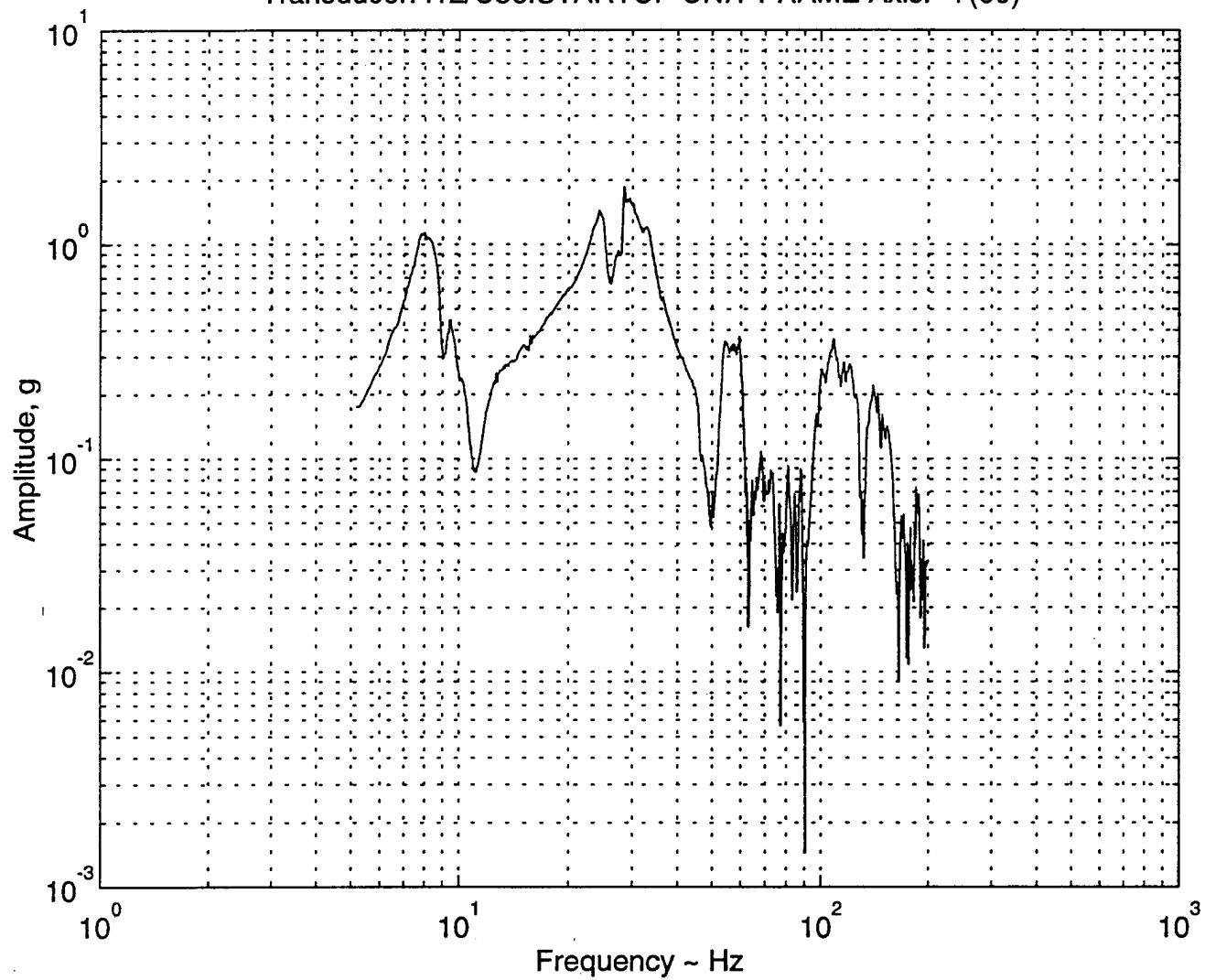
APPENDIX E.

This Appendix contains the experimental data obtained from analysis of the graphs of Appendix D. Prominent peaks were located and the corresponding frequencies tabulated. A table was made corresponding to each graph.

Pages 170-175 contain results from the longitudinal sine-vibration test. Pages 176-183 contain results from the lateral sine-vibration test.

TOPAZ 4 X-AXIS SINE (LONGITUDINAL)		EXPERIMENTAL DATA

TRANSDUCER: A1:RESP.;INBD.SPIDER FX.LEG Axis:+X

MODE	FREQUENCY (Hz)	AMPLITUDE (g)
1	7.26411	0.979038
2	38.5593	2.55313

TRANSDUCER: A2:CTL.;TBL.FX.NEAR INB.SPDR. Axis: +X

MODE	FREQUENCY (Hz)	AMPLITUDE (g)
1	7.26411	0.949486
2	40.4287	1.16645

TRANSDUCER: I08/C01:REAC. LEG BRACKET/+Y Axis: -X(20)

MODE	FREQUENCY (Hz)	AMPLITUDE (g)
1	7.25590	0.830437
2	39.1799	3.21519
3	119.168	0.840745

TRANSDUCER: I10/C02:REAC.TOP PLENUM/+Y AXIS: +Y

MODE	FREQUENCY (Hz)	AMPLITUDE (g)
1	7.25590	0.130444
2	26.7471	0.396580
3	43.7505	1.47043
4	75.4438	0.220682

TRANSDUCER: I10/C03:REAC.TOP PLENUM/+Y Axis: -X

MODE	FREQUENCY (Hz)	AMPLITUDE (g)
1	7.25590	0.949505
2	39.1799	4.51255

TRANSDUCER:	I07/C05:REAC. LEG BRACKET/-Z Axis: -X(20)	
MODE	FREQUENCY (Hz)	AMPLITUDE (g)
1	7.25590	0.964197
2	40.0062	6.00587
3	111.373	0.552872

TRANSDUCER:	I09/C09:REACT. TOP PLENUM/-Z Axis: -X	
MODE	FREQUENCY (Hz)	AMPLITUDE (g)
1	7.25590	0.986588
2	35.3706	6.14214

TRANSDUCER:	I09/C12:REAC.TOP PLENUM/-Z Axis: -Z	
MODE	FREQUENCY (Hz)	AMPLITUDE (g)
1	39.4811	0.998568
2	51.3925	0.889658

TRANSDUCER:	I01/C13:-Z LEG @ BASE Axis: -X	
MODE	FREQUENCY (Hz)	AMPLITUDE (g)
1	7.26411	0.933774
2	39.5012	2.36357
3	118.356	1.00910

TRANSDUCER:	I01/C14:-Z LEG @ BASE Axis: -Z	
MODE	FREQUENCY (Hz)	AMPLITUDE (g)
1	37.9520	0.378004
2	72.3113	0.226455
3	148.181	0.398491

171

TRANSDUCER:	I01/C15:-Z LEG @ BASE Axis: -Y	
MODE	FREQUENCY (Hz)	AMPLITUDE (g)
1	7.26411	4.428413E-02
2	15.1196	0.217778
3	39.0735	1.24001

TRANSDUCER:	I02/C16:LEG/+Y AND +Z/BASE Axis: -X	
MODE	FREQUENCY (Hz)	AMPLITUDE (g)
1	7.26411	0.956400
2	38.0587	1.68669
3	103.69	0.884210

TRANSDUCER:	I02/C17:LEG/+Y AND +Z/BASE Axis: +Y	
MODE	FREQUENCY (Hz)	AMPLITUDE (g)
1	7.26411	0.130565
2	39.5012	0.780018
3	64.2438	0.187713
4	83.3868	0.249129
5	154.734	0.250545

TRANSDUCER:	I06/C19:LEG/+Y AND +Z/RAD. TOP Axis: -X	
MODE	FREQUENCY (Hz)	AMPLITUDE (g)
1	7.26411	0.947660
2	39.5012	5.00209
3	107.438	0.670597

TRANSDUCER:	I04/C24:BOTTOM COLL.RAD./+Y Axis: +X	
MODE	FREQUENCY (Hz)	AMPLITUDE (g)
1	7.26411	0.916813
2	38.4494	6.19911
3	112.567	1.61763

TRANSDUCER:	I03/C27:BOTTOM COLL.RAD./-Z Axis: +X	
MODE	FREQUENCY (Hz)	AMPLITUDE (g)
1	7.26411	0.957385
2	38.4494	4.70091
3	109.031	1.38565
4	153.015	0.480957

TRANSDUCER:	I11/C28:HARD POINT/CESIUM UNIT Axis: -X	
MODE	FREQUENCY (Hz)	AMPLITUDE (g)
1	7.25590	1.08319
2	39.7964	11.0903
3	123.496	2.02739

TRANSDUCER:	I11/C29:HARD POINT/CESIUM UNIT Axis: -Y	
MODE	FREQUENCY (Hz)	AMPLITUDE (g)
1	23.6227	1.32583
2	40.9289	2.26666
3	58.1368	2.83179
4	84.0117	1.94570
5	123.977	0.913474

173

TRANSDUCER:	I11/C30:HARD POINT/CESIUM UNIT Axis: -Z	
MODE	FREQUENCY (Hz)	AMPLITUDE (g)
1	8.67318	3.010930E-02
2	28.8288	1.42810
3	69.7589	0.597402
4	113.349	0.901246

TRANSDUCER:	I05/C31:JOINT ON LEG Axis: -X	
MODE	FREQUENCY (Hz)	AMPLITUDE (g)
1	7.26411	0.936477
2	38.5593	3.58424
3	101.861	0.693603
4	144.553	0.628134

TRANSDUCER:	I12/C34:STARTUP UNIT FRAME Axis: -X	
MODE	FREQUENCY (Hz)	AMPLITUDE (g)
1	7.25590	0.981654
2	39.5960	8.74582
3	123.977	0.874155
4	169.133	0.584549

TRANSDUCER:	I12/C35:STARTUP UNIT FRAME Axis: -Z(60)	
MODE	FREQUENCY (Hz)	AMPLITUDE (g)
1	25.2811	0.312611
2	33.8624	0.434271
3	39.7120	0.862081
4	52.9984	0.437670
5	71.5108	0.342384
6	101.493	0.246964
7	150.347	0.162090
8	181.722	0.234352

TRANSDUCER:	I12/C36:STARTUP UNIT FRAME Axis: -Y(60)	
MODE	FREQUENCY (Hz)	AMPLITUDE (g)
1	7.25590	0.114642
2	34.0583	3.08350
3	38.9664	6.18548
4	101.493	0.546350
5	172.147	0.555203

Z-AXIS SINE (LATERAL)		EXPERIMENTAL DATA

TRANSDUCER: A1:SINE CTL.1;INBOARD LEG(N.) Axis: +Z

PEAK	FREQUENCY (Hz)	AMPLITUDE (g)
1	7.5904	0.750334
2	28.4307	0.895611
3	169.748	0.844949

TRANSDUCER: A2:SINE CTL.2;OUTBOARD LEG(E.) Axis: +Z

PEAK	FREQUENCY (Hz)	AMPLITUDE (g)
1	7.5904	0.777016
2	28.4307	0.948742

TRANSDUCER: I08/C04:REACT. LEG BRAKET/+Y Axis: +Z

PEAK	FREQUENCY (Hz)	AMPLITUDE (g)
1	24.9373	1.38918
2	81.8337	0.13952
3	85.0912	0.178205
4	89.5111	0.210022
5	96.9556	0.219762
6	119.427	0.206647

TRANSDUCER: I07/C08:REACT. LEG BRAK./-Z Axis: -Z(15)

PEAK	FREQUENCY (Hz)	AMPLITUDE (g)
1	53.5097	0.440174
2	59.7097	0.318055
3	76.1284	0.176809
4	81.2433	0.269399
5	85.0912	0.214570
6	89.8642	0.268446
7	163.492	5.619752E-02

TRANSDUCER:	I09/C09:REACT. TOP PLENUM/-Z Axis: -X	
MODE	FREQUENCY (Hz)	AMPLITUDE (g)
1	81.4916	5.806199E-02
2	84.7875	5.008457E-02
3	94.4956	4.543561E-02
4	98.3362	4.003127E-02
5	119.001	8.006853E-02
6	140.005	8.117978E-02
7	158.818	1.432525E-02
8	164.039	1.186877E-02
9	170.054	7.224624E-03
10	171.907	8.513646E-03

TRANSDUCER:	I09/C11:REACT. TOP PLENUM/-Z Axis: +Y	
MODE	FREQUENCY (Hz)	AMPLITUDE (g)
1	8.76736	1.95501
2	15.3975	9.637231E-02
3	15.7615	8.896597E-02
4	28.3918	2.16219
5	54.1565	0.603319
6	59.8494	0.212064
7	69.5546	0.141099
8	84.2027	0.188112
9	111.574	2.786758E-02
10	118.594	2.285344E-02
11	143.565	2.197792E-02
12	190.176	1.028353E-02

TRANSDUCER:	I09/C12:REACT. TOP PLENUM/-Z Axis: -Z	
MODE	FREQUENCY (Hz)	AMPLITUDE (g)
1	9.40651	4.61358
2	29.4789	3.97788
3	53.8231	1.36627
4	100.092	0.138697
5	133.096	5.688959E-02
6	175.661	1.350727E-02

TRANSDUCER:	I01/C13:-Z LEG @ BASE Axis: -X	
MODE	FREQUENCY (Hz)	AMPLITUDE (g)
1	7.59040	0.548643
2	24.5878	9.492084E-02
3	28.0407	0.114665
4	32.1489	8.869818E-02
5	46.3899	4.471105E-02
6	56.3866	5.088181E-02
7	68.8677	4.105160E-02
8	81.9021	1.659305E-02
9	85.1832	2.000362E-02
10	120.925	0.140088
11	138.978	0.265800
12	177.79	0.110414

TRANSDUCER:	I01/C14:-Z LEG @ BASE Axis: -Z	
MODE	FREQUENCY (Hz)	AMPLITUDE (g)
1	7.76132	0.270319
2	10.5609	1.10978
3	143.486	1.13443

TRANSDUCER:	I01/C15:-Z LEG @ BASE Axis: -Y	
MODE	FREQUENCY (Hz)	AMPLITUDE (g)
1	6.31161	1.959258E-02
2	8.56065	6.319125E-02
3	12.5204	5.286855E-02
4	28.0407	0.291127
5	138.978	0.518210

TRANSDUCER:	I02/C17:LEG/+Y AND +Z/BASE Axis: +Y	
MODE	FREQUENCY (Hz)	AMPLITUDE (g)
1	7.71202	0.502636
2	28.53	0.625009
3	60.5565	0.728032
4	133.629	0.683575

TRANSDUCER:	I02/C18:LEG/+Y AND +Z/BASE Axis: -Z	
MODE	FREQUENCY (Hz)	AMPLITUDE (g)
1	7.59040	0.807592
2	26.8651	1.05284
3	131.239	1.16256

TRANSDUCER:	I06/C19:LEG/+Y AND +Z/RAD. TOP Axis: -X	
MODE	FREQUENCY (Hz)	AMPLITUDE (g)
1	8.28011	0.625170
2	28.4307	0.209106
3	44.6078	0.180537
4	59.7707	0.154713
5	81.3292	0.109272
6	100.051	0.152750
7	161.436	8.821841E-02

TRANSDUCER:	I06/C20:LEG/ +Y AND +Z/RAD. TOP Axis: +Z(30)	
MODE	FREQUENCY (Hz)	AMPLITUDE (g)
1	7.75082	1.56896
2	24.1758	2.22697
3	28.8881	2.56046
4	55.9942	0.349077
5	96.9556	0.466277
6	136.480	0.899289

TRANSDUCER:	I04/C23:BOTT. COLL. RAD./ +Y Axis: +Y	
MODE	FREQUENCY (Hz)	AMPLITUDE (g)
1	9.86712	0.105801
2	27.943	2.34252
3	48.6237	4.5289
4	69.3226	2.20957
5	88.3314	3.07370
6	130.777	2.95019
7	154.658	2.88126

TRANSDUCER:	I03/C25:BOTT. COLL. RAD./ -Z Axis: -Z	
MODE	FREQUENCY (Hz)	AMPLITUDE (g)
1	7.71202	0.866554
2	27.2555	1.15438
3	48.2127	1.22134

TRANSDUCER:	I11/C28:HARD POINT/CESIUM UNIT Axis: -X	
MODE	FREQUENCY (Hz)	AMPLITUDE (g)
1	8.76736	0.281597
2	13.1312	0.125737
3	28.8881	5.36258
4	59.9416	0.819486
5	81.4916	0.468706
6	140.465	0.537631
7	192.935	0.201526

TRANSDUCER:	I11/C29:HARD POINT/CESIUM UNIT Axis: -Y	
MODE	FREQUENCY (Hz)	AMPLITUDE (g)
1	8.83778	1.23716
2	25.1265	5.35297
3	38.5431	1.97241
4	60.1536	3.74441
5	87.5979	0.767632
6	97.6267	0.604192
7	135.027	0.270747

TRANSDUCER:	I11/C30:HARD POINT/CESIUM UNIT Axis: +Z	
MODE	FREQUENCY (Hz)	AMPLITUDE (g)
1	7.81651	2.05755
2	24.9373	9.57841
3	60.0392	0.904517
4	71.8386	0.974768
5	97.2413	0.865449
6	135.027	0.232790
7	161.199	8.948593E-02

TRANSDUCER:	I05/C31:JOINT ON LEG Axis: -X	
MODE	FREQUENCY (Hz)	AMPLITUDE (g)
1	7.76132	0.410090
2	28.53	0.241601
3	51.9497	0.122066
4	73.0626	0.256050
5	144.013	0.365256

TRANSDUCER:	I05/C33:JOINT ON LEG Axis: -Z	
MODE	FREQUENCY (Hz)	AMPLITUDE (g)
1	7.71202	1.01215
2	27.2555	1.40077
3	140.974	2.00604

TRANSDUCER:	I12/C34:STARTUP UNIT FRAME Axis: -X	
MODE	FREQUENCY (Hz)	AMPLITUDE (g)
1	8.26743	0.459574
2	29.4789	0.831606
3	53.8231	0.136480
4	106.063	0.593274

TRANSDUCER:	I12/C35:STARTUP UNIT FRAME Axis: -Z(60)	
MODE	FREQUENCY (Hz)	AMPLITUDE (g)
1	7.75082	1.83180
2	27.8961	4.99722
3	55.9942	0.397595
4	132.123	0.834946

182

TRANSDUCER:	I12/C36:STARTUP UNIT FRAME Axis: -Y(60)	
MODE	FREQUENCY (Hz)	AMPLITUDE (g)
1	7.97612	1.13312
2	24.2569	1.43728
3	28.3918	1.85856
4	59.4898	0.371952
5	108.367	0.362733
6	139.493	0.220601

INITIAL DISTRIBUTION LIST

No. Copies

1. Defense Technical Information Center 2
   Cameron Station
   Alexandria VA 22301-6145

2. Library, Code 052 2
   Naval Postgraduate School
   Monterey CA 93943-5101

3. Dr. Rudolph Panholzer 1
   Chairman, Space Systems Academic Group
   Code SP
   Naval Postgraduate School
   Monterey CA 93943-5002

4. Dr. Daniel J. Collins 1
   Chairman, Aeronautics and Astronautics Department
   Code AA/Co
   Naval Postgraduate School
   Monterey CA 93943-5106

5. Dr. Sandra L. Scrivener 3
   Code AA/Ss
   Naval Postgraduate School
   Monterey CA 93943-5106

6. Dr. Oscar Biblarz 1
   Code AA/Bi
   Naval Postgraduate School
   Monterey CA 93943-5106

7. TOPAZ International Program 2
   Attn: Frank Thome
              Frank Wyant
   901 University Blvd, S.E.
   Albuquerque, NM 87106

8. LT Elisa A. Raney 4
   Air Department
   USS NIMITZ (CVN 68)
   FPO AP   96697-2820